FUNCTIONAL ANALYSIS OF EGFR USING A CONDITIONAL ALLELE

Tang-Cheng Lee

A dissertation submitted to the faculty of the University of North Carolina at Chapel Hill in partial fulfillment of the requirements for the degree of Doctor of Philosophy in the Curriculum of Genetics & Molecular Biology

Chapel Hill
2008

Approved by:

Dr. Terry Magnuson

Dr. David Threadgill

Dr. Beverly Koller

Dr. Fernando Pardo-Manuel de Villena

Dr. Eva Anton

ABSTRACT

Tang-Cheng Lee: Functional Analysis of EGFR Using a Conditional Allele
(Under the direction of David Threadgill)

Epidermal growth factory receptor (EGFR) is a member of the ERBB family of tyrosine kinase receptors, which includes ERBB2, ERBB3 and ERBB4. EGFR signaling is complicated and involved in a variety of cellular processes, including proliferation, differentiation, migration, adhesion and anti-apoptosis.

EGFR has been studied using gene targeting to investigate the *in vivo* role of the receptor. Constitutional knockout of *Egfr* in mice results in placental defects with mice dying pre- or perinatally depending on the genetic backgroud. All *Egfr* null mice that survive to term eventually develop neurodegeneration that is primarily restricted to the cortex and olfactory bulb. Because the existing knockout models are unable to distinguish the cell lineage(s) (*ie* neuron, astrocyte or both) that depend on EGFR signaling for survival, and also result in pre- or peritnatal lethality limiting the ability to study the role of EGFR in physiological functions or diseases of adults *in vivo*, thus the generation of an *Egfr* conditional allele is necessary to overcome this limitation. Herein gene targeting was used in combination with the Cre/*loxp* system to generate an *Egfr* conditional allele. This allele was used to develop tissue-specific deletion of EGFR to explore its function in the central nervous system in order to understand the mechanism by which loss of EGFR results in neurodegeneration.

After the *Egfr* conditional allele (*Egfr*^{tm1Dwt}) was generated, the *Egfr*^{tm1Dwt} and *Egfr*$^{\Delta}$, which is generated by Cre-mediated excision in the *Egfr*^{tm1Dwt}, were characterized showing that the *Egfr*^{tm1Dwt} possesses wildtype activity and can be inactivated tissue-specially, and the *Egfr*$^{\Delta}$ is a null allele.

To investigate the underlying mechanism responsible for neurodegeneration of *Egfr* null mice, three *Cre* transgenic lines expressed in the embryonic epiblast (*Sox2-Cre*) or neuroprogenitor cells (*Nestin-Cre* and *hGFAP-Cre*) were crossed with mice carrying the *Egfr*^{tm1Dwt} conditional allele to generate *Egfr*$^{tm1Dwt/tm1Dwt}$, *Sox2-Cre* (as well as *Nestin-Cre* or *hGFAP-Cre*) mice. *Egfr*$^{tm1Dwt/tm1Dwt}$ mice also carrying *Sox2-Cre* or *Nestin-Cre* displayed neurodegeneration in the cortex, olfactory bulb and areas surrounding lateral ventricle including corpus callosum, the fimbria of the hippocampus and subventricular zone (SVZ) and rostral extension (RE). These results were consistent with the phenotype of *Egfr* null mice. Conversely, *Egfr*$^{tm1Dwt/tm1Dwt}$, *hGFAP-Cre* mice showed no damage within the brain. To locate differences in the distribution of *Cre* expression in the brain that leads to different phenotypes in the brain between *Egfr*$^{tm1Dwt/tm1Dwt}$, *Nestin-Cre* and *Egfr*$^{tm1Dwt/tm1Dwt}$, *hGFAP-Cre* mice, *Nestin-Cre* and *hGFAP-Cre* mice were crossed with the ROSA26-*lacZ* reporter mice (*R26R*). Results indicated that the *hGFAP-Cre* line expresses *Cre* in the progenitors of the cortex, olfactory bulb, SVZ, RE and rostral migratory stream (RMS) but unlike *Nestin-Cre* not the choroid plexus, despite the lack of neurodegeneration in *Egfr*$^{tm1Dwt/tm1Dwt}$, *hGFAP-Cre* mice. These results suggest that neuronal or astrocytic death in the absence of EGFR signaling is a secondary effect, possibly mediated by the choroid plexus.

ACKNOWLEDGEMENTS

Pursuing a Ph.D. is a long-term process and requires a lot of effort, not only from myself but also from many others. I would like to express my deep appreciation to my advisor, Dr. David Threadgill for his support, instruction and the way he leads the lab. He puts his full trust in his students and allows them to pursue their work in an independent manner. Scientific research can be challenging but his lab always provides the encouragement necessary to succeed.

I would like to thank my committee members: Dr. Terry Magnuson, Dr. Beverly Koller, Dr. Fernando Pardo-Manuel de Villena and Dr. Eva Anton, for their support and valuable suggestions during the course of my project.

I have encountered many difficulties in my research and without the help of my fellow lab members would not have succeeded. I would like to thank all current and former lab members, especially Daekee Lee, Karen Strunk and Reade Roberts for providing their experience, knowledge and advice to assist me in resolving dilemmas. Daekee Lee is an excellent scientist and has been a great help to me. I relied greatly on his experience and knowledge in molecular cloning as well as many experimental protocols optimized by him for my own research.

I would also like to thank my friends, Yau-Sheng Tsai and Steve Wu for their support and providing their experience from their projects, which was very helpful to me.

TABLE OF CONTENTS

LIST OF FIGURES

Figure

ABBREVIATIONS

ADAM	a disintegrin and metalloprotease
AREG	amphiregulin
BTC	betacellulin
ChAT	acetyltransferase
CIN85	Cbl interacting protein of 85 kDa
CNS	central nervous system
Cre	cyclization recombination recombinase
CSF	cerebrospinal fluid
CSPG	chondroitin sulfate proteoglycan
DMEM	Dulbecco's modified eagle medium
DMSO	dimethyl sulfoxide
d.p.c.	days postcoitum
Dsk 5	dark skin 5
DSS	dextran sulfate sodium
DTR	diphtheria toxin receptor/heparin-binding EGF-like growth factor
E	embryonic day
ECL	enhanced chemiluminescent
ECM	extracellular matrix
EDTA	ethylenediamine-tetraacetic acid
EGF	epidermal growth factor

EGFR	epidermal growth factor receptor
EGFRvIII	variant III EGFR deletion
EGTA	ethylenebis(oxyethylenenitrilo) tetraacetic acid
ENU	N-ethyl-N-nitrosourea
EPGN	epigen
EREG	epiregulin
Eps15	EGFR pathway substrate 15
ES	embryonic stem
ESCRT	endosome sorting complex required to transport
F1	the first filial generation
FAK	focal adhesion kinase
FBS	fetal bovine serum
GPCR	G-protein coupled receptor
hGFAP	human glial fibrillary acidic protein
HRP	horseradish peroxidase
Hrs	hepatocyte growth factor-regulated tyrosine kinase substrate
IgG	immunoglobulin G
K14	keratin 14
LPC	lysolecithin
MAPK	mitogen-activated protein kinase
MEK	MAPK kinase
MVE/MVB	multivesicular endosome/multivesicular body
NBF	neutral formalin solution

NF-κB	transcription factor nuclear factor κB
NGF	nerve growth factor
NSCLC	non-small cell lung cancer
NT-4	neurotrophin-4
OCT	tissue freezing medium
PBS	phosphate-buffered saline
PCR	polymerase chain reaction
PI3K	phosphoinositide-3 kinase
PKC	protein kinase C
PLCγ	phospholipase Cγ
PMSF	phenyl sulfonyl fluoride
RAS	renin-angiotensin system
RE	rostral extension
ROS	Reactive oxygen species
RMS	rostral migratory stream
R26R	Rosa26 LacZ reporter
RT-PCR	reverse transcriptase-PCR
SCN	suprachiasmatic nucleus
SDS-PAGE	sodium dodecyl sulfate polyacrylamide gel electrophoresis
SOCS2	suppressor of cytokine signaling-2
Sox2	SRY-box containing gene 2
SPF	specific pathogen-free
STAM	signal transduction adapter molecule

STAT	signal transducer and activator of transcription
SVZ	subventricular zone
TGFA	transforming growth factor-α
TSG 101	tumor susceptibility gene 101
TUNEL	terminal uridine deoxytransferase dUTP nick end labeling
UIM	ubiquitin-interacting motif
VZ	ventricular zone
Wa-2	waved-2
Wa-5	waved-5

CHAPTER 1

INTRODUCTION

EGFR and ERBB family

Epidermal growth factory receptor (EGFR) is a member of the ERBB family of tyrosine kinase receptors, which includes ERBB2, ERBB3 and ERBB4 (Fig.1-1). EGFR as well as other members are membrane-bound glycoproteins whose basic structure contains extracellular (including L1 [ligand-binding], CR1 [cysteine-rich], L2, and CR2 subdomains), transmembrane, juxtamembrane and kinase domains as well as a C-terminal tail with several tyrosine residues that can serve as docking sites after being phosphorylated. The active unit of ERBB receptors is a dimer or higher order oligomer. Upon ligand binding, ERBB receptors can form homo- or hetero-dimers with other members of the ERBB family. ERBB2 is an orphan receptor that has no recognized ligand (Klapper et al., 1999), while ERBB3 lacks kinase activity (Guy et al., 1994) due to the substitution of highly conserved residues in the kinase catalytic domain (Plowman et al., 1990), such that ERBB3 can only transmit signals through heterodimerization with other ERBB receptors. The formation of receptor dimers activates the intrinsic ERBB kinase activities, through trans-phosphorylation of tyrosine residues in the C-terminal tail of the receptors. Phosphotyrosines also serve as docking sites to recruit proteins containing SH2 or phosphotyrosine binding (PTB) domains that trigger intracellular signaling cascades.

EGFR ligands

EGFR ligands include epidermal growth factor (EGF), transforming growth factor-α (TGFA), amphiregulin (AREG), diphtheria toxin receptor/heparin-binding EGF-like growth factor (DTR), epiregulin (EREG), betacellulin (BTC), and epigen (EPGN) (Fig.1-1). All EGFR ligands contain EGF-like domains with six spatially conserved cysteine residues (CX7 CX4-5 CX10-13 CXCX8 C) that form three intramolecular disulfide bonds (C1-C3, C2-C4, C5-C6). This EGF-like domain is important for binding to ERBB receptors (Guy et al., 1994; Harris et al., 2003). The progenitors of the ligands are type 1 transmembrane proteins that are cleaved by ADAM (a disintegrin and metalloprotease) proteins to release mature growth factor ligands (Blobel, 2005). EGF was first discovered in the submaxillary gland of mouse, and it was found that EGF injection into newborn mice led to precocious eyelid opening and eruption of teeth (Cohen, 1962). Unexpectedly, EGF deficient mice do not display overt phenotypes of the hair or eyes, nor in other organs like lung, kidney and the gastrointestinal tract. Furthermore, *Egf* null mice are viable and fertile (Luetteke et al., 1999). However, EGF is a major accelerator of wound healing. Administration of EGF accelerates the healing of burn wounds on the skin of the Wistar rats, and attenuates tissue neutrophil accumulation (Jahovic et al., 2004). By contrast, *Tgfa* null mice exhibit wavy coats and curly whiskers, and dramatic derangement of hair follicles throughout the dermal layer. In addition, a number of *Tgfa* null mice display partial eyelid closure defects at birth, and exhibit clear corneal inflammation by five weeks of age (Mann et al., 1993). TGFA is also involved in blood vessel remodeling. Blood vessels are continuously subjected to dynamic mechanical forces, including stretch and shear stress. Those mechanical factors generate reactive oxygen species (ROS) that activate the transcription factor Nuclear Factor κB (NF-κB), which regulates both

blood vessel growth and the development and progression of vessel disease. TGFA/EGFR signaling is a mediator during the vascular process. Mechanical factor-induced ROS activates TGFA/EGFR signaling, which in turn activates downstream NF-κB signaling leading to vascular remodeling (Lemarie et al., 2006).

Areg null mice do not display overt phenotypes. However female *Areg* null mice have an abnormal mammary gland phenotype (Luetteke et al., 1999). Virgin mice lacking AREG have underdeveloped mammary glands with less ductal outgrowth and branching. Pregnant and postpartum *Areg* null mice have abnormal lobuloalveolar development that affects milk production and impairs lactation resulting in perinatal morbidity of pups. AREG also protects against parasite infection. The immune response to nematode infection is primarily through T-helper 2 (T_H2) lymphocytes and other cells secreting cytokines, including interleukin 4 (IL-4), IL-5, IL-10, and IL-13. AREG is highly expressed in T_H2 lymphocytes to enhance the clearance of nematodes from the mouse intestine (Zaiss et al., 2006). Unlike other EGFR ligands, DTR plays a more essential role in survival since it is important for normal heart development. Hearts from *Dtr* null mice have dilated and enlarged ventricular chambers with cardiomyocyte hypertrophy, and enlarged semilunar (aortic and pulmoic) and atrioventricular (mitral and tricuspid) valves (Iwamoto et al., 2003; Jackson et al., 2003). Like TGFA, DTR is also involved in the process of eyelid closure. DTR is expressed at the tips of two leading edges of the eyelid, and promotes epithelial cell migration through the EGFR-MAPK signaling pathway until the two leading edges of both eyelids meet and fuse at the center of eye (Mine et al., 2005).

Ereg null mice exhibit no overt phenotypes. However, *Ereg* deficiency causes mice to be more susceptible to dextran sulfate sodium (DSS)-induced colitis (Lee et al., 2004). In

addition, *Ereg* null mice develop chronic dermatitis under specific pathogen-free (SPF) conditions that is mediated by non-bone-marrow-derived cells (Shirasawa et al., 2004). BTC has been implicated in pancreatic development. However, *Btc* null mice are viable and fertile, and in newborn *Btc* null mice, there are no morphological changes in pancreas. Adult *Btc* null mice also display normal expression of insulin, glucagon, cytokeratin and amylase (Jackson et al., 2003). Although BTC is not essential for pancreas development, an *in vitro* study has shown that BTC promotes beta cell differentiation (Thowfeequ et al., 2007). This result suggests a therapeutic potential for BTC against type 1 diabetes. EPGN is the most recently discovered EGFR ligand, having been cloned from a mouse keratinocyte cDNA library. EPGN expression is detected in mouse testis, liver and heart, and induces phosphorylation of MAPK (Strachan et al., 2001).

EGFR signaling and biological function

EGFR signaling is complicated and involved in a variety of cellular processes, including proliferation, differentiation, migration, adhesion and anti-apoptosis (Fig.1-2) (Yarden and Sliwkowski, 2001; Zaczek et al., 2005). For proliferation, one of the most important mitogenic pathways is the RAS-RAF-MEK-MAPK pathway. Activated EGFR recruits adapters such as SHC and GRB2 by using phosphotyrosine residues as docking sites in the C-terminal tail. GRB2-bound SOS, a guanylnucleotide exchange factor, activates RAS by changing GDP-bound RAS to GTP-bound RAS, triggering the intracellular signaling cascade. EGFR-activated MAPK pathway is involved in the progression of the cell cycle from G1 to S phase (Suhardja and Hoffman, 2003). Other important EGFR-activated pathways include PI3K/AKT and STAT pathways. In cerebral cortical cultures from mouse

brain, DTR promotes cell proliferation through the EGFR-activated PI3K/AKT pathway (Jin et al., 2005). The PI3K/AKT pathway is activated by EGFR not only in normal cell types but also in different cancer cells such as those from the prostate and esophagus. STAT proteins can be activated by direct binding to EGFR through their SH2 domain or can be activated through SRC proteins. EGFR-activated STAT pathways are involved in cell proliferation and survival of different types of solid tumors (Quesnelle et al., 2007).

EGFR signaling is also required for cell differentiation as best exemplified in *Drosophila* eye development (Voas and Rebay, 2004). The *Drosophila* compound eye comprises about 750-800 individual units called ommatidia. Each ommatidia contains 20 cells including eight photoreceptors (R1-R8), which collect visual inputs and transmit the stimuli to the optic lobes. Additionally, four cone cells secrete the lens and eight pigment cells optically insulate the individual ommatidia. During ommatidial development, EGFR signaling through the RAS/RAF/MEK/MAPK pathway provides the primary signal for recruitment all cells except R8 within ommatidia. R8 is the first cell recruited into the ommatidia in a process requiring the proneural gene *Atonal*. R8 secretes *Spitz*, the *Drosophila* ortholog of TGFA, to activate the EGFR signaling pathway within cells adjacent to R8, and results in recruitment of R2 and R5. By activating the EGFR signaling pathway, photoreceptors recruit more flanking cells into ommatidia as R3 and R4, then R1 and R6, and finally R7, as well as subsequent recruitment of cone and pigment cells.

EGFR also prevents cell apoptosis and enhances cell survival through different downstream pathways. Many cancer cells overexpress EGFR and exert EGFR signaling pathways to escape chemotherapeutic drug- or radiation-induced apoptosis by upregulating anti-apoptotic proteins like BCL2 or BCLX, which block the release of cytochrome c from

mitochondria that is needed to induce a caspase-mediated cascade resulting in apoptosis. Similarly, EGFR can activate pathways that inhibit pro-apoptotic proteins like BAD, BAX, and BAK, which promote the release of cytochrome c from mitochondria causing apoptosis (Danielsen and Maihle, 2002). EGFR signaling can also promote cell migration, which is import for processes such as tumor invasion, wound healing and eyelid closure in newborn mice. Cell migration requires signals from the extracellular matrix (ECM) to activate receptor signaling pathways that induce the rearrangement of the actin cytoskeleton. One example is osteopontin, a secreted, intergrin-binding glycophosphoprotein that induces cell migration of mammary epithelial cells by activating EGFR and the downstream PLCγ/PKC pathway (Tuck et al., 2003).

EGFR also crosstalks with integrins to mediate adhesion between cells and the ECM, which not only serves as a scaffold to stabilize the physical structure of tissues, but also is involved in regulating cell behaviors that can influence cell survival, differentiation, migration, proliferation, shape, and function. Upon integrin binding to the ECM, β-integrin binds to cytoskeletal proteins such as tailin and paxillin, which in turn recruit focal adhesion kinase (FAK) to activate downstream signaling cascades. Active FAK can also bind to EGFR and activate EGFR signaling (Miranti and Brugge, 2002). Another example of pathway crosstalk is between G-protein coupled receptor (GPCR) and EGFR signaling, where ADAMs play a role as a bridge. Upon agonist binding to GPCR, a signaling cascade is activated that causes some kinases (PKC, PYK2, SRC) or molecules (e.g. Ca2+, ROS) involved in the cascade to activate ADAMs, which in turn, result in ectodomain shedding of growth factor progenitors and release of active growth factor ligands that bind and activate EGFR (Ohtsu et al., 2006). Less well understood are results that suggest EGFR can

translocate to the nucleus directly, although the nuclear EGFR pathway is similar to traditional pathways in regulating gene expression and mediating cellular processes (Lo and Hung, 2006).

Endocytosis and degradation of EGFR

Once activated membrane-bound receptors are usually destined for lysosomal degradation through receptor endocyosis, a process of protein sorting and internalization from the cell membrane. Other than basal endocytosis or nonclathrin-mediated endocytosis, ligand-induced and clathrin-mediated EGFR endocytosis has attracted the most investigation. Growth factor-induced EGFR endocytosis requires activation of EGFR, thus also providing a way to downregulate receptor activity. During the process of EGFR endocytosis, monoubiquitination of EGFR is a critical step since ubiquitin functions as a signal for protein sorting (Fig. 1-3) (Haglund et al., 2003; Le Roy and Wrana, 2005; Williams and Urbe, 2007). Upon EGFR activation, phosphorylated EGFR recruits and phosphorylates CBL, an E3 ubiqiutin ligase, which in turn ubiquitylates activated EGFR. Phosphorylated CBL will interact with CIN85 (CBL interacting protein of 85 kDa) and CIN85 in turn binds to endophilin, which is regulatory component of clathrin-coated pits that can bind to lipid bilayers and induce local changes in membrane curvature. Activated EGFR also phophorylates clathrin and EPS15 (EGFR pathway substrate 15) and Epsin. Phosphorylation of clathrin causes its redistribution at the cell periphery and EPS15 as well as Epsin recognize ubiquitylated EGFR by their ubiquitin-interacting motifs (UIMs). Epsin also interacts with clathrin and clathrin adapter protein AP2. EPS15 and Epsin are critical components for the internalization of EGFR from cell membranes. At the early endosome

stage, EGFR is either recycled back to the cell surface or is sorted into multivesicular endosome/multivesicular body (MVE/MVB). Also at the early endosome stage, a UIM-containing protein, HRS (hepatocyte growth factor-regulated tyrosine kinase substrate) complexes with two other UIM-containing proteins, EPS15 and STAM (signal transduction adapter molecule) to sort cargo like EGFR to the ESCRT-I complex (endosomal sorting complex required to transport-I). In the HRS-STAM-EPS15 complex, both HRS and EPS15 bind to multiply ubiquitylated EGFR, and importantly, those UIM-containing proteins themselves are also ubiquitylated by ubiquitin ligase. Thus, EPS15 can regulate intramolecular interactions between its own UIM and ubiquitin, and dissociate from ubiquitylated EGFR to transfer EGFR to HRS. Using the same mechanism, HRS sorts EGFR into MVE/MVB through an interaction with another UIM-containing protein, TSG101 (tumor susceptibility gene 101), another component of the ESCRT-I complex. Subsequently, EGFR is transported from ESCRT-I to ESCRT-II then ESCRT-III, before finally being sorted into intralumenal vesicles of MVE/MVB that are formed through invagination and pinching-off the endosome membrane. Eventually, MVE/MVB fuses with the lysosome, resulting in degradation of EGFR by lysosomal acidic hydrolases.

EGFR and disease

EGFR mutations and EGFR-mediated signaling pathways are involved in the development of many diseases. It is well known that EGFR is overexpressed in different types of cancer including those of the lung, colon, head and neck, prostate, breast, ovary, stomach, esophagous and glia. Many cancer cells use the EGFR signaling pathway for cell proliferation, survival, and even metastasis. In non-small-cell lung cancer (NSCLC), *EGFR*

mutations occur in exons 18-21, which codes for the tyrosine kinase domain. Exon 19 deletions account for 44% of *EGFR* mutations in NSCLC, while the single nucleotide substitution L858R in exon 21 for 41%, the in-frame insertion in exon 20 for 5%, and other point mutations in exons 18-21 for 10% (Shigematsu and Gazdar, 2006). The exon 19 deletion and single nucleotide substitution L858R in exon 21 of *EGFR* codes for receptors that increase the magnitude and duration of signal activation compared with wildtype receptors. Cancer cells that possess these *EGFR* mutations are more sensitive to tyrosine kinase inhibitors, such as gefitinib and erlotinib. Another *EGFR* mutation, the variant III *EGFR* deletion (EGFRvIII) is commonly observed in glioma, and has been reported to occur in other types of cancer such as those of the prostate, breast, ovary and stomach. EGFRvIII is an in-frame deletion encompassing part of the extracellular domain of EGFR and ablating its ligand-binding ability, resulting in constitutive activation of EGFR. Since EGFRvIII appears in several different types of cancer, it has been proposed as a prognostic and therapeutic target (Nicholas et al., 2006).

The Apc^{Min} mouse model for colorectal cancer has shown that intestinal adenoma multiplicity relies on EGFR signaling; reduction of EGFR activity significantly decreases polyp number (Roberts et al., 2002). About 60-80% of colorectal cancers express EGFR, which may be associated with response to radiotherapy, adverse prognosis and shorter survival time (Zlobec et al., 2007). This has caused EGFR to be a therapeutic target for colorectal cancer.

EGFR is connected to other diseases as well. Psoriasis is a skin disease characterized by epidermal hyperproliferation, disturbed differentiation, inflammation, excessive dermal angiogenesis and abnormal keratinization. EGFR and its ligands, EGF as well as TGFA have

been indicated to be significantly increased in psoriatic epidermis and keratinocytes (Ben-Bassat and Klein, 2000). EGFR activation also contributes to angiotensin-II-induced hypertension, cardiac hypertrophy, atherosclerosis, and kidney disease (Shah and Catt, 2003, 2006). Angiotensin II is the dominant effector of the renin-angiotensin system (RAS), which has an important physiological role in the regulation of blood pressure and aldosterone secretion. However, overactivity of RAS can result in renal disease and disorders of the cardiovascular system. The mechanism by which angiotensin II leads to disease is through the transactivation of EGFR that is mediated by ADAMs. Angiotensin II is a peptide hormone that binds to the AT1 receptor, which is a GPCR that activates downstream molecules PLC and PLC that in turn activate kinases such as PKC, SRC, PYK2, increasing the release of Ca^{2+} and ROS. Activation of PKC, SRC, and PYK2 or release of Ca^{2+} and ROS can induce ADAM activity resulting in ectodomain shedding of DTR and TGFA, leading to activation of EGFR signaling. In the heart, elevated EGFR signaling can cause cardiac hypertrophy and fibroblast proliferation and in the kidney, renal lesions by promoting cell proliferation, mesenchymal epithelial transdifferentiation, collagen production, matrix deposition and glomerulosclerosis.

Menetrier's disease is a stomach disease characterized by selective expansion of surface mucous cells in the body and fundus of the stomach (Coffey et al., 2007). The symptoms of this disease include abdominal pain, nausea, vomiting, anemia (due to gastric blood lose), hypochlorhydria (due to markedly reduced numbers of parietal cells), and edema of peripheral tissues (due to leakage of protein across the gastric mucosa). It is believed that Menetrier's disease results from the elevated EGFR signaling in the gastric mucosa caused by local overproduction of TGFA; patients with Menetrier's disease exhibit enhanced

immunoreactivity of TGFA in the expanded surface mucous cell compartment. Transgenic mice overexpressing TGFA in the stomach display phenotypes similar to Menetrier's disease. As EGFR is widely expressed in different organs and tissues, and the EGFR signaling network is involved in many cellular processes, it is not surprising that homeostasis of EGFR signaling is important for developmental processes and physiological functions. Lack or overproduction of EGFR signaling results in developmental defects or abnormalities of physiological functions.

EGFR has been studied using gene targeting to investigate the *in vivo* role of the receptor. Constitutional knockout of *Egfr* in mice results in placental defects with mice dying pre- or perinatally depending on the genetic background (Sibilia and Wagner, 1995; Threadgill et al., 1995). All *Egfr* null mice that survive to term eventually develop neurodegeneration that is primarily restricted to the cortex and olfactory bulb. The placental defect in *Egfr* null mice can be rescued in chimeras generated by aggregation of 2N $Egfr^{-/-}$ zygotes with 4N wildtype embryos or ES cells, where the 4N cells contribute entirely to extraembryonic tissues including the placenta. However, *Egfr* null chimeras that have a normal placenta also develop neurodegeneration after birth and die within one month of birth. The existing models cannot distinguish the cell lineage(s) (*ie* neuron, astrocyte or both) that depend on EGFR signaling for survival. In addition, the current models result in pre- or postnatal lethality limiting the ability to study the role of EGFR in physiological functions or diseases of adults *in vivo*. Thus, the generation of an *Egfr* conditional allele is necessary to overcome this limitation. Herein gene targeting was used in combination with the Cre/*loxp* system to generate an *Egfr* conditional allele. This allele was used to develop tissue-specific

deletion of EGFR to explore its function in the central nervous system in order to understand the mechanism by which loss of EGFR results in neurodegeneration.

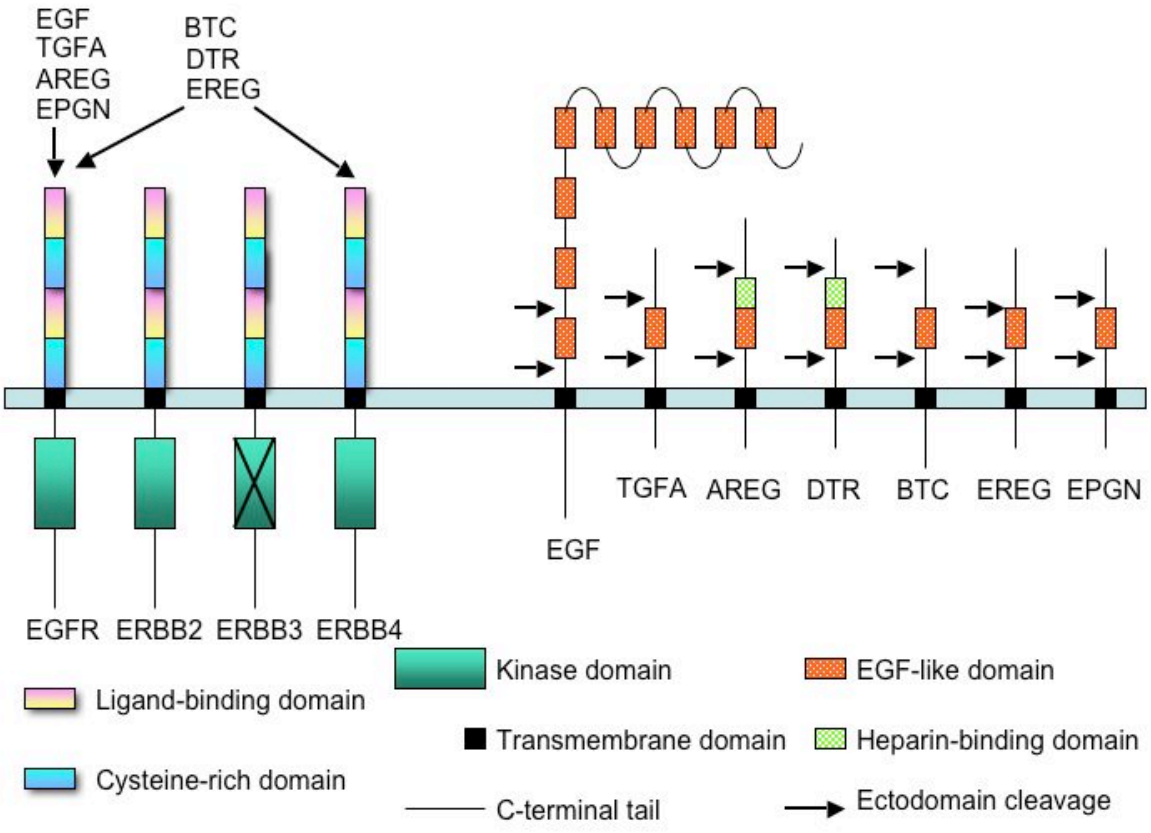

Fig. 1-1 The structure of EGFR and other ERBB receptors and their ligands. EGFR and other ERBB receptors contain an extracellular domain (including two ligand-binding domains and two cysteine-rich domains), a transmembrane domain, a juxtamembrane region, a kinase domain, and a C-terminal tail. Progenitor lignads of EGFR are membrane-bound proteins containing EGF-like domain(s), some with an additional heparin-binding domain. Modified from (Harris et al., 2003)

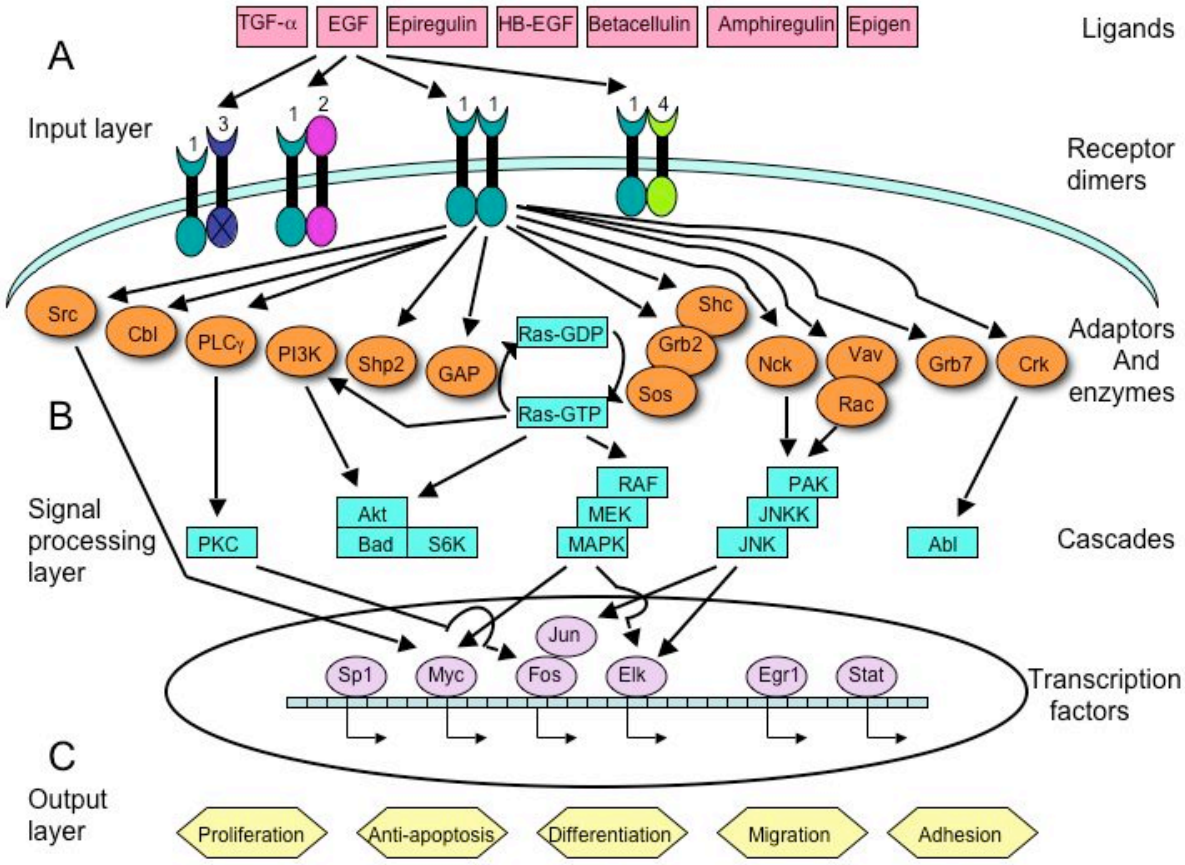

Fig. 1-2 Layers of the EGFR signaling network. (A) The input layer represents the lignad binding and activation of EGFR. (B) The signal processing layer is where EGFR triggers different downstream signaling pathways including RAS/RAF/MEK/MAPK, PI3K/AKT, PLCγ/PKC among other pathways. (C) The output layer is the results of EGFR signaling, which eventually induces distinct cellular events including proliferation, anti-apoptosis, differentiation, migration and adhesion. Modified from (Yarden and Sliwkowski, 2001)

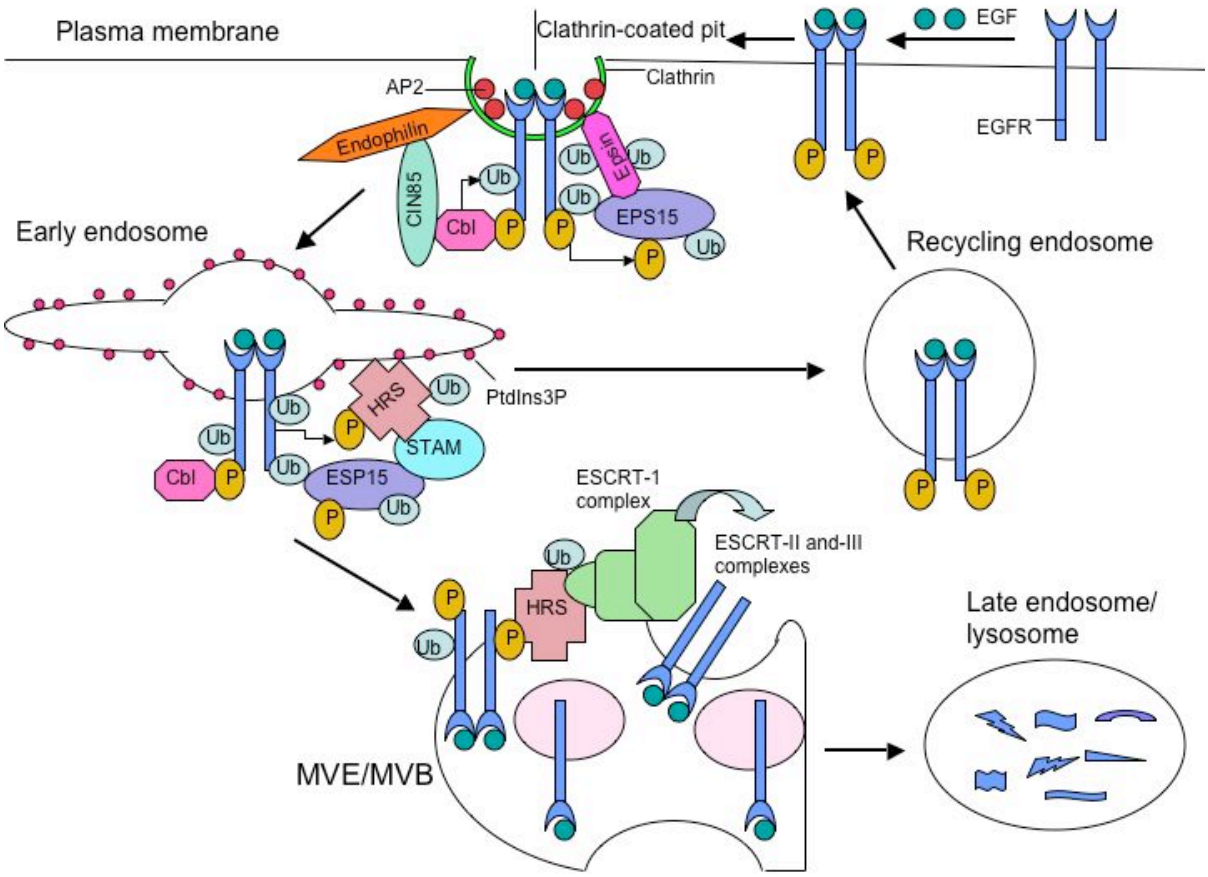

Fig. 1-3 EGFR endocytosis. Upon ligand stimulation, activated EGFR recruits and phosphorylates CBL, which in turn multiubiquitylates EGFR and associates CIN85 and endophilin. Ubiquitylated EGFR recruits ubiquitin receptors, EPS15 and Epsin, the latter of which interacts with clathrin and AP2. After EGFR is sorted into early endosomes, EPS15 complexes with two other ubiquitin receptors, HRS and STAM and dissociates from ubiquitylated EGFR. From the early endosome, ubiquitylated EGFR can be either recycled to cell membrane or sorted into MVE/MVB through the interaction between HRS and the ESCRT-I complex. Ubiquitylated EGFR targeted for degradation is transported to ESCRT-II, ESCRT-III, and then to intralumenal vesicles. The MVE/MVB fuses with the lysosome resulting in degradation of EGFR by lysosomal acidic hydrolases. Modified from (Le Roy and Wrana, 2005)

References

Ben-Bassat, H., and Klein, B.Y. (2000). Inhibitors of tyrosine kinases in the treatment of psoriasis. Curr Pharm Des *6*, 933-942.

Blobel, C.P. (2005). ADAMs: key components in EGFR signalling and development. Nat Rev Mol Cell Biol *6*, 32-43.

Coffey, R.J., Washington, M.K., Corless, C.L., and Heinrich, M.C. (2007). Menetrier disease and gastrointestinal stromal tumors: hyperproliferative disorders of the stomach. J Clin Invest *117*, 70-80.

Cohen, S. (1962). Isolation of a mouse submaxillary gland protein accelerating incisor eruption and eyelid opening in the new-born animal. J Biol Chem *237*, 1555-1562.

Danielsen, A.J., and Maihle, N.J. (2002). The EGF/ErbB receptor family and apoptosis. Growth Factors *20*, 1-15.

Guy, P.M., Platko, J.V., Cantley, L.C., Cerione, R.A., and Carraway, K.L., 3rd (1994). Insect cell-expressed p180erbB3 possesses an impaired tyrosine kinase activity. Proc Natl Acad Sci U S A *91*, 8132-8136.

Haglund, K., Di Fiore, P.P., and Dikic, I. (2003). Distinct monoubiquitin signals in receptor endocytosis. Trends Biochem Sci *28*, 598-603.

Harris, R.C., Chung, E., and Coffey, R.J. (2003). EGF receptor ligands. Exp Cell Res *284*, 2-13.

Iwamoto, R., Yamazaki, S., Asakura, M., Takashima, S., Hasuwa, H., Miyado, K., Adachi, S., Kitakaze, M., Hashimoto, K., Raab, G.*, et al.* (2003). Heparin-binding EGF-like growth factor and ErbB signaling is essential for heart function. Proc Natl Acad Sci U S A *100*, 3221-3226.

Jackson, L.F., Qiu, T.H., Sunnarborg, S.W., Chang, A., Zhang, C., Patterson, C., and Lee, D.C. (2003). Defective valvulogenesis in HB-EGF and TACE-null mice is associated with aberrant BMP signaling. Embo J *22*, 2704-2716.

Jahovic, N., Guzel, E., Arbak, S., and Yegen, B.C. (2004). The healing-promoting effect of saliva on skin burn is mediated by epidermal growth factor (EGF): role of the neutrophils. Burns *30*, 531-538.

Jin, K., Mao, X.O., Del Rio Guerra, G., Jin, L., and Greenberg, D.A. (2005). Heparin-binding epidermal growth factor-like growth factor stimulates cell proliferation in cerebral cortical cultures through phosphatidylinositol 3'-kinase and mitogen-activated protein kinase. J Neurosci Res *81*, 497-505.

Klapper, L.N., Glathe, S., Vaisman, N., Hynes, N.E., Andrews, G.C., Sela, M., and Yarden, Y. (1999). The ErbB-2/HER2 oncoprotein of human carcinomas may function solely as a shared coreceptor for multiple stroma-derived growth factors. Proc Natl Acad Sci U S A *96*, 4995-5000.

Le Roy, C., and Wrana, J.L. (2005). Clathrin- and non-clathrin-mediated endocytic regulation of cell signalling. Nat Rev Mol Cell Biol *6*, 112-126.

Lee, D., Pearsall, R.S., Das, S., Dey, S.K., Godfrey, V.L., and Threadgill, D.W. (2004). Epiregulin is not essential for development of intestinal tumors but is required for protection from intestinal damage. Mol Cell Biol *24*, 8907-8916.

Lemarie, C.A., Tharaux, P.L., Esposito, B., Tedgui, A., and Lehoux, S. (2006). Transforming growth factor-alpha mediates nuclear factor kappaB activation in strained arteries. Circ Res *99*, 434-441.

Lo, H.W., and Hung, M.C. (2006). Nuclear EGFR signalling network in cancers: linking EGFR pathway to cell cycle progression, nitric oxide pathway and patient survival. Br J Cancer *94*, 184-188.

Luetteke, N.C., Qiu, T.H., Fenton, S.E., Troyer, K.L., Riedel, R.F., Chang, A., and Lee, D.C. (1999). Targeted inactivation of the EGF and amphiregulin genes reveals distinct roles for EGF receptor ligands in mouse mammary gland development. Development *126*, 2739-2750.

Mann, G.B., Fowler, K.J., Gabriel, A., Nice, E.C., Williams, R.L., and Dunn, A.R. (1993). Mice with a null mutation of the TGF alpha gene have abnormal skin architecture, wavy hair, and curly whiskers and often develop corneal inflammation. Cell *73*, 249-261.

Mine, N., Iwamoto, R., and Mekada, E. (2005). HB-EGF promotes epithelial cell migration in eyelid development. Development *132*, 4317-4326.

Miranti, C.K., and Brugge, J.S. (2002). Sensing the environment: a historical perspective on integrin signal transduction. Nat Cell Biol *4*, E83-90.

Nicholas, M.K., Lukas, R.V., Jafri, N.F., Faoro, L., and Salgia, R. (2006). Epidermal growth factor receptor - mediated signal transduction in the development and therapy of gliomas. Clin Cancer Res *12*, 7261-7270.

Ohtsu, H., Dempsey, P.J., and Eguchi, S. (2006). ADAMs as mediators of EGF receptor transactivation by G protein-coupled receptors. Am J Physiol Cell Physiol *291*, C1-10.

Plowman, G.D., Whitney, G.S., Neubauer, M.G., Green, J.M., McDonald, V.L., Todaro, G.J., and Shoyab, M. (1990). Molecular cloning and expression of an additional epidermal growth factor receptor-related gene. Proc Natl Acad Sci U S A *87*, 4905-4909.

Quesnelle, K.M., Boehm, A.L., and Grandis, J.R. (2007). STAT-mediated EGFR signaling in cancer. J Cell Biochem *102*, 311-319.

Roberts, R.B., Min, L., Washington, M.K., Olsen, S.J., Settle, S.H., Coffey, R.J., and Threadgill, D.W. (2002). Importance of epidermal growth factor receptor signaling in establishment of adenomas and maintenance of carcinomas during intestinal tumorigenesis. Proc Natl Acad Sci U S A *99*, 1521-1526.

Shah, B.H., and Catt, K.J. (2003). A central role of EGF receptor transactivation in angiotensin II -induced cardiac hypertrophy. Trends Pharmacol Sci *24*, 239-244.

Shah, B.H., and Catt, K.J. (2006). TACE-dependent EGF receptor activation in angiotensin-II-induced kidney disease. Trends Pharmacol Sci *27*, 235-237.

Shigematsu, H., and Gazdar, A.F. (2006). Somatic mutations of epidermal growth factor receptor signaling pathway in lung cancers. Int J Cancer *118*, 257-262.

Shirasawa, S., Sugiyama, S., Baba, I., Inokuchi, J., Sekine, S., Ogino, K., Kawamura, Y., Dohi, T., Fujimoto, M., and Sasazuki, T. (2004). Dermatitis due to epiregulin deficiency and a critical role of epiregulin in immune-related responses of keratinocyte and macrophage. Proc Natl Acad Sci U S A *101*, 13921-13926.

Sibilia, M., and Wagner, E.F. (1995). Strain-dependent epithelial defects in mice lacking the EGF receptor. Science *269*, 234-238.

Strachan, L., Murison, J.G., Prestidge, R.L., Sleeman, M.A., Watson, J.D., and Kumble, K.D. (2001). Cloning and biological activity of epigen, a novel member of the epidermal growth factor superfamily. J Biol Chem *276*, 18265-18271.

Suhardja, A., and Hoffman, H. (2003). Role of growth factors and their receptors in proliferation of microvascular endothelial cells. Microsc Res Tech *60*, 70-75.

Thowfeequ, S., Ralphs, K.L., Yu, W.Y., Slack, J.M., and Tosh, D. (2007). Betacellulin inhibits amylase and glucagon production and promotes beta cell differentiation in mouse embryonic pancreas. Diabetologia *50*, 1688-1697.

Threadgill, D.W., Dlugosz, A.A., Hansen, L.A., Tennenbaum, T., Lichti, U., Yee, D., LaMantia, C., Mourton, T., Herrup, K., Harris, R.C.*, et al.* (1995). Targeted disruption of mouse EGF receptor: effect of genetic background on mutant phenotype. Science *269*, 230-234.

Tuck, A.B., Hota, C., Wilson, S.M., and Chambers, A.F. (2003). Osteopontin-induced migration of human mammary epithelial cells involves activation of EGF receptor and multiple signal transduction pathways. Oncogene *22*, 1198-1205.

Voas, M.G., and Rebay, I. (2004). Signal integration during development: insights from the Drosophila eye. Dev Dyn *229*, 162-175.

Williams, R.L., and Urbe, S. (2007). The emerging shape of the ESCRT machinery. Nat Rev Mol Cell Biol *8*, 355-368.

Yarden, Y., and Sliwkowski, M.X. (2001). Untangling the ErbB signalling network. Nat Rev Mol Cell Biol *2*, 127-137.

Zaczek, A., Brandt, B., and Bielawski, K.P. (2005). The diverse signaling network of EGFR, HER2, HER3 and HER4 tyrosine kinase receptors and the consequences for therapeutic approaches. Histol Histopathol *20*, 1005-1015.

Zaiss, D.M., Yang, L., Shah, P.R., Kobie, J.J., Urban, J.F., and Mosmann, T.R. (2006). Amphiregulin, a TH2 cytokine enhancing resistance to nematodes. Science *314*, 1746.

Zlobec, I., Vuong, T., Hayashi, S., Haegert, D., Tornillo, L., Terracciano, L., Lugli, A., and Jass, J. (2007). A simple and reproducible scoring system for EGFR in colorectal cancer: application to prognosis and prediction of response to preoperative brachytherapy. Br J Cancer *96*, 793-800.

CHAPTER 2

GENERATION OF GERMLINE CHIMERAS

Abstract

In order to investigate the tissue-specific function of *Egfr*, a conditional knockout mouse model was produced. The first two constructs engineered did not produce any targeted events or targeted *Egfr* at a very low frequency. The third construct was designed with much longer homologous regions, resulting in a greater targeting efficiency than the previous two constructs. The third construct resulted in 13 targeted embryonic stem (ES) cell clones out of 300 screened clones. Southern blot and PCR analyses confirmed that among the 13 targeted clones, 11 clones had the predicted genomic organization after targeting. Two of the 11 targeted clones were chosen to prepare for microinjection and then producing chimeras. First, Cre recombinase was transiently expressed in the targeted ES cells to remove the *neo* cassette, followed by RT-PCR to confirm that two remaining *loxp* sites in the targeted *Egfr* gene did not alter the RNA splcing pattern. Subsequently, the targeted ES cells were microinjected into blastocysts from CD1 mice, and four chimeras were generated, all with low coat color chimerism. Of the four chimeras, one was sterile and the others were fertile. The fertile chimeras, however, did not transmit the modified allele to any progeny within the first ten litters produced. Consequently, the targeted ES cells were used for microinjection into blastocysts from C57BL/6 mice to generate chimeras; the modified allele was found in

the progeny of these chimeras, and a colony of mice carrying the *Egfr* condtional allele established for functional studies.

Introduction

Gene targeting technique is frequently used to generated knockout or null alleles for creating mouse models lacking specific genes. In this way, the function of individual genes can be determined *in vivo* through careful phenotypic analysis. Thus, gene targeting provides a powerful tool for gene function studies. Mice that are deficient for specific genes can show phenotypes from early embryonic stages through adults. Deletion of some genes will result in no phenotype or an undetectable phenotype due to genetic redundancy or compensation by other genes or the lack of appropriate physiological stress. It is also very common that genes may play multiple roles in different tissues or organs, or at different stages of development. In particular, embryonic lethality will prevent the study of postnatal or adult physiological functions. In order to overcome the limitation of embryonic lethality, conditional alleles are commonly generated that allow the deletion of specific genes to be controlled spatially and temporally.

Studies have shown that homozygosity for targeted mutations in any member of the *Erbb* family of receptor tyrosine kinases results in embryonic lethality. *Egfr* deficient mice die prenatally from placental abnormalities or perinatally with abnormalities in skin, lung, brain and gastrointestinal tract depending on genetic background (Miettinen et al., 1995; Sibilia and Wagner, 1995; Threadgill et al., 1995). Embryos homozygous for a null mutation in *Erbb2* die before embryonic day (E) 11 with defects in cardiac trabeculation and impaired neural development (Lee et al., 1995). Deficiency for *Erbb3* causes mid-gestation lethality from abnormal cardiac cushion development and a lack of Schwann cell precursors, which in turn results in degeneration of the peripheral nervous system and death of motor and sensory neurons in the dorsal root ganglia owing to a lack of neurotrophic factors provided by

developing Schwann cells (Lee et al., 1995; Riethmacher et al., 1997). *Erbb4* mutant embryos die at E10-11 due to the failure of trabeculation in the heart ventricle, which is similar to the phenotype in *Erbb2* null mice. *ErbB4* deficiency also results in abnormal development of the hindbrain leading to mis-innervation (Gassmann et al., 1995).

Since embryonic lethality limits studies of post-natal phenotypes for all members of the *Erbb* gene family, including *Egfr*, it is necessary to create conditional mutations to selectively remove the genes from specific tissues. Although conditional alleles have been generated for *Erbb2*, *Erbb3* and *Erbb4* (Crone et al., 2002; Fitch et al., 2003; Garcia-Rivello et al., 2005; Long et al., 2003; Qu et al., 2006), there are no available *Egfr* conditional knockout mouse models. In this study, an *Egfr* conditional knockout mouse model was generated using the *Cre*/*loxp* system (Lewandoski, 2001; Nagy, 2000). Cre is a 38-KDa monomeric protein encoded by bacteriaphage P1 (Abremski and Hoess, 1984), while *Loxp* is a 34-bp sequence consisting of two 13-bp inverted repeats and an 8-bp asymmetric core sequence, which provides directionality. Cre cooperatively binds to *loxp* sites with one Cre monomer contacting each of 13-bp inverted repeats. Association of two dimers of Cre on each *loxp* site forms a synaptic structure and catalyzes recombination between two *loxp* sites (Ghosh and Van Duyne, 2002). Cre-mediated *loxp* recombinations include excision/integration, inversion and translocation depending on the alignment and direction of two *loxp* sites (Fig.2-1) (Kwan, 2002; Nagy, 2000). The general strategy used to develop a conditional knockout mouse model for *Egfr* includes several steps: (a) construction of a targeting vector. (b) identification of targeted ES cell clones. (c) removal of the *neo* selection cassette. (d) microinjection of targeted ES cells into blastocysts. (e) transfer of blastocysts into uteri of psedopregnant recipients. (f) generation of chimeras. (g) germline transmission

of the modified alleles (Fig. 2-2). In this chapter, the development of an *Egfr* conditional knockout mouse model is presented.

Materials and methods

Construction of targeting vectors

Vector 1 and Vector 2

For constructing vectors 1 and 2, clone 158K10, containing the *Egfr* locus was isolated from the RPCI-22 129S6/SvEvTAC BAC library (BacPac Resources, Children's Hospital Oakland Research Institute), and was used as a template to amplify DNA fragments of *Egfr*. Construction of vector 1 began with the ligation of a 1.3 kb PCR fragment containing part of first intron into pCR2.1-TOPO to serve as the 5' homologous region. A *neo* cassette flanked by two *loxp* sites that includes unique *Cla*1 and a *Sal*1 sites was inserted into the *Xho*1 site of pCR2.1-TOPO. Subsequently, a 4.0 kb fragment consisting of a *loxp* site, part of first intron, exons 2-4, and part of fourth intron was inserted into *Cla*1 site. Finally, a 5.0 kb fragment containing part of intron 4, exon 5, intron 5 as well as part of exon 6 was inserted into *Sal*1 site to serve as the 3' homologous region. Vector 2 was similar to vector 1 except with a 2.6 kb 5' homologous region rather than 1.3 kb as in vector 1.

Vector 3

Because of the targeting inefficiency of vectors 1 and 2, vector 3 was designed to have longer homologous regions. BAC clone 158K10 was cut with *Eco*R1 to obtain two DNA fragments of 6.0 kb and 12.8 kb, respectively. The 6.0 kb *Eco*R1 fragment was further cut with *Nhe*1 to produce a 4.3 kb *Eco*R1-*Nhe*1 fragment that was inserted into plox-neo-lox as the 5' homologous region. The remaining 1.7 kb *Nhe*1-*Eco*R1 fragment was ligated with a

7.5 kb *Eco*R1-*Xma*1 fragment that was generated from the 12.8 kb *Eco*R1 fragment cut with *Xma*1. After subcloning this 9.2 kb *Nhe*1-*Xma*1 fragment, a *loxp* site was inserted into the *Spe*1 site within intron 3 before cloning this fragment into plox-neo-lox to complete vector 3.

ES cell culture

The TL1 ES cells, derived from 129S6/SvEvTAC were a gift from Dr. Brigid Hogan (Duke University). ES cells were cultured in Dulbecco's modified eagle medium (DMEM) (Gibco-BRL), with 15% heat-inactivated fetal bovine serum (FBS) (Gibco-BRL), 2mM L-glutamine (Gibco-BRL), 0.1mM non-essential amino acids solution (Gibco-BRL), 50 units/ml penicillin-50 μg/ml streptomycin (Gibco-BRL), 0.1mM 2-mercaptoethanol (Sigma), as well as 1000 units/ml ESGRO (murine leukemia inhibitory factor; Gibco-BRL). For selecting neomycin-resistant ES cell clones, the ES cell medium were supplemented with Geneticin selective antibiotic (G418) (Gibco-BRL) at 200 μg/ml.

Electroporation

Cultured ES cells were trypsinized, washed once with phosphate-buffered saline (PBS) and resuspended as a single cell suspension at a concentration of 1×10^7 cells/ml in Ca^{2+}/Mg^{2+}-free PBS. For electroporation, 0.8 ml of cells were placed in a 0.4 cm wide curvette, and mixed with 10 μg of linearized targeting vector. The cuvette was set at room temperature for 5 minutes before applying a 240 V, 500 μF pulse to the cells using a Gene Pulser II (Bio-Rad). After electroporation, the ES cells were cultured in ES cell medium with 200 μg/ml G418.

Colony picking

G418-resistent ES cell colonies were picked and cultured in 96-well plates. When ES cells reached confluency, they were passaged into two plates. An equal volume of 2X freezing

medium (DMEM with 40% FBS and 20% dimethylsulfoxide [DMSO]) to each well of one plate before topping with 100 μl of sterile light paraffin oil. This plate was placed in a styroform box, stored at -70°C for at least 24 hours, and then transferred to liquid nitrogen for long-term storage. The cells in second other plate were further grown to confluency for analysis.

Molecular analysis of ES cell clones

ES cells were washed twice with PBS and 50 μl of lysis buffer (10 mM Tris [pH 7.7], 10 mM ethylenediamine tetraaceticacid [EDTA], 10 mM NaCl, 0.5% sarcosyl, and fresh-prepared 1 mg/ml proteinase K) was added to each well. The plate was then placed in a Tupperware-type container with wet towels and incubated at 60°C oven overnight. The next day, 100 μl of precipitation solution (150 μl of 5 M NaCl to 10 ml of cold absolute ethanol) was added to each well. The plate sat at room temperature for 30 minutes before discarding the solution by inversion of the plate. The precipitated genomic DNA remained on the bottom of the wells. Each well was washed three times with 70% of ethanol before drying the genomic DNA. Finally, 30 μl of restriction digestion mixture containing 10 units of *Pfl*F1, *Eco*N1 or *Nde*1 was added to each well and incubated at 37°C overnight.

Digested genomic DNA was subjected to agarose gel electrophoresis, and afterwards, the gel was soaked in denaturation solution (0.4M NaOH, 3M NaCl). The restriction fragments were transferred from the agarose gel to a nylon transfer membrane (Schleicher & Schuell, Nytran supercharge). After UV crosslinking the transferred DNA to the membrane, a 1.3 kb ^{32}P labeled probe from upstream of the 5' homologous region of targeting vector was hybridized overnight to detect targeted and wildtype alleles. The membrane was washed

and then exposed to X-ray film to detect the hybridized bands, which corresponded to a 6.9 kb *Pfl*F1 fragment for targeted allele and a 9.4 kb fragment for the wildtype allele.

Transient expression of Cre and removal of the *neo* cassette

To remove the *neo* cassette, correctly targeted ES cells were electroporated with 5 μg pCMV-Cre vector containing *Cre* driven by a human cytomegarovirus major immediate early promoter (CMV promoter). The procedures of electroporation and genomic DNA extraction were identical to those used to generate the targeted ES cells clones. The genomic DNA from each colony was subjected to PCR screening to identify colonies with an appropriately removed *neo* cassette.

PCR genotyping

To determine whether the third *loxp* site was present in the 13 targeted ES cell clones, genomic DNA was amplified for 35 cycles (30 s at 94°C, 1 min at 60°C and 1 min at 72°C) using Taq DNA polymerase (Qiagen) and a GeneAmp PCR system 9700 (Applied Biosystems). The primers were lox3s 5'-CTTTGGAGAACCTGCAGATC-3' and lox3as 5'-CTGCTACTGGCTCAAGTTTC-3'. A 375 bp PCR product resulted if the third *loxp* site was present, while a 320 bp PCR product was generated if the *loxp* site was not present.

To screen ES cell clones after Cre-mediated partial *loxp* recombination, genomic DNA from each ES cell colony was amplified for 35 cycles (30 s at 94°C, 1 min at 60°C and 1 min at 72°C). The primers were CTE-1 5'-CCAGGGACTACCAGTGGGTT-3' and CTE-2 5'-GAGGTGGCTCCTAATGGCTT-3'. The flox specific band was 431 bp and the wildtype band was 336 bp.

Reverse transcriptase-polymerase chain reaction (RT-PCR)

To determine whether *loxp* sites within introns affect *Egfr* expression or spicing, RT-PCR was performed. Total mRNA was extracted from targeted and wildtype ES cell clones using TRizol reagent (Invitrogen) according to manufacturer's instructions. The targeted or wildtype ES cells were mixed with TRizol reagent (5-10 × 10^5 cells/ml) and repetitively pipeted to lyse the cells. For each ml of Trizol reagent, 0.2 ml of chloroform was then added. After centrifugation (12,000 ×g, 15 min), the upper aqueous phase was removed to a fresh tube and isopropyl alcohol was added (TRizol : isopropyl = 1 : 2) to precipitate RNA. The RNA was pelleted by centrifugation (12.000 ×g, 10 min) and the pellet washed once with 70% ethanol before drying briefly. Finally, the RNA was dissolved in RNase-free water. One μg of mRNA was used as template for synthesis of cDNA using random primers (Gibco-BRL) and SuperScript II RT (Gibco-BRL) in a total reaction volume of 20 μl. The cDNA was used as template for PCR amplification of exons 2-4 for 35 cycles (30 s at 93°C, 1 min at 58°C and 1 min at 72 °C). The primers were RNA2 5'-TGCCAAGGCACAAGTAACAG-3' and RNA4 5'-GCTCGGATGGCTCTGTAAGT-3'. The predicted wildtype band was 465 bp.

Microinjection, uterine transfer and chimera generation

Blastocysts were prepared by flushing the uteri of 3.5 days postcoitum (dpc) pregnant CD1 females with M2 medium (Chemicon). Approximately 10-15 targeted ES cells in KSOM medium (Chemicon) were microinjected into each blastocyst. ES cell-injected blastocysts were then transferred into the uteri of 2.5 d.p.c. pseudopregnant recipient CD1 females that had been mated with vasectomized males. The ES cell-injected chimeras were easily

differentiated by two coat colors, one derived from the albino CD1 blastocysts and the other derived from agouti ES cells.

Results

Construction of targeting vectors

To generate an *Egfr* conditional allele, a Cre-*loxp* strategy was employed. Two vectors were designed to inactivate *Egfr* by Cre-mediated excision of a *loxp*-flanked region including exons 2-4, which encodes an essential part of the EGFR ligand-binding domain. Vector 2 has longer 5' homologous arm compared to vector 1 (2.6 kb vs 1.3 kb), and both have the same 3' homologous arm (5.0 kb). Instead of disrupting *Egfr* by deleting exons 2-4 as planned for vectors 1 and 2, vector 3 was designed to inactivate *Egfr* by deleting exon 3, which would introduce a frameshift in the reading frame after Cre-mediated excision. Vector 3 also has much longer 5' and 3' homologous regions (4.3 kb and 8.4 kb, respectively), and is expected to have higher targeting efficiency than vectors 1 and 2 (Fig. 2-3).

Targeting efficiency and targeted ES cell clones

One thousand G418-resistant ES cell clones from an electroporation with vector 1 were screened by Southern blot analysis, but no targeted clone was obtained. For vector 2 electroporated ES cells, 300 ES cell clones were screened and only one was correctly targeted. As anticipated, vector 3 had a much higher targeting efficiency, resulting in 13 targeted ES cell clones out of 300 G418-resistant ES cell clones (Table 2-1). The targeted allele was identified as a 6.9 kb *Pfl*F1 fragment by Southern blot analysis as opposed to the wildtype allele that was a 9.4 kb fragment. All 13 targeted ES cell clones were subjected to

further confirmation. One of the 13 targeted clones had lost the third *loxp* site as determined by PCR screening, indicating that in this clone homologous recombination occurred in the region between the second and the third *loxp* sites. Another clone contained a correctly targeted allele but the other allele differed from the predicted wildtype allele. The remaining 11 ES cell clones were correctly targeted clones (Fig. 2-4).

Table 2-1 Targeting frequencies

	Number of ES cell clones screened	Number of targeted ES cell clones	Percentage of targeted ES cell clone (%)
Vector 1	1000	0	0
Vector 2	300	1	0.33
Vector 3	300	13	4.33

Removal of *neo* cassette by transient Cre expression

Based on colony morphology and karyotyping, two clones were chosen for further preparation. Considering that the selectable *neo* cassette may influence the expression of the targeted allele (Fiering et al., 1995; Meyers et al., 1998), Cre was transiently expressed to remove the *neo* cassette by partial *loxp* recombination between the first and the second *loxp* sites, thus, removing the *neo* cassette but retaining two *loxp* sites in the targeted allele franking a region including exon 3. Two primers were designed, one located upstream of the first *loxp* site and the other located in the region between the second and the third *loxp* sites

(Fig. 2-5A). PCR was performed to screen the ES cell colonies, and several clones were identified that had partial recombination occurring between the first and the second *loxp* sites as indicated by a 431 bp PCR product. Most ES colonies underwent complete recombination that excised not only the *neo* cassette but also exon 3 (Fig. 2-5B). The allele that possesses two *loxp* sites flanking exon 3 was called the *Egfr*^{tm1Dwt} allele, while the allele with complete *loxp* recombination as the *Egfr*$^{\Delta}$ allele (Fig. 2-6).

Insertions of *loxp* sites do not alter *Egfr* splicing

To examine if the insertions of *loxp* sites in *Egfr*^{tm1Dwt} disturb gene expression or alter splicing, RT-PCR analysis was conducted. RNA extracted from wildtype ES cells and targeted ES cells containing the *Egfr*^{tm1Dwt} allele was used as template, and primers were designed to be located in exons 2 and 4. The resulting RT-PCR product amplified from the *Egfr*^{tm1Dwt} allele was identical in size and quantity to that from the wildtype allele, suggesting that insertions of *loxp* sites in the *Egfr*^{tm1Dwt} allele do not alter the splicing pattern or reduce gene expression (Fig. 2-7). This result suggests that the *Egfr*^{tm1Dwt} allele should function as a wildtype allele.

Generation of chimeras

To generate chimeras, 10-15 ES cells carrying the *Egfr*^{tm1Dwt} allele were injected into 3.5 d.p.c. blastocysts from CD1 mice, and the injected blastocysts were transferred into the uteri of 2.5 d.p.c. pseudopregnant CD1 recipients. Four chimeras with low coat color chimerism (5-30%) were generated and mated with wildtype female CD1 mice (Fig. 2-8). Germline transmission was not obtained from any of the CD1 chimeras. A second round of

chimeras was produced by injection of targeted ES cells into C57BL/6 blastocysts. Ten chimeras were obtained, all with much higher coat color chimerism (45-100%) than with CD1 chimeras. Five high contribution male chimeras (85-100%) were chosen to mate with wildtype C57BL/6 and 129SvEv females, which produced agouti pups containing the *Egfr*^{tm1Dwt} allele as determined by PCR. The pups carrying *Egfr*^{tm1Dwt} allele will be used for functional studies of EGFR.

Discussion

Mice homozygous for an *Egfr* null allele die pre- or peri-natally depending on genetic background (Sibilia and Wagner, 1995; Threadgill et al., 1995). This prevents the study of EGFR function in postnatal tissues or organs. To overcome this limitation, an *Egfr* conditional allele was generated using the Cre-*loxp* system, which supports inactivation of *Egfr* in a spatially and/or temporally controlled manner. To inactivate genes in a spatially controlled manner, mice with conditional alleles are crossed to mice carrying a *Cre* transgene in which *Cre* is expressed under control of a tissue-specific promoter. To inactivate a gene of interest in a spatially and temporally controlled manner, a combination of an inducible system with the cre/*loxp* system is required.

Although the Cre/*loxp* system can be used to knockout a gene of interest in a tissue-specific pattern, mosaicism commonly occurs. Many *Cre* transgenic lines are not 100% efficient causing partial deletion of the conditional allele. This can complicate interpretation of the results if a small population of wildtype cells can prevent abnormal phenotypes, like when the target gene acts in noncell-autonomous manner (Kwan, 2002; Nagy, 2000).

Three targeting vectors were built to generate an *Egfr* conditional allele. However, vectors 1 and 2 had very low targeting frequencies. There are several factors that can affect targeting frequency, including position effect and the amount of homology. To improve the targeting frequency, the homologous region in vector 3 was greatly increased and the size of the selection cassette reduced. This was achieved by replacing a *tk-neo* cassette (3.5 kb) in vectors 1 and 2 with a *neo* cassette (2.1 kb) in vector 3. As the results shown (Table 2-1), the targeting efficiency was greatly improved in vector 3. In order to increase the size of the homologous region in vector 3, a different design was used. The design of vectors 1 and 2 was to inactivate *Egfr* by deletion of exons 2-4, while in vector 3, the design was to inactivate *Egfr* by deleting only exon 3. Deletion of exon 3 introduces a frameshift resulting in two stop codons in exon 4 and early termination of translation. In addition, exon 3 encodes residues 57-117, which is part of the L1 subdomain of the extracellular domain that is essential for lignd-binding (Garrett et al., 2002; Reiter et al., 2001). Thus, removal of exon 3 should ensure an inactive *Egfr* allele upon Cre-mediated recombination.

For gene targeting, the *neo* selectable marker provides resistance to G418 allowing the identification of ES cell colonies that have been potentially targeted by positive selection. However, the presence of the *neo* cassette within an intron may interfere with expression of the targeted allele by reducing gene expression or causing aberrant splicing, thus creating a hypomorphic allele. This result may be due to the fact that the *neo* cassette contains cryptic splice sites (Meyers et al., 1998; Nagy et al., 1998). To avoid the possibility of interference of gene expression, transient expression of *Cre* in targeted ES cells was performed by electroporation to remove the *neo* cassette that is flanked by two *loxp* insertions. However, a third *loxp* insertion exists within another intron of *Egfr* to permit gene inactivation that may

also interfere with splicing. Therefore, an RT-PCR analysis was performed to show that no alternative splicing occurs in the targeted *Egfr* locus.

The success of the knockout technology relies on the pluripotency of ES cells, which allows ES cells to contribute to all cell lineages, including the germ line of resulting chimeras. Of four chimeras from CD1 embryos, one was sterile. It is likely to be an XX ↔ XY chimera, which was morphologically male but was sterile due to the presence of female germ cells in the gonads (Koopman et al., 1991). The remaining fertile chimeras each produced ten litters, but none transmitted the agouti coat color predicted from the ES cell contribution. These chimeras had very low coat color chimerism (5-25%), suggesting that CD1 embryos are not suitable hosts for microinjection of 129-derived ES cells. Previous studies with CD1 and MF1 embryo-derived chimeras reached similar conclusions, consistent with our result. It was concluded that the genetic background has a profound influence on the degree of ES cell colonization to different tissues (Schwartzberg et al., 1989). Most likely CD1 embryos are predominant over the injected 129 ES cells in contributing to the germ line, possibly due to the faster growth of CD1 embryos. Ten high coat color contribution chimeras were obtained when using C57BL/6 host blastocysts. Since the coat color chimerism is positively correlated with germ line transmission (Forsthoefel et al., 1983; Mystkowska et al., 1979), five chimeras with over 85% coat color chimerism were chosen to cross with C57BL/6 and 129 SvEv females. As expected, agouti progeny were obtained from the crosses that carried the *Egfr*^{tm1Dwt} conditional allele.

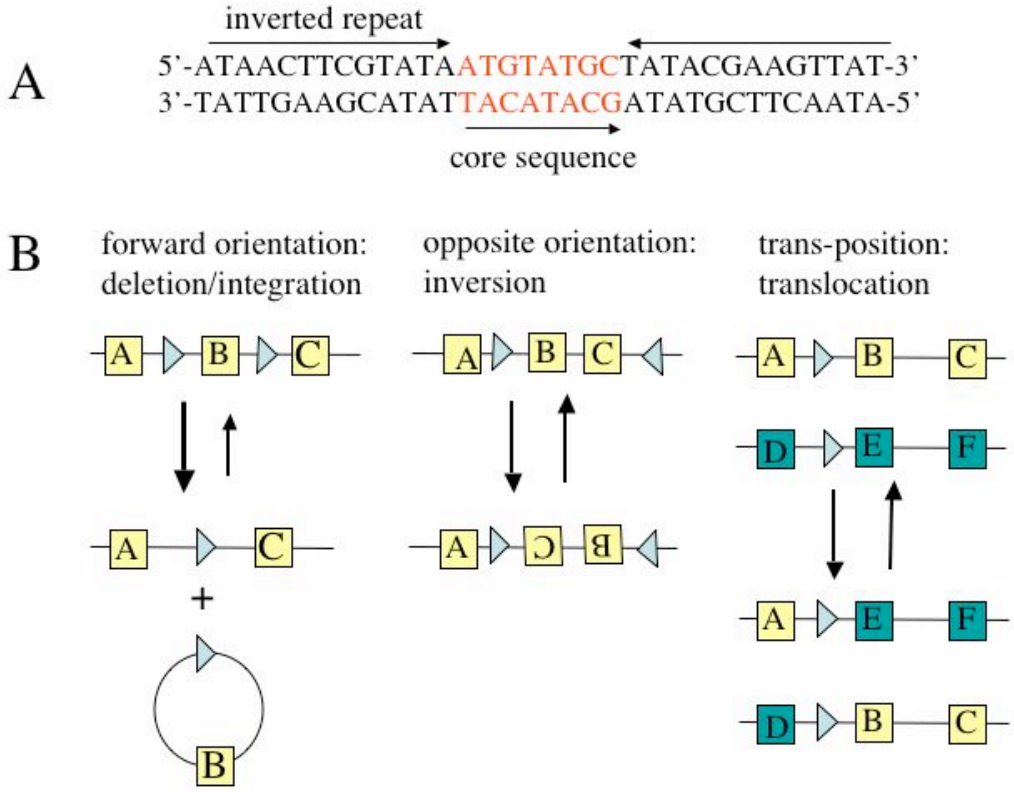

Fig. 2-1 Cre/*loxp* system. (A) *Loxp* contains two 13-bp inverted repeats and an 8-bp core sequence which defines the orientation of *loxp* site. (B) The Cre-mediated *loxp* recombinations can result in deletions/integrations or inversions when two *loxp* sites are aligned in *cis*, and translocations when two *loxp* sites are aligned *in trans*. Figure modified from (Kwan, 2002).

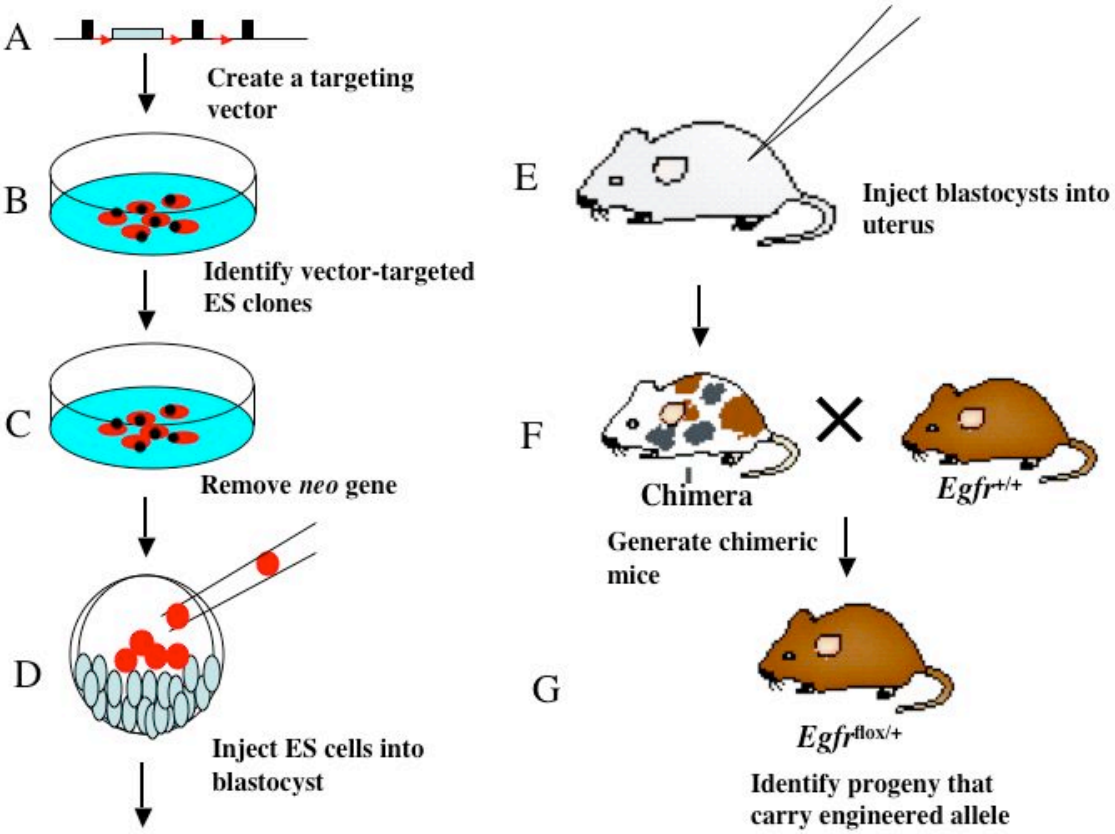

Fig. 2-2 Strategy for generating chimeras. (A) Creation of targeting vector. (B) Identification of targeted ES cell clones. (C) Removal of the *neo* cassette. (D) Injection of targeted ES cells into host blastocysts. (E) Transfer of blastocysts into uteri of surrogate dams. (F) Birth of chimeras. (E) Identification of progeny from chimeras carrying the engineered allele. Figure modified from (Yu and Bradley, 2001).

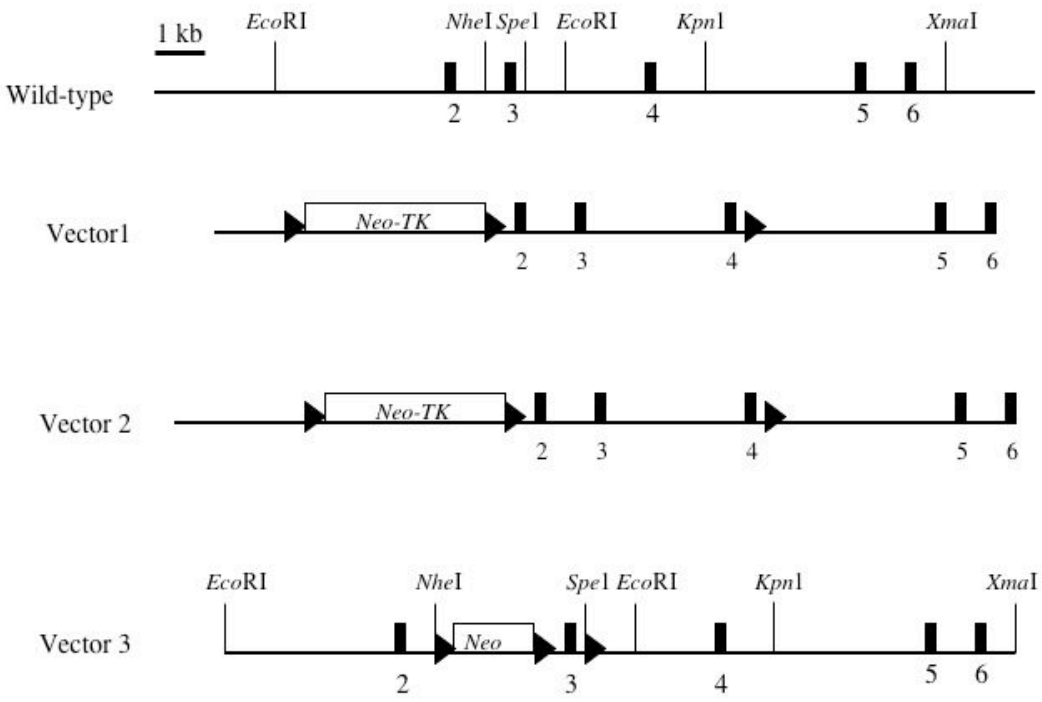

Fig. 2-3 Constructs for generating an *Egfr* conditional allele. The targeting efficiency was increased as the amount of homologous regions was increased and the amount of mismatch region was decreased.

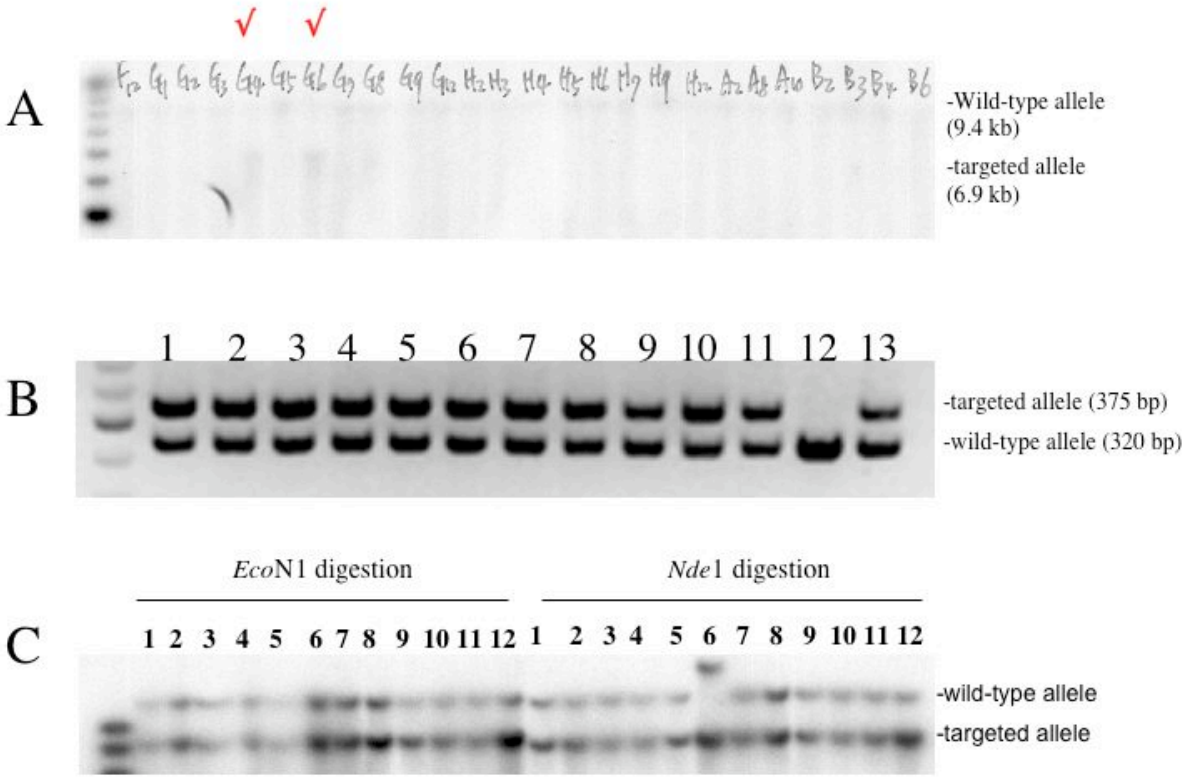

Fig. 2-4 Targeting efficiency of vector 3. (A) *Neo* resistant colonies analyzed by Southern blot for proper targeting (check-marked lanes have targeted clones). (B) One in 13 targeted clones lost the intronic *loxp* site (No. 12). (C) Verification of the remaining 12 targeted clones confirmed by Southern blot analysis with *Eco*N1 and *Nde*1 digestions. Note that No. 6 may have an extra insertion.

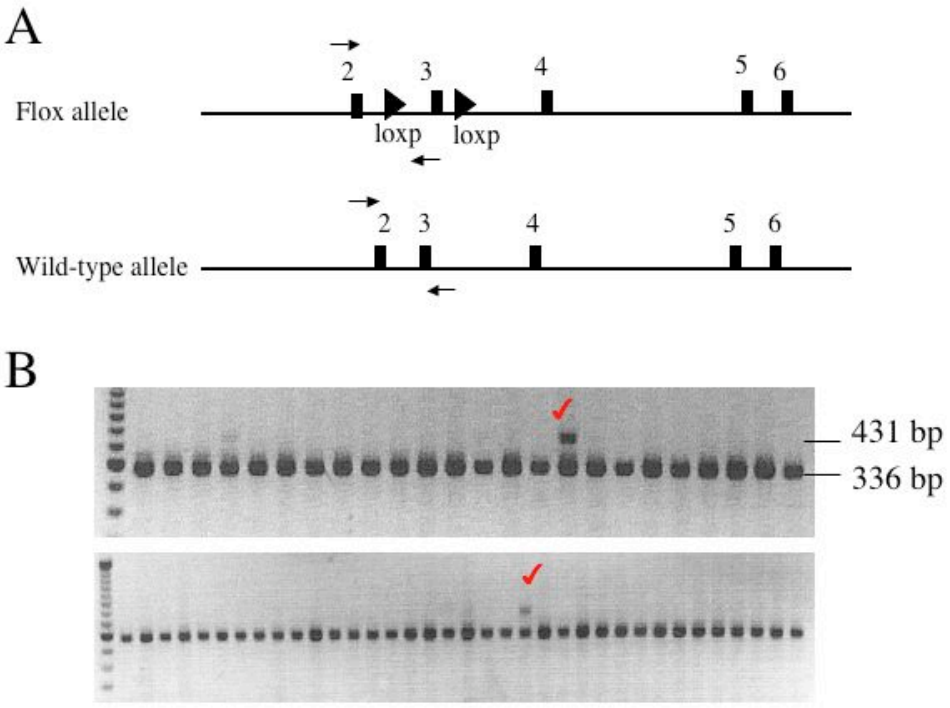

Fig. 2-5 Removal of the *neo* cassette by partial Cre-mediated *loxp* recombination. (A) Structure of floxed and wildtype alleles. The arrows indicate locations of the forward and reverse primers for PCR. (B) PCR results indicating the clones in which partial *loxp* recombination was correct (check-marks).

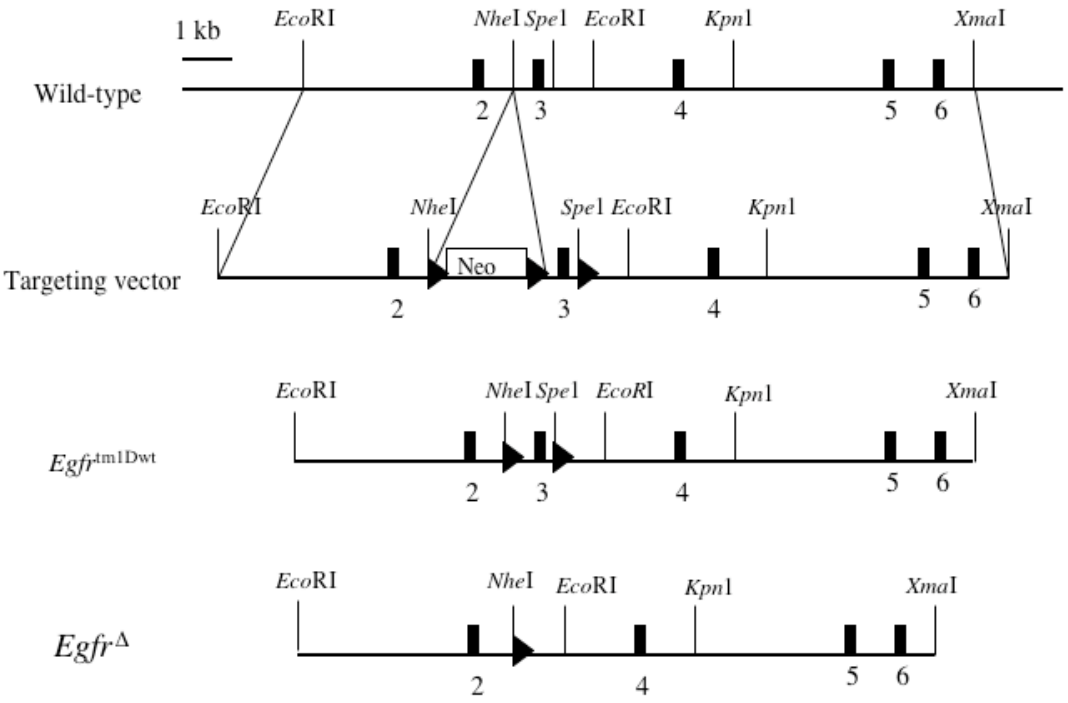

Fig. 2-6 Structure of wildtype and engineered *Egfr* alleles. The *Egfr*^{tm1Dwt} allele was generated by removing the *neo* cassette from the vector 3 allele in ES cells, while the *Egfr*$^{\Delta}$ allele can be created by deleting *loxp*-flanked exon 3 from the *Egfr*^{tm1Dwt} allele.

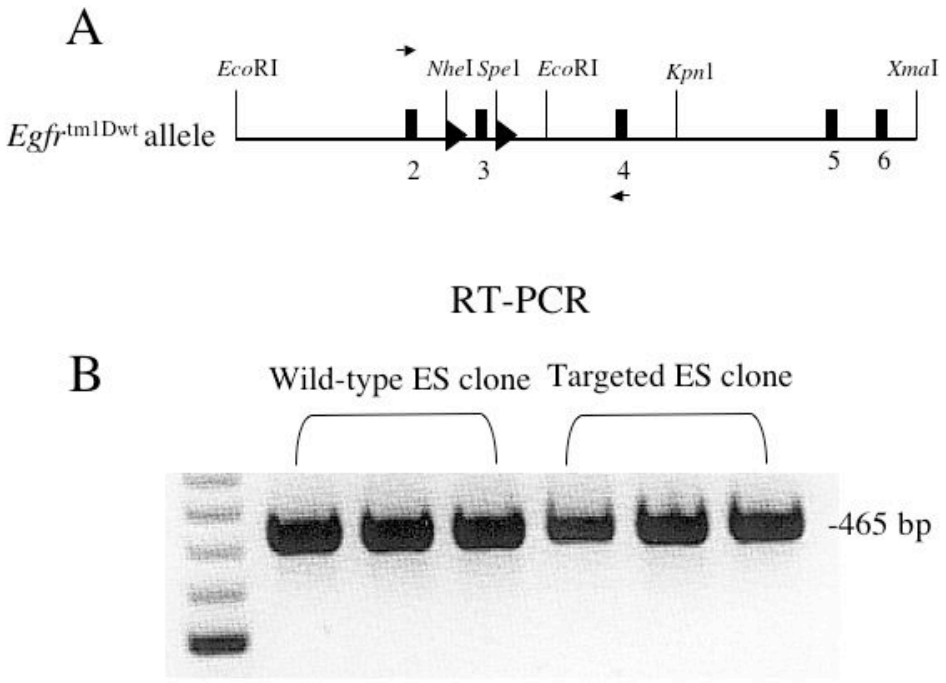

Fig. 2-7 Splicing from the *Egfr*^{tm1Dwt} allele. (A) The structure of the *Egfr*^{tm1Dwt} allele. Arrows indicate the location of forward and reverse primers in exons 2 and 4 for RT-PCR. (B) RT-PCR results from targeted ES clones was identical to that from wildtype clones.

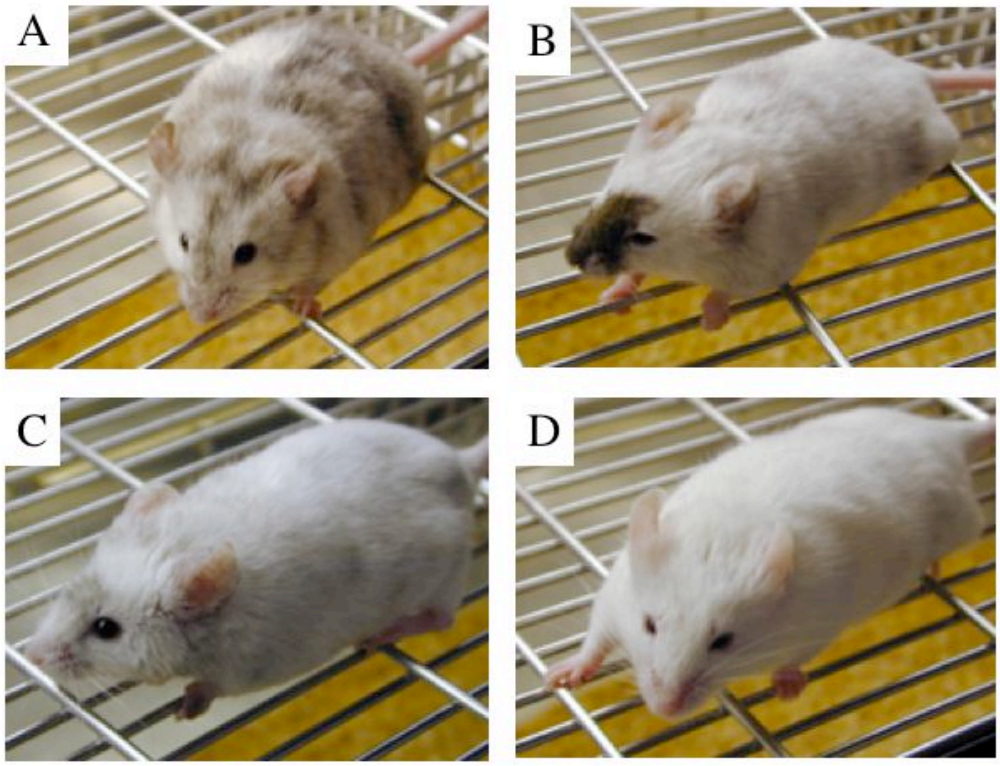

Fig. 2-8 Generation of chimeras. (A-D) Four chimeras with low coat color chimerism (estimated 5-30%) were generated using CD1 blastocysts as host embryos.

References

Abremski, K., and Hoess, R. (1984). Bacteriophage P1 site-specific recombination. Purification and properties of the Cre recombinase protein. J Biol Chem *259*, 1509-1514.

Crone, S.A., Zhao, Y.Y., Fan, L., Gu, Y., Minamisawa, S., Liu, Y., Peterson, K.L., Chen, J., Kahn, R., Condorelli, G.*, et al.* (2002). ErbB2 is essential in the prevention of dilated cardiomyopathy. Nat Med *8*, 459-465.

Fiering, S., Epner, E., Robinson, K., Zhuang, Y., Telling, A., Hu, M., Martin, D.I., Enver, T., Ley, T.J., and Groudine, M. (1995). Targeted deletion of 5'HS2 of the murine beta-globin LCR reveals that it is not essential for proper regulation of the beta-globin locus. Genes Dev *9*, 2203-2213.

Fitch, K.R., McGowan, K.A., van Raamsdonk, C.D., Fuchs, H., Lee, D., Puech, A., Herault, Y., Threadgill, D.W., Hrabe de Angelis, M., and Barsh, G.S. (2003). Genetics of dark skin in mice. Genes Dev *17*, 214-228.

Forsthoefel, P.F., Kanjananggulpan, P.B., and Harmon, S. (1983). Developmental interactions of cells mutant for Strong's luxoid gene with normal cells in chimeric mice. J Hered *74*, 153-162.

Garcia-Rivello, H., Taranda, J., Said, M., Cabeza-Meckert, P., Vila-Petroff, M., Scaglione, J., Ghio, S., Chen, J., Lai, C., Laguens, R.P.*, et al.* (2005). Dilated cardiomyopathy in Erb-b4-deficient ventricular muscle. Am J Physiol Heart Circ Physiol *289*, H1153-1160.

Garrett, T.P., McKern, N.M., Lou, M., Elleman, T.C., Adams, T.E., Lovrecz, G.O., Zhu, H.J., Walker, F., Frenkel, M.J., Hoyne, P.A.*, et al.* (2002). Crystal structure of a truncated epidermal growth factor receptor extracellular domain bound to transforming growth factor alpha. Cell *110*, 763-773.

Gassmann, M., Casagranda, F., Orioli, D., Simon, H., Lai, C., Klein, R., and Lemke, G. (1995). Aberrant neural and cardiac development in mice lacking the ErbB4 neuregulin receptor. Nature *378*, 390-394.

Ghosh, K., and Van Duyne, G.D. (2002). Cre-loxP biochemistry. Methods *28*, 374-383.

Koopman, P., Gubbay, J., Vivian, N., Goodfellow, P., and Lovell-Badge, R. (1991). Male development of chromosomally female mice transgenic for Sry. Nature *351*, 117-121.

Kwan, K.M. (2002). Conditional alleles in mice: practical considerations for tissue-specific knockouts. Genesis *32*, 49-62.

Lee, K.F., Simon, H., Chen, H., Bates, B., Hung, M.C., and Hauser, C. (1995). Requirement for neuregulin receptor erbB2 in neural and cardiac development. Nature *378*, 394-398.

Lewandoski, M. (2001). Conditional control of gene expression in the mouse. Nat Rev Genet *2*, 743-755.

Long, W., Wagner, K.U., Lloyd, K.C., Binart, N., Shillingford, J.M., Hennighausen, L., and Jones, F.E. (2003). Impaired differentiation and lactational failure of Erbb4-deficient mammary glands identify ERBB4 as an obligate mediator of STAT5. Development *130*, 5257-5268.

Meyers, E.N., Lewandoski, M., and Martin, G.R. (1998). An Fgf8 mutant allelic series generated by Cre- and Flp-mediated recombination. Nat Genet *18*, 136-141.

Miettinen, P.J., Berger, J.E., Meneses, J., Phung, Y., Pedersen, R.A., Werb, Z., and Derynck, R. (1995). Epithelial immaturity and multiorgan failure in mice lacking epidermal growth factor receptor. Nature *376*, 337-341.

Mystkowska, E.T., Ozdzenski, W., and Niemierko, A. (1979). Factors regulating the degree and extent of experimental chimaerism in the mouse. J Embryol Exp Morphol *51*, 217-225.

Nagy, A. (2000). Cre recombinase: the universal reagent for genome tailoring. Genesis *26*, 99-109.

Nagy, A., Moens, C., Ivanyi, E., Pawling, J., Gertsenstein, M., Hadjantonakis, A.K., Pirity, M., and Rossant, J. (1998). Dissecting the role of N-myc in development using a single targeting vector to generate a series of alleles. Curr Biol *8*, 661-664.

Qu, S., Rinehart, C., Wu, H.H., Wang, S.E., Carter, B., Xin, H., Kotlikoff, M., and Arteaga, C.L. (2006). Gene targeting of ErbB3 using a Cre-mediated unidirectional DNA inversion strategy. Genesis *44*, 477-486.

Reiter, J.L., Threadgill, D.W., Eley, G.D., Strunk, K.E., Danielsen, A.J., Sinclair, C.S., Pearsall, R.S., Green, P.J., Yee, D., Lampland, A.L.*, et al.* (2001). Comparative genomic sequence analysis and isolation of human and mouse alternative EGFR transcripts encoding truncated receptor isoforms. Genomics *71*, 1-20.

Riethmacher, D., Sonnenberg-Riethmacher, E., Brinkmann, V., Yamaai, T., Lewin, G.R., and Birchmeier, C. (1997). Severe neuropathies in mice with targeted mutations in the ErbB3 receptor. Nature *389*, 725-730.

Schwartzberg, P.L., Goff, S.P., and Robertson, E.J. (1989). Germ-line transmission of a c-abl mutation produced by targeted gene disruption in ES cells. Science *246*, 799-803.

Sibilia, M., and Wagner, E.F. (1995). Strain-dependent epithelial defects in mice lacking the EGF receptor. Science *269*, 234-238.

Threadgill, D.W., Dlugosz, A.A., Hansen, L.A., Tennenbaum, T., Lichti, U., Yee, D., LaMantia, C., Mourton, T., Herrup, K., Harris, R.C.*, et al.* (1995). Targeted disruption of

mouse EGF receptor: effect of genetic background on mutant phenotype. Science *269*, 230-234.

Yu, Y., and Bradley, A. (2001). Engineering chromosomal rearrangements in mice. Nat Rev Genet *2*, 780-790.

CHAPTER 3

CHARACTERIZATION OF *Egfr*^{tm1Dwt} AND *Egfr*$^{\Delta}$ ALLELES

Abstract

After the *Egfr* conditional knockout mouse model was generated, the *Egfr*^{tm1Dwt} and *Egfr*$^{\Delta}$ alleles were characterized. To determine whether the *Egfr*^{tm1Dwt} allele has wildtype activity, *Egfr*$^{tm1Dwt/+}$ mice were crossed with *Egfr*$^{tm1Mag/+}$ mice carrying a null allele to generate *Egfr*$^{tm1Dwt/tm1Mag}$ offspring as well as control littermates. All mice from this cross were viable, fertile and normal in appearance, indicating that the *Egfr*^{tm1Dwt} allele possesses wildtype activity. To prove that *Egfr*$^{\Delta}$ allele functions as a null allele, *Egfr*$^{\Delta/\Delta}$, *EIIa-Cre* mice were generated, which all died at mid-gestation and displayed moderate to severe placental defects with a reduced spongiotrophoblast layer and a disorganized architecture of the labyrinth layer that was identical to the phenotype reported for *Egfr* null mice. Thus, the *Egfr*$^{\Delta}$ allele functions as a null allele. In addition, to test if the *Egfr*^{tm1Dwt} allele can be inactivated tissue-specifically, *Egfr*$^{tm1Dwt/tm1Dwt}$, *K14-Cre* mice were produced. As expected, these mice were viable but exhibited wavy coat phenotype, highly similar to *Egfr*$^{wa2/wa2}$ mice, homozygous for a hypomorphic allele of *Egfr*. Overall, these results reveal that this new mouse model can be used to inactivate *Egfr* conditionally for functional analysis of EGFR in adult tissues.

Introduction

Egfr has been extensively studied to investigate its physiological role in many organs and tissues using mouse models with different *Egfr* alleles, including targeted, spontaneous, N-ethyl-N-nitrosourea (ENU)-mutated and transgenic alleles. Three targeted null mouse models ($Egfr^{tm1Mag}$, $Egfr^{tm1Wag}$ and $Egfr^{tm1Rdk}$) have been created, and depending on genetic background, die of placental defect at mid-gestation or perinatal stages. The placental defect includes a greatly reduced spongiotrophoblast layer and a disorganization of the labyrinth layer indicating that EGFR signaling is required for normal placental development. Phenotypes observed in *Egfr* null mice surviving to term include abnormalities of the skin and gastrointestinal tract, immature lungs, and cell death in the cortex and olfactory bulb (Miettinen et al., 1995; Sibilia and Wagner, 1995; Threadgill et al., 1995). *Egfr* null mice also have abnormal craniofacial development including defects in palate closure, elongated snouts, and underdeveloped lower jaws (Miettinen et al., 1999).

Another allele that has been frequently utilized for analysis of EGFR function is the $Egfr^{wa2}$ allele that has a spontaneously arising point mutation causing a Val743Gly substitution in the ATP-binding site of the tyrosine kinase domain. The receptor produced from the $Egfr^{wa2}$ allele has an 80-95% reduction in EGFR activity. Studies using $Egfr^{wa2}$ homozygous mice have shown an important role for EGFR signaling during anagen phase of the hair cycle (Mak and Chan, 2003); EGFR is normally localized to the outer root sheath of hair follicles (Luetteke et al., 1994). $Egfr^{wa2}$ homozygous dams display smaller mammary glands with lower milk production that causes increased mortality of their neonates (Fowler et al., 1995). $Egfr^{wa2}$ homozygous mice also exhibit enlarged aortic valves that are enhanced

by heterozygosity for a targeted mutantion in *Ptpn11*, which encodes the protein-tyrosine-phosphatase SHP2 (Chen et al., 2000).

There are two ENU-induced *Egfr* mutant alleles that have been reported, $Egfr^{Wa5}$ and $Egfr^{Dsk5}$. The $Egfr^{Wa5}$ allele is an antimorphic allele, also called a dominant-negative, containing a point mutation leading to an Asp833Gly substitution in a highly conserved DFG motif within the kinase domain. Mice heterozygous for *the* $Egfr^{Wa5}$ allele have open eyes and wavy coats similar to $Egfr^{wa2/wa2}$ mice, while $Egfr^{Wa5}$ homozygous embryos die at mid-gestation owing to placental defects that are similar to those of *Egfr* null embryos. In addition, the $Egfr^{Wa5}$ allele enhances the $Egfr^{wa2}$ hypomorphic phenotype in compound heterozygotes (Du et al., 2004; Lee et al., 2004). The other ENU-induced allele is the hypermorphic $Egfr^{Dsk5}$ allele that contains a missense mutation resulting in a Leu863Gln substitution lying within the tyrosine kinase domain; receptors produced by $Egfr^{Dsk5}$ have increased kinase activity. Mice heterozygous or homozygous for $Egfr^{Dsk5}$ display pigment accumulation and melanocytosis progressively with age, which is secondary to hyperkeratosis and epidermal thickening (Fitch et al., 2003).

A humanized allele, $Egfr^{KI}$ has also been created, containing a human *EGFR* cDNA that replaces the mouse *Egfr* allele. Mice homozygous for $Egfr^{KI}$ can live up to six months, but display growth retardation, hair follicle defects, increase in differentiated chondrocytes and osteoblasts in bone and heart hypertrophy with abnormal semilunar valves (Sibilia et al., 2003). Taken altogether, mice carrying different *Egfr* alleles have been proven to be important tools for analyzing EGFR functions *in vivo*, and have revealed a diversity of EGFR functions across multiple tissues. After generating an *Egfr* conditional knockout mouse

model, its activity was functionally characterized to show that the *Egfr*^{tm1Dwt} allele will be a useful tool for more detailed analyses of EGFR functions, especially in the adult mice.

Materials and methods

Mice and crosses

Egfr mutant mice used in these experiments include *Egfr*$^{tm1Dwt/+}$ (129 background), *Egfr*$^{tm1Dwt/tm1Dwt}$ (129,B6 mixed background) and *Egfr*$^{tm1Mag/+}$ (129 background) (chapter 2; Threadgill et al., 1995). *EIIa-Cre* (B6,FVB mixed background) transgenic mice were a gift from Dr. Mark Majesky (UNC), and *K14-Cre* (FVB background) transgenic mice were obtained from The Jackson Laboratory.

The activity of the *Egfr*^{tm1Dwt} allele was evaluated by crossing *Egfr*$^{tm1Dwt/+}$ mice with *Egfr*$^{tm1Mag/+}$ mice. *Egfr*$^{tm1Dwt/tm1Mag}$ and *Egfr*$^{tm1Mag/+}$ F1 mice were used as experimental and control groups, respectively. Body weights were measured and compared by gender.

To verify if *Egfr*$^{\Delta}$ allele is a null allele, *Egfr*$^{tm1Dwt/tm1Dwt}$ mice were crossed to *EIIa-Cre* mice to generate *Egfr*$^{\Delta/+}$, *EIIa-Cre* progeny. *Egfr*$^{\Delta/+}$, *EIIa-Cre* mice were then crossed with *Egfr*$^{tm1Dwt/tm1Dwt}$ mice to generate *Egfr*$^{\Delta/+}$, *EIIa-Cre and Egfr*$^{\Delta/\Delta}$, *EIIa-Cre* mice. The placentas at E12.5 were histologically examined.

To identify whether the *Egfr*^{tm1Dwt} allele functions as a tissue-specific conditional allele, *Egfr*$^{tm1Dwt/tm1Dwt}$ mice were crossed to *K14-Cre* mice to obtain *Egfr*$^{tm1Dwt/+}$, *K14-Cre* progeny, which were crossed to *Egfr*$^{tm1Dwt/tm1Dwt}$ mice to generate *Egfr*$^{tm1Dwt/tm1Dwt}$, *K14-Cre* and *Egfr*$^{tm1Dwt/+}$, *K14-Cre* offspring that were used as experimental and control groups, respectively. The coat phenotypes were examined by visual inspection.

Histological examination

Placentas from E12.5 embryos were isolated and fixed in 10% neutral buffered formalin solution (NBF) for 24 hours. After fixation, the samples were dehydrated using a graded alcohol series, 70% (1 hr), 85% (1 hr), 95% (1 hr), 100% (1 hr) and 100% (1 hr) alcohol followed by xylene twice (1 hr for each). Finally, the samples were infiltrated with paraffin at 60 °C twice (1 hr for each) before embedding and sectioning (7 μm). Sections were stained with hematoxylin and eosin and after mounting, examined under light microscopy.

PCR genotyping

Tail DNA samples were examined for the *Egfr*^{tm1Dwt} allele by amplifying for 35 cycles (30 s at 94°C, 1 min at 60°C and 1 min at 72°C) using Taq DNA polymerase (Qiagen) and a GeneAmp PCR system 9700 (Applied Biosystems). The primers were lox3s 5'-CTTTGGAGAACCTGCAGATC-3' and lox3as 5'-CTGCTACTGGCTCAAGTTTC-3'. A 375 bp PCR product was detected from the *Egfr*^{tm1Dwt} allele and a 320 bp PCR product from the wildtype allele. For *Egfr*$^{\Delta}$ allele, genomic DNA from embryos at E10.5 or E12.5 was amplified for 40 cycles (30 s at 94°C, 20 s at 60°C and 20 s at 72°C). The primers were Delta-3 5'-CTCAGCCAGATGATGTTGAC-3' and Delta-4 5'-CCTCGTCTGTGGAAGAACTA-3'. A 129 bp PCR fragment was amplified from the *Egfr*$^{\Delta}$ allele. The *Egfr* null allele, *Egfr*^{tm1Mag}, was detected by amplifying DNA for 40 cycles (30 s at 94°C, 30 s at 55°C and 1 min at 72°C). The primers were EGFR common 5'-GCCCTGCCTTTCCCACCATA-3' and EGFR knockout 5'-AACGTCGTGACTGGGAAAAC-3'. A 450 bp PCR product was detected from the *Egfr* null allele.

For *EIIa*- and *K14-Cre* transgenes, genomic DNA was amplified for 38 cycles (30 s at 94°C, 1 min at 56°C and 1 min at 72°C). The primers were CRE-1 5'-GTGATGAGGTTCGCAAGAAC-3' and CRE-2 5'-AGCATTGCTGTCACTTGGTC-3'. A 278 bp PCR fragment was amplified from the *Cre* transgenes.

Western blot analysis

E10.5 embryos and yolk sac with *Egfr*$^{+/\Delta}$, *EIIa-Cre* and *Egfr*$^{\Delta/\Delta}$, *EIIa-Cre* genotypes were homogenized with tissue lysis buffer at a ratio of 10 ml tissue lysis buffer/g of tissue. The tissue lysis buffer contained 20 mM HEPES, pH 7.4, 150 mM MaCl; 2 mM EDTA, pH 8.0, 2 mM ethylenebis(oxyethylenenitrilo) tetraacetic acid (EGTA), pH 8.0, 1% Triton X-100, and 10% glycerol adjusted to final pH 7.4 before adding protease inhibitors (1 mM phenyl sulfonyl fluoride [PMSF] in isopropanol, 10 μg/ml leupeptin and 10 μg/ml aprotinin) and phosphatase inhibitors (1 mM sodium orthovanadate [Na3VO4] and 1 mM NaF).

Twenty five micrograms of total protein from each sample in homogenized lysate was separated by sodium dodecyl sulfate polyacrylamide gel electrophoresis (SDS-PAGE), and then transferred to PVDF membrane. The membrane was placed in a blocking solution containing 5% milk in TBST (150 mM NaCl, 10 mM Tris-HCl, pH 8.0, 0.1% Tween-20), and probed with a primary antibody, sheep anti-EGFR polyclonal IgG (Upstate) in blocking solution (1:500) overnight. The membrane was then washed with TBST four times (15 min each), and incubated in blocking solution with second antibody, rabbit anti-sheep polyclonal IgG conjugated with horseradish peroxidase (HRP) (1:10000) for 1 hour. The membrane was washed with TBST four times again, incubated with enhanced chemiluminescent (ECL) substrate (Pierce) for 1-5 minutes and subjected to X-ray film photography. The amount of ß-tubulin in each sample was used as an internal control. The primary antibody for ß-tubulin

was mouse anti- ß-tubulin polyclonal IgG (1:1000), and the second antibody was goat anti-mouse polyclonal IgG with HRP conjugated (1:15000).

Statistical analysis

An unpaired t-test was used for all comparisons. The data was expressed as mean ± SEM.

Results

Egfr^{tm1Dwt} allele possesses wildtype function

To evaluate the activity of the *Egfr*^{tm1Dwt} allele, *Egfr*$^{tm1Dwt/+}$ mice were crossed to *Egfr*$^{tm1Mag/+}$ mice. Progeny with *Egfr*$^{tm1Dwt/tm1Mag}$ and *Egfr*$^{tm1Mag/+}$ genotypes were observed for abnormal phenotypes and their body weights were measured at two months of age. *Egfr*$^{tm1Dwt/tm1Mag}$ mice developed normally with a wildtype appearance, including their coat appearance, and also had wildtype fertility (Fig. 3-1). The average body weights of *Egfr*$^{tm1Dwt/tm1Mag}$ males (n=7) and females (n=5) were 22.07 ± 0.60 and 17.54 ± 0.92 g, respectively, while the average body weights of control *Egfr*$^{tm1Mag/+}$ males (n=6) and females (n=6) were 22.63 ± 1.02 and 17.78 ± 0.85 g, respectively. Statistically, there was no significant difference between genotypes (p = 0.63 and 0.85 for males and females) (Fig. 3-2). This result shows that the *Egfr*^{tm1Dwt} allele produces an EGFR with wildtype function.

Egfr$^{\Delta}$ allele is a null allele

The *Egfr*$^{\Delta}$ allele, predicted to act like a null allele, is produced after Cre-mediated recombination. To test this prediction, the *Egfr*$^{\Delta}$ allele was produced by crossing *Egfr*$^{tm1Dwt/tm1Dwt}$ mice with *EIIa-Cre* transgenic mice. The adenovirus *EIIa* promoter expresses *Cre* during preimplantation development, as early as the one-cell embryo stage

(Lakso et al., 1996). After intercrossing the progeny, placentas from *Egfr*$^{\Delta/\Delta}$, *EIIa-Cre* embryos were grossly smaller in size than those of wildtype littermates. Histological analysis showed that the spongiotrophoblast and labyrinth layers were affected. In the spongiotrophoblast layer, the numbers of spongiotrophoblast and glycogen cells were moderately to severely decreased, with few spongiotrophoblast cells remaining in some *Egfr*$^{\Delta/\Delta}$, *EIIa-Cre* placentas. The labyrinth layer in the mutant placentas had a disorganized architecture, which was also reduced in size (Fig. 3-3). Amorphous materials were commonly observed in the *Egfr* mutant placentas with aggregates of multiple nuclei, which have been reported in placentas from other gene knockouts (Parekh et al., 2004; Ware et al., 1995). Western blot analysis for EGFR revealed total loss of EGFR in placentas from *Egfr*$^{\Delta/\Delta}$, *EIIa-Cre* embryos at E10.5 (Fig.3-4). Taken together, these results are consistent with *Egfr*$^{\Delta}$ being a null allele (Sibilia and Wagner, 1995; Threadgill et al., 1995).

The *Egfr*^{tm1Dwt} allele can be inactivated tissue-specifically

To test whether the *Egfr*^{tm1Dwt} allele can be inactivated tissue-specifically, *Egfr*$^{tm1Dwt/tm1Dwt}$ mice were crossed to *K14-Cre* mice that express high levels of Cre recombinase activity in the developing skin at E14.5 (Dassule et al., 2000). *Egfr*$^{tm1Dwt/tm1Dwt}$, *K14-Cre* mice were obtained and were viable and fertile. However, unlike their wildtype littermates that had normal, straight coat hairs, *Egfr*$^{tm1Dwt/tm1Dwt}$, *K14-Cre* mice displayed wavy hair (Fig. 3-5), remarkably similar to the phenotype of *Egfr*$^{wa2/wa2}$ mice (Keeler; 1935; Luetteke et al., 1994; Miettinen et al., 1995; Sibilia and Wagner, 1995; Threadgill et al., 1995). This result indicates that the *Egfr*^{tm1Dwt} allele can be inactivated in a tissue specific pattern.

Discussion

Insertions of *loxp* sites have been considered to interfere with gene expression. Consequently, the *Egfr*^{tm1Dwt} allele was extensively characterized and shown to possess wildtype function. Although *in vitro* analysis using RT-PCR revealed that no alternative RNA splicing was detectable in targeted ES cells (Chapter 2, Fig. 2-7), further *in vivo* confirmation was performed. *Egfr*$^{tm1Dwt/tm1Mag}$ mice developed normally and were fertile indicating that the *Egfr*^{tm1Dwt} allele produces sufficient EGFR to function normally.

Inactivation of the *Egfr*^{tm1Dwt} allele by Cre recombinase at an early embryonic stage was used to generate *Egfr*$^{\Delta/\Delta}$, *EIIa-Cre* embryos, which displayed the same defective placental phenotype as reported previously for constitutional *Egfr* null alleles (Sibilia and Wagner, 1995; Threadgill et al., 1995). Placentas from *Egfr*$^{\Delta/\Delta}$, *EIIa-Cre* embryos had a greatly reduced spongiotrophoblast layer and an abnormal labyrinth architecture. The proper function of the *Egfr*^{tm1Dwt} allele was validated through tissue-specific generation of *Egfr*$^{\Delta/\Delta}$ in skin using *K14-Cre*. Overall, these results provide evidence to show that the *Egfr* conditional allele can be inactivated in a spatially and temporally controlled manner.

Although the results conclusively showed proper function for the *Egfr*^{tm1Dwt} allele, mutant mice from the same litter frequently had different levels of phenotypic severity. It is unclear whether this mosaicism is due to variable expression levels of Cre recombinase in individual mice, different accessibility of Cre recombinase to the conditional allele or for another unknown reason. Nonetheless, awareness potential mosaicism is important, especially when the conditional alleles code for proteins that act in a non-cell-autonomous manner such that a small fraction of wildtype cells may completely rescue a mutant phenotype (Kwan, 2002). However, for subtle phenotypes, a sufficient and constantly

expressed *Cre* transgene could be crucial for experimental success. Fortunately, for *Egfr*^{tm1Dwt}, the phenotypes were evident.

Despite the uncertainty, conditional knockout mouse models provide significant benefits. The major benefit is that genes can be inactivated spatially and temporally, overcoming the limitations caused by embryonic lethality of some constitutional knockout alleles. Since conditional alleles have been generated for all four *Erbb* genes (Crone et al., 2002; Long et al., 2003; Qu et al., 2006), it is now possible to create double mutations to enhance understanding of ERBB interaction.

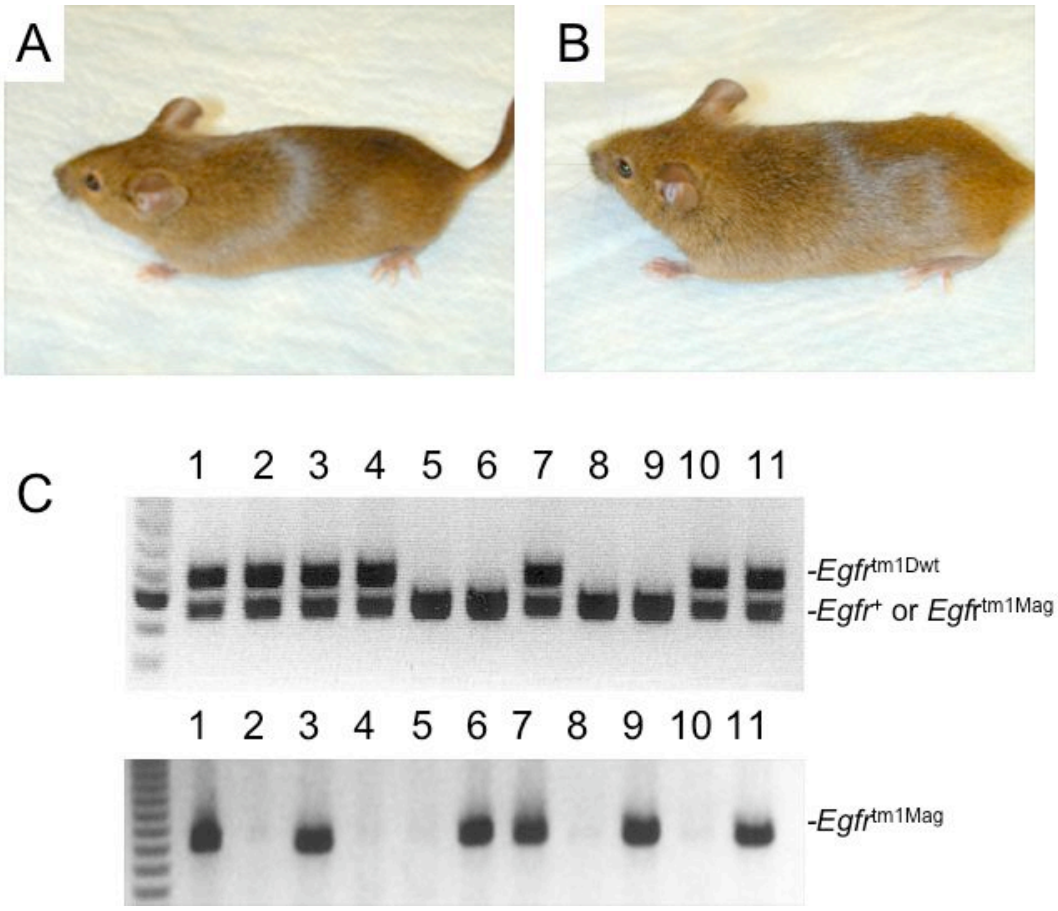

Fig. 3-1 Normal activity of the *Egfr*^{tm1Dwt} allele. (A) *Egfr*$^{tm1Mag/+}$ mouse. (B) *Egfr*$^{tm1Dwt/tm1Mag}$ mouse. (C) Genotypes of eleven mice. No. 1, 3, 7, and 11 are *Egfr*$^{tm1Dwt/tm1Mag}$ mice.

Fig. 3-2 Comparison of body weight between *Egfr*$^{tm1Dwt/tm1Mag}$ and *Egfr*$^{tm1Mag/+}$ mice (p=0.85 for females and 0.63 for males).

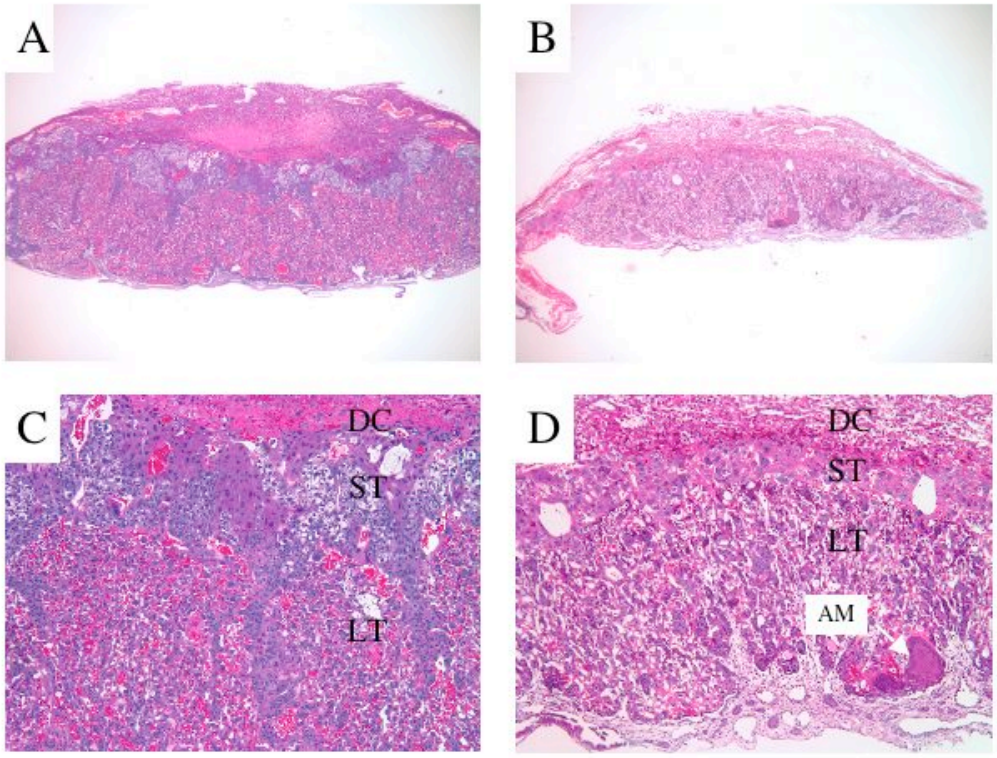

Fig. 3-3 Placental defect in *Egfr*$^{\Delta/\Delta}$, *EIIa-Cre* mice. (A) Wildtype placenta (30X, H&E stain). (B) *Egfr*$^{\Delta/\Delta}$, *EIIa-Cre* placenta, which is thinner and smaller than wildtype (30X, H&E stain). (C) Wildtype placenta at higher magnification (100X, H&E stain). (D) *Egfr*$^{\Delta/\Delta}$, *EIIa-Cre* placenta with reduced spogiotrophoblast layer and disorganized labyrinth layer. Amorphous material, indicated by white arrow, is common in mutant placentas (100X, H&E stain). DC, decidua; ST, spongiotrophoblast layer; LT, labyrinth layer.

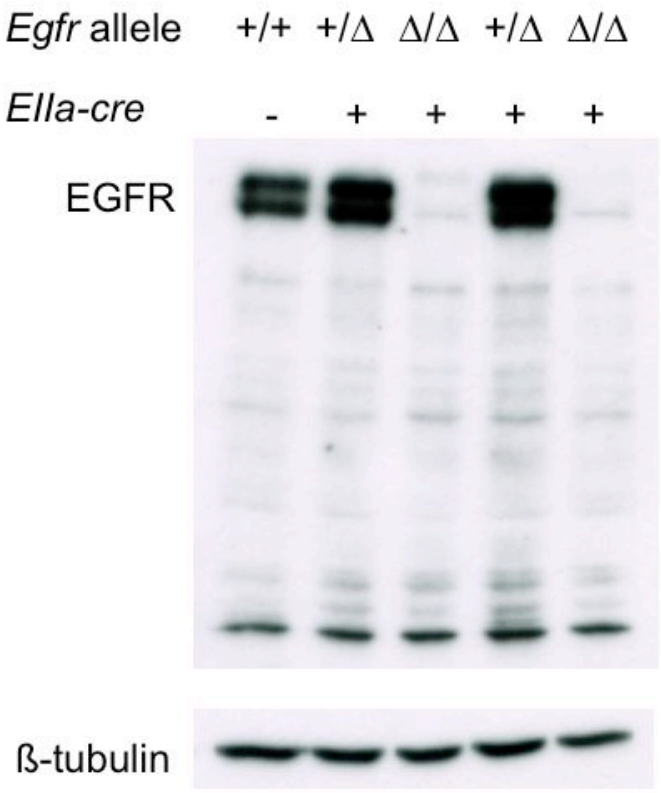

Fig. 3-4 Western blot analysis displaying loss of EGFR of protein in *Egfr*$^{\Delta/\Delta}$, *EIIa-Cre* embryos at E10.5.

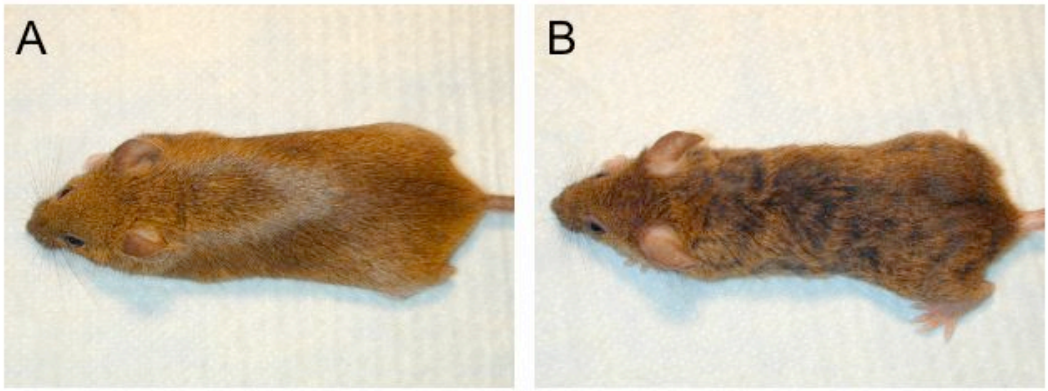

Fig. 3-5 Tissue-specific deletion of *Egfr*. (A) *Egfr*$^{tm1Dwt/+}$, *K14-cre* mouse (3 months old). (B) *Egfr*$^{tm1Dwt/tm1Dwt}$, *K14-cre* mouse (3 months old) displaying a wavy coat.

References

Chen, B., Bronson, R.T., Klaman, L.D., Hampton, T.G., Wang, J.F., Green, P.J., Magnuson, T., Douglas, P.S., Morgan, J.P., and Neel, B.G. (2000). Mice mutant for Egfr and Shp2 have defective cardiac semilunar valvulogenesis. Nat Genet *24*, 296-299.

Crone, S.A., Zhao, Y.Y., Fan, L., Gu, Y., Minamisawa, S., Liu, Y., Peterson, K.L., Chen, J., Kahn, R., Condorelli, G.*, et al.* (2002). ErbB2 is essential in the prevention of dilated cardiomyopathy. Nat Med *8*, 459-465.

Dassule, H.R., Lewis, P., Bei, M., Maas, R., and McMahon, A.P. (2000). Sonic hedgehog regulates growth and morphogenesis of the tooth. Development *127*, 4775-4785.

Du, X., Tabeta, K., Hoebe, K., Liu, H., Mann, N., Mudd, S., Crozat, K., Sovath, S., Gong, X., and Beutler, B. (2004). Velvet, a dominant Egfr mutation that causes wavy hair and defective eyelid development in mice. Genetics *166*, 331-340.

Fitch, K.R., McGowan, K.A., van Raamsdonk, C.D., Fuchs, H., Lee, D., Puech, A., Herault, Y., Threadgill, D.W., Hrabe de Angelis, M., and Barsh, G.S. (2003). Genetics of dark skin in mice. Genes Dev *17*, 214-228.

Fowler, K.J., Walker, F., Alexander, W., Hibbs, M.L., Nice, E.C., Bohmer, R.M., Mann, G.B., Thumwood, C., Maglitto, R., Danks, J.A.*, et al.* (1995). A mutation in the epidermal growth factor receptor in waved-2 mice has a profound effect on receptor biochemistry that results in impaired lactation. Proc Natl Acad Sci U S A *92*, 1465-1469.

Keeler, C.E. (1935). A second rexoid coat character in the house mouse. J Hered *26*, 189-191.

Kwan, K.M. (2002). Conditional alleles in mice: practical considerations for tissue-specific knockouts. Genesis *32*, 49-62.

Lakso, M., Pichel, J.G., Gorman, J.R., Sauer, B., Okamoto, Y., Lee, E., Alt, F.W., and Westphal, H. (1996). Efficient in vivo manipulation of mouse genomic sequences at the zygote stage. Proc Natl Acad Sci U S A *93*, 5860-5865.

Lee, D., Cross, S.H., Strunk, K.E., Morgan, J.E., Bailey, C.L., Jackson, I.J., and Threadgill, D.W. (2004). Wa5 is a novel ENU-induced antimorphic allele of the epidermal growth factor receptor. Mamm Genome *15*, 525-536.

Long, W., Wagner, K.U., Lloyd, K.C., Binart, N., Shillingford, J.M., Hennighausen, L., and Jones, F.E. (2003). Impaired differentiation and lactational failure of Erbb4-deficient mammary glands identify ERBB4 as an obligate mediator of STAT5. Development *130*, 5257-5268.

Luetteke, N.C., Phillips, H.K., Qiu, T.H., Copeland, N.G., Earp, H.S., Jenkins, N.A., and Lee, D.C. (1994). The mouse waved-2 phenotype results from a point mutation in the EGF receptor tyrosine kinase. Genes Dev *8*, 399-413.
Mak, K.K., and Chan, S.Y. (2003). Epidermal growth factor as a biologic switch in hair growth cycle. J Biol Chem *278*, 26120-26126.

Miettinen, P.J., Berger, J.E., Meneses, J., Phung, Y., Pedersen, R.A., Werb, Z., and Derynck, R. (1995). Epithelial immaturity and multiorgan failure in mice lacking epidermal growth factor receptor. Nature *376*, 337-341.

Miettinen, P.J., Chin, J.R., Shum, L., Slavkin, H.C., Shuler, C.F., Derynck, R., and Werb, Z. (1999). Epidermal growth factor receptor function is necessary for normal craniofacial development and palate closure. Nat Genet *22*, 69-73.

Parekh, V., McEwen, A., Barbour, V., Takahashi, Y., Rehg, J.E., Jane, S.M., and Cunningham, J.M. (2004). Defective extraembryonic angiogenesis in mice lacking LBP-1a, a member of the grainyhead family of transcription factors. Mol Cell Biol *24*, 7113-7129.

Qu, S., Rinehart, C., Wu, H.H., Wang, S.E., Carter, B., Xin, H., Kotlikoff, M., and Arteaga, C.L. (2006). Gene targeting of ErbB3 using a Cre-mediated unidirectional DNA inversion strategy. Genesis *44*, 477-486.

Sibilia, M., Wagner, B., Hoebertz, A., Elliott, C., Marino, S., Jochum, W., and Wagner, E.F. (2003). Mice humanised for the EGF receptor display hypomorphic phenotypes in skin, bone and heart. Development *130*, 4515-4525.

Sibilia, M., and Wagner, E.F. (1995). Strain-dependent epithelial defects in mice lacking the EGF receptor. Science *269*, 234-238.

Threadgill, D.W., Dlugosz, A.A., Hansen, L.A., Tennenbaum, T., Lichti, U., Yee, D., LaMantia, C., Mourton, T., Herrup, K., Harris, R.C.*, et al.* (1995). Targeted disruption of mouse EGF receptor: effect of genetic background on mutant phenotype. Science *269*, 230-234.

Ware, C.B., Horowitz, M.C., Renshaw, B.R., Hunt, J.S., Liggitt, D., Koblar, S.A., Gliniak, B.C., McKenna, H.J., Papayannopoulou, T., Thoma, B.*, et al.* (1995). Targeted disruption of the low-affinity leukemia inhibitory factor receptor gene causes placental, skeletal, neural and metabolic defects and results in perinatal death. Development *121*, 1283-1299.

CHAPTER 4

CHARACTERIZATION OF EGFR FUNCTION WITHIN THE BRAIN

Abstract

In order to analyze EGFR function within the brain and to investigate the underlying mechanism responsible for neurodegeneration of *Egfr* null mice, three *Cre* transgenic lines expressed in the embryonic epiblast (*Sox2-Cre*) or neuroprogenitor cells (*Nestin-Cre* and *hGFAP-Cre*) were crossed with mice carrying the $Egfr^{tm1Dwt}$ conditional allele to generate $Egfr^{tm1Dwt/tm1Dwt}$, *Sox2-Cre* (as well as *Nestin-Cre* or *hGFAP-Cre*) mice. $Egfr^{tm1Dwt/tm1Dwt}$ mice also carrying *Sox2-Cre* or *Nestin-Cre* displayed growth retardation and neurodegeneration in the cortex, olfactory bulb and areas surrounding lateral ventricle including corpus callosum, the fimbria of the hippocampus and subventricular zone (SVZ) and rostral extension (RE). These results were consistent with the phenotype of *Egfr* null mice. Conversely, $Egfr^{tm1Dwt/tm1Dwt}$, *hGFAP-Cre* mice showed no damage within the brain. At E18.5 there were no differences between body weights of $Egfr^{tm1Dwt/tm1Dwt}$ mice also carrying *Sox2-Cre*, *Nestin-Cre* or *hGFAP-Cre*, although $Egfr^{tm1Dwt/tm1Dwt}$, *Sox2-Cre* (or *Nestin-Cre)* showed postnatal growth defects. TUNEL analysis revealed that the neurodegeneration was caused by induction of apoptosis. *Nestin-Cre* and *hGFAP-Cre* mice were crossed with the ROSA26-*lacZ* reporter mice (*R26R*) to locate differences in the distribution of *Cre* expression in the

brain. Results indicated that the *hGFAP-Cre* line expresses Cre in the progenitors of the cortex, olfactory bulb, SVZ, RE and rostral migratory stream (RMS) but unlike *Nestin-Cre* not the choroid plexus, despite the lack of neurodegeneration in *Egfr*$^{tm1Dwt/tm1Dwt}$, *hGFAP-Cre* mice. These results suggest that neuronal or astrocytic death in the absence of EGFR signaling is a secondary effect, possibly mediated by the choroid plexus.

Introduction

EGFR is widely expressed in the central nervous system (CNS). *Egfr* transcripts are primarily restricted to the hindbrain at E13 but more broadly in the ventricular zone (VZ) and SVZ of forebrain at E17. *Egfr* is also expressed in the cortex, striatum, hippocampus and cerebellum of the developing and adult mouse brains (Fox and Kornblum, 2005). Compared with primary rat neuron culture, *Egfr* is highly expressed in astrocytes and oligodendrocytes (Mazzoni and Kenigsberg, 1994; Wang et al., 1989), implying the importance of EGFR signaling in development, function or survival of astrocytes and oligodendrocytes.

During postnatal development of the rat optic nerve, activation of EGFR directs astrocytes to form cribriform structures that group axons into bundles (Liu and Neufeld, 2004a, b). EGFR signaling is also required for the proliferation of both retinal progenitors and Muller glial cells, but *Egfr* expression declines when the retina matures (Close et al., 2006). Along with TGFA stimulation, overexpression of EGFR promotes retinal progenitor cells to differentiate into Muller glial cells rather than rod photoreceptors (Lillien, 1995), indicating that a balance in EGFR signal is essential for normal retinal development. Other studies have shown that after unilateral lysolecithin (LPC)-induced demyelination of the mouse corpus callosum, overexpression of EGFR enhances oligodendrocyte progenitor proliferation, increasing the number of oligodendrocytes distributed throughout the lesion, promoting axonal remyelination (Aguirre et al., 2007). Studies have also confirmed that neural stem cells from the developing or adult mouse germinal zones increase proliferation in response to EGFR activation (Ciccolini, 2001; Gritti et al., 1999; Reynolds et al., 1992; Tropepe et al., 1999). Additionally, the timing and level of EGFR expression in neural stem cells influence their migration properties and cell fate choices during cortical development

(Burrows et al., 1997). EGFR has been further demonstrated to promote cell migration in neural stem cells or other cell types in the developing telencephalon, possibly through HB-EGF, or other ligands serving as chemoattractant (Caric et al., 2001).

EGFR signaling appears to have opposing functions on neurite outgrowth. In some reports, EGFR signaling enhances neurite outgrowth induced by suppressor of cytokine signaling-2 (SOCS2) in the cortical neurons (Goldshmit et al., 2004); EGFR mediates the enhancement of neurite outgrowth and synaptic transmission by versican G3 domain in the embryonic hippocampal neurons (Xiang et al., 2006). Conversely, in other cases EGFR signaling displays inhibitory effect on neurite outgrowth. Calcium-dependent activation of EGFR mediates the inhibition of neurite outgrowth by myelin-associated inhibitors and chondroitin sulfate proteoglycans (CSPGs) (Koprivica et al., 2005); EGFR can be transactivated by binding fibrinogen to β3 integrin to mediate the inhibition of neurite outgrowth (Schachtrup et al., 2007).

Egfr null mice develop neurodegeneration exclusively in the cortex and olfactory bulb (Sibilia et al., 1998; Threadgill et al., 1995). In order to further understand how the loss of EGFR leads to neurodegeneration, an *Egfr* conditional allele (*Egfr*^{tm1Dwt}) was used to remove EGFR specifically in the brain.

Materials and methods

Mice and crosses

The conditional *Egfr*^{tm1Dwt} on a 129,B6 mixed background was previously described (Chapter 2). *Sox2-Cre* (B6,CBA mixed backgound), *Nestin-Cre* (B6,CBA mixed background), and

hGFAP-Cre (FVB/N background) mice were obtained from The Jackson Laboratory. The Rosa26 reporter (R26R) was a gift from Dr. Terry Van Dyke (University of North Carolina).

To analyze the requirement for EGFR in the brain, *Egfr*$^{tm1Dwt/tm1Dwt}$ mice were crossed with *Sox2-Cre*, *Nestin-Cre* or *hGFAP-Cre* mice to generate *Egfr*$^{tm1Dwt/+}$, *Sox2-Cre* (*Nestin-Cre* and *hGFAP-Cre*) F1 mice, which were then backcrossed to *Egfr*$^{tm1Dwt/tm1Dwt}$ mice to generate *Egfr*$^{tm1Dwt/tm1Dwt}$, *Sox2-Cre* (*Nestin-Cre* and *hGFAP-Cre*) and control littermates. In general, *Egfr*$^{tm1Dwt/tm1Dwt}$, *Sox2-Cre* (*Nestin-Cre* and *hGFAP-Cre*) experimental mice were compared with *Egfr*$^{tm1Dwt/+}$, *Sox2-Cre* (*Nestin-Cre* and *hGFAP-Cre*) control mice.

To locate differences in *Cre* expression between *Nestin-Cre* and *hGFAP-Cre*, crosses were performed with *R26R* reporter mice to generate *R26R, Nestin-Cre* and *R26R, hGFAP-Cre* mice.

PCR genotyping

The *Egfr*^{tm1Dwt} allele was amplified from genomic DNA for 35 cycles (30 s at 94°C, 1 min at 60°C and 1 min at 72°C) using Taq DNA polymerase (Qiagen) and a GeneAmp PCR system 9700 (Applied Biosystems). The primers were lox3s 5'-CTTTGGAGAACCTGCAGATC-3' and lox3as 5'-CTGCTACTGGCTCAAGTTTC-3'. A 375 bp PCR product was detected from the *Egfr*^{tm1Dwt} allele and a 320 bp PCR product from the wildtype allele. For the *Egfr*$^{\Delta}$ allele, genomic DNA was amplified for 40 cycles (30 s at 94°C, 20 s at 60°C and 20 s at 72°C). The primers were Delta-3 5'-CTCAGCCAGATGATGTTGAC-3' and Delta-4 5'-CCTCGTCTGTGGAAGAACTA-3'. A 129 bp PCR fragment was detected from the *Egfr*$^{\Delta}$ allele.

For the *Sox2-Cre* and *Nestin-Cre* transgenes, genomic DNA was amplified for 38 cycles (30 s at 94°C, 1 min at 56°C and 1 min at 72°C). The primers were cre-1 5'-

GTGATGAGGTTCGCAAGAAC-3' and CRE-2 5'-AGCATTGCTGTCACTTGGTC-3'. A 278 bp PCR fragment was amplified that corresponded to the *Cre* transgenes. For the *hGFAP-Cre* transgene, genomic DNA was amplified for 38 cycles (30 s at 94°C, 1 min at 51°C and 1 min at 72°C). The primers were MR1900 5'-ACTCCTTCATAAAGCCCT-3' and MR1901 5'-ATCACTCGTTGCATCGACC-3'. A 190 bp PCR fragment was amplified from the *hGFAP-Cre* transgene. For the *R26R* transgene, genomic DNA was amplified for 38 cycles (30 s at 94°C, 1 min at 60°C and 1 min at 72°C). The primers were Rosascom 5'-AAAGTCGCTCTGAGTTGTTAT-3' and Rosasneo 5'-GCGAAGAGTTTGTCCTCAACC-3'. A 300 bp PCR fragment was amplified from the *R26R* transgene.

Measurement of blood glucose

Mice at 24 days of age were fasted for 24 hours before taking blood glucose measurements. Blood glucose was measured from the tail using a Freestyle blood glucose monitoring system (TheraSense) and Freestyle flash test strips.

Histology

Mice were anesthetized by isoflurane (Abbott) and perfused with 4% paraformaldehyde. Mouse brains were collected and fixed in 4% paraformaldehyde for 24 hours before dehydrating through a 70% (1 hr), 85% (1 hr), 95% (1 hr) and 100% (2 x 1 hr) alcohol series. Samples were washed twice in xylene (1 hr for each), and then infiltrated in paraffin at 60 °C twice (1 hr each). Finally, the samples were embedded in paraffin and sectioned (7 μm) with a microtome (Leica). Sections were stained with hematoxylin and eosin and after mounting, examined by light microscopy.

TUNEL assay

TUNEL was performed using the ApopTag Plus Peroxidase *In Situ* Apoptosis Detection Kit (Chemicon) according the protocol provided by the manufacturer. The process included (1) deparaffinization of tissue sections with xylene, (2) pretreatment of tissues with proteinase K (20 μg/ml), (3) quenching of endogenous peroxidase with 3% hydrogen peroxide, (4) application of equilibration buffer, (5) application of working strength TdT enzyme, (6) application of stop/wash buffer, (7) application of anti-digoxigenin conjugate, (8) washing in PBS, (9) development of color in peroxidase substrate, (10) washing specimens, and (11) counterstaining the specimens with 0.5% methyl green.

Cryosectioning

R26R, Nestin-Cre and *R26R, hGFAP-Cre* mice at 6 weeks of age were anesthetized by isoflurane (Abbott) and perfused with cold PBS. Mouse brains were collected and fixed in 2% paraformaldehyde for 30 min. Brain samples were then infiltrated with 30% sucrose phosphate buffer at 4°C overnight before placing in the cryomolds, embedding with tissue freezing medium (OCT) and immersing in cold isopentane. The sample blocks were sectioned (10 μm) with a cryostat (Leica).

X-gal staining

Cryosections of brain samples were fixed with 2% paraformaldehyde on ice for 10 min, and washed in rinse buffer (2 mM $MgCl_2$, 1X PBS, pH 7.2) followed by detergent rinse buffer (2 mM $MgCl_2$, 0.02% Igepal CA630, 0.01% sodium deoxycholate, 1X PBS, pH 7.2) for 10 min each. X-gal staining solution (5 mM potassium ferricyanide, 5 mM potassium ferrocyanide, 0.1% X-gal [5-bromo-4-chloro-3-indolyl-β-D-galactopyranoside; Denville Scientific], 2 mM $MgCl_2$, 0.02% Igepal CA630, 0.01% sodium deoxycholate) was applied to the brain

cryosections and incubated at 37°C for 4-5 hours in a dark, humidified box. Cryosections were counterstained with 0.1X hematoxylin and 1X eosin Y.

Western blot analysis

Brains were collected from mice at 8 days of age, cut into two parts (the prosencephalon and the combined mesencephalon and rhombencephalon) and homogenized with tissue lysis buffer using a ratio of 10 ml tissue lysis buffer/g of tissue. The tissue lysis buffer contained 20 mM HEPES, pH 7.4, 150 mM MaCl; 2 mM EDTA, pH 8.0, 2 mM EGTA, pH 8.0, 1% Triton X-100, and 10% glycerol, adjusted to final pH 7.4; also added with protease inhibitors (1 mM phenyl sulfonyl fluoride [PMSF] in isopropanol, 10 µg/ml leupeptin and 10 µg/ml aprotinin) and phosphatase inhibitors (1 mM sodium orthovanadate [Na3VO4] and 1 mM NaF).

Forty micrograms of total protein from each sample were separated using SDS-PAGE, and then transferred to PVDF membrane. Subsequently, the membrane was blocked in 5% milk in TBST (150 mM NaCl, 10 mM Tris-HCl, pH 8.0, 0.1% Tween-20), and probed with primary antibody, sheep anti-EGFR polyclonal IgG (Upstate), in blocking solution (1:500) over night. The membrane was then washed with TBST four times (each time for 15 min), incubated with secondary antibody, rabbit anti-sheep polyclonal IgG conjugated with horseradish peroxidase (HRP) in blocking solution (1:10000) for 1 hour. The membrane was washed with TBST four times, incubated with enhanced chemiluminescent (ECL) substrate (Pierce) for 1-5 minutes, and subjected to X-ray film photography. An anti-ß-tubulin antibody was used as a loading control. The primary antibody was a mouse anti-ß-tubulin polyclonal IgG (1:1000), and the second antibody was a goat anti-mouse polyclonal IgG conjugated with HRP (1:15000).

Statistical analysis

The logrank test was used to analyze survival curves. For other experiments, an unpaired Student's t-test was used. The data was expressed as mean ± SEM, *p<0.05, **p<0.01, ***p<0.001.

Results

Three *Cre* lines, *Sox2-Cre*, *Nestin-Cre* and *hGFAP-Cre*, were used to analyze the function of EGFR in the mouse brain. *Sox2-Cre* is epiblast-specific (Hayashi et al., 2002), which should result in Cre-mediated deletion of $Egfr^{tm1Dwt}$ in all cells of the embryo properly, but not extraembryonic cells like those contributing to the placenta. *Nestin-Cre* expresses in neural stem cells (Betz et al., 1996; Tronche et al., 1999), which should result in Cre-mediated deletion of $Egfr^{tm1Dwt}$ in all cells of the adult brain. Similarly, the *hGFAP-Cre* line expresses Cre in neural stem cells before being extinguished and re-expressed in glial cells (astrocytes, oligodendrocytes and microglias) (Zhuo et al., 2001). Since it has been shown that *Sox2-Cre* female mice can transmit Cre activity via a maternal effect to their offspring irrespective of whether the *Cre* transgene is inherited (Hayashi et al., 2003), only male $Egfr^{tm1Dwt/+}$, *Sox2-Cre* mice were used as parents.

$Egfr^{tm1Dwt/tm1Dwt}$, *Sox2-Cre* (and *Nestin-Cre*) mice display postnatal lethality and growth retardation

$Egfr^{tm1Dwt/tm1Dwt}$, *Sox2-Cre* mice had open eyes at birth, curly whiskers and a wavy coat, and were much smaller than their littermates (Fig. 4-1A). The phenotype in the Sox2-Cre crosses was very similar to the *Egfr* null mice surviving past birth. Survival curve for

Egfr$^{tm1Dwt/tm1Dwt}$, *Sox2-Cre* mice was significantly different from those of the three control genotypes (logrank test, $p<0.0001$; Fig. 4-2A). Over 80% of *Egfr*$^{tm1Dwt/tm1Dwt}$, *Sox2-Cre* mice died within two weeks after birth (17/21). However, the remaining mice survived although they displayed classical *Egfr*-mediated hair phenotype. The most likely explanation for the variable survival of some *Egfr*$^{tm1Dwt/tm1Dwt}$, *Sox2-Cre* mice is mosaicism in Cre recombinase expression.

Egfr$^{tm1Dwt/tm1Dwt}$, *Nestin-Cre* mice were smaller in size compared with their littermates (Fig. 4-1B); and there was also a significant difference in the survival curves between *Egfr*$^{tm1Dwt/tm1Dwt}$, *Nestin-Cre* mice and the three control genotypes (logrank test, $p<0.0001$; Fig. 4-2B). Over 50% of *Egfr*$^{tm1Dwt/tm1Dwt}$, *Nestin-Cre* mice died within one month after birth (17/31), with the surviving mice having only mild defects including reduced growth (Fig. 4-3). Both *Egfr*$^{tm1Dwt/tm1Dwt}$, *Sox2-Cre* and *Nestin-cre* mice displayed dehydration and severe growth retardation or weight loss before death, although the phenotype of *Egfr*$^{tm1Dwt/tm1Dwt}$, *Sox2-Cre* mice was more severe than that of *Egfr*$^{tm1Dwt/tm1Dwt}$, *Nestin-Cre* mice. Since *Cre* is more widely expressed from the *Sox2* promoter than *Nestin*, the higher death rate of *Egfr*$^{tm1Dwt/tm1Dwt}$, *Sox2-Cre* mice may have been due to additional abnormalities of the skin and immature lungs (Sibilia and Wagner, 1995; Threadgill et al., 1995), which did not occur in *Egfr*$^{tm1Dwt/tm1Dwt}$, *Nestin-Cre* mice.

In contrast to mice from *Sox2-Cre* or *Nestin-Cre* crosses, *Egfr*$^{tm1Dwt/tm1Dwt}$, *hGFAP-Cre* mice did not display elevated levels of postnatal lethality, but did show wavy coats indicative of Cre expression in the skin (Fig. 4-1D). There was no significant difference in survival curves (Fig. 4-2C), although the average body weight of *Egfr*$^{tm1Dwt/tm1Dwt}$, *hGFAP-Cre* mice was less than that of their control littermates at 24 days of age (11.05 ± 0.64 vs

13.02 ± 0.56 g, $p<0.05$ in female; 11.50 ± 0.74 vs 14.18 ± 0.71 g, $p<0.05$ in male; Fig. 4-4A). Nonetheless, all groups reached a similar weight by two months of age (21.25 ± 0.58 vs 20.63 ± 0.64 g, $p=0.48$ in female; 26.86 ± 0.64 vs 28.37 ± 0.73 g, $p=0.14$ in male; Fig. 4-4B).

In order to determine when the growth retardation of *Egfr*$^{tm1Dwt/tm1Dwt}$, *Sox2-Cre* (*Nestin-Cre* and *hGFAP-Cre*) mice begins, body weights were measured at E18.5 (Fig. 4-5). No significant differences in body weight were detected between the genotypic groups, indicating that the growth retardation begins after birth. Surviving *Egfr*$^{tm1Dwt/tm1Dwt}$, *Nestin-Cre* mice also had much lower levels of blood sugar at 24 days after birth (65.5 ± 6.5 vs 117.5 ± 6.7 mg/dl, $p<0.001$ in female; 67.9 ± 8.4 vs 115.7 ± 6.8 mg/dl, $p<0.001$ in male; Fig. 4-6A), suggesting that neurodegeneration may affect feeding behavior or metabolism. *Egfr*$^{tm1Dwt/tm1Dwt}$, *hGFAP-Cre* mice also had significantly lower levels of blood sugar compared with their littermates (123.4 ± 4.3 vs 137.1 ± 3.8 mg/dl, $p<0.05$ in female; 122.8 ± 6.4 vs 140.1 ± 4.1 mg/dl, $p<0.05$ in male; Fig. 4-6B).

Egfr$^{tm1Dwt/tm1Dwt}$, _Sox2-Cre_ and _Nestin-Cre_ but not _hGFAP-Cre_ mice display neurodegeneration in the cortex, olfactory bulb and areas surrounding the lateral ventricle

Histology of the brains from *Egfr*$^{tm1Dwt/tm1Dwt}$, *Sox2-Cre*, (and *Nestin-Cre* and *hGFAP-Cre*) mice was compared to their control littermates. Grossly, the brains of *Egfr*$^{tm1Dwt/tm1Dwt}$, *Sox2-cre* (and *Nestin-Cre*) mice were smaller than those of their littermates. It was common to see bleeding in the cortex and olfactory bulb of *Egfr*$^{tm1Dwt/tm1Dwt}$, *Sox2-Cre* (and *Nestin-Cre*) mice. Histological analysis showed that significant cell death in the frontal areas of the cortex, caused the cortex to shrink or cavity formation (Fig. 4-7B and D). Apoptotic bodies

were found in the cortical cells indicating that the cells were dieing of apoptosis. Six layers of cortical plates were comparably complete, suggesting that cortical lamination was not affected. In the lateral ventricle of *Egfr*$^{tm1Dwt/tm1Dwt}$, *Sox2-Cre* (and *Nestin-Cre*) mice, the thickness of the corpus callosum was reduced, and the fimbria of the hippocampus was shrunk. Cell loss was apparent in the SVZ and RE, where neural stem cells reside. Cells surrounding the lateral ventricle of *Egfr*$^{tm1Dwt/tm1Dwt}$, *Sox2-Cre* (and *Nestin-Cre*) brains appeared to gradually die, making the lateral ventricle larger than that of control littermates (Fig. 4-8B and D).

In the olfactory bulb, hemorrhage usually occurred near the glomerular layer. The mitral cell layer in *Egfr*$^{tm1Dwt/tm1Dwt}$, *Sox2-Cre* (and *Nestin-Cre*) brains was greatly reduced or complete absent. Cell loss was also found in the granular cell layer of the olfactory bulb (Fig. 4-9B and D), the destination of the neural stem cell descendants from the SVZ that migrate through RMS while differentiating into granular interneurons (Lois et al., 1996). The cell loss in the granular cell layer of olfactory bulb may reflect damage in the SVZ and RE that caused fewer migrating cells along the RMS required to replenish cells in the granular cell layer. By contrast, brains from *Egfr*$^{tm1Dwt/tm1Dwt}$, *hGFAP-Cre* mice did not show any neurodegeneration in their cortex, lateral ventricle or olfactory bulb (Fig. 4-7F, 4-8F and 4-9F).

TUNEL analysis was performed to confirm that neurodegeneration was due to the induction of apoptosis. Sections of cortex and olfactory bulb from *Egfr*$^{tm1Dwt/tm1Dwt}$, *Nestin-Cre* brains had apoptotic cells lining of the areas of damage in the cortex and were also scattered throughout the olfactory bulb (Fig. 4-10B and D).

Because of the abnormality in the lateral ventricle of *Egfr*$^{tm1Dwt/tm1Dwt}$, *Sox2-Cre* (and *Nestin-Cre*) brains, it was speculated that there may also be damage or cell death in the

choroid plexus, which produces the cerebrospinal fluid (CSF). The choroid plexus from *Egfr*$^{tm1Dwt/tm1Dwt}$, *Sox2-Cre* (and *Nestin-Cre*) brains had a less well-organized villi structure. Some fibroblasts and collagen fibrils in the connective tissue of villi appeared reduced. The fenestrations of the endothelial cells of the capillaries in the connective tissue were not distinct. The choroid epithelial cells, which primarily secrete CSF and form a lining covering of villi, had less cytoplasm altering the normal cuboidal shape (Fig. 4-11B and D). However, the choroid plexus from *Egfr*$^{tm1Dwt/tm1Dwt}$, *hGFAP-Cre* brains did not display any morphological change when compared to that from control littermates (Fig. 4-11F).

Overlapping Cre expression from *Nestin-Cre* and *hGFAP-Cre* suggests neurodegeneration is a secondary effect

Since results showed that the neurodegeneration occured in the cortex, olfactory bulb, SVZ and RE from *Egfr*$^{tm1Dwt/tm1Dwt}$, *Sox2-Cre* (and *Nestin-Cre*) mouse brains, but not in the brains of *Egfr*$^{tm1dwt/tm1dwt}$, *hGFAP-Cre* mice, *Nestin-Cre* and *hGFAP-Cre* mice were crossed to the *R26R lacZ* reporter mice to locate differences in Cre expression driven by *Nestin* and *hGFAP* promoters. The reporter mice express lacZ only in the presence of Cre recombinase (Soriano, 1999). LacZ expression, as detected by X-gal staining, was throughout the entire brains of *R26R/Nestin-Cre* mice (Fig. 4-12B), confirming that Cre is expressed in neural stem cells when driven by the *Nestin* promoter. The *R26R/hGFAP-Cre* showed an equally extensive pattern of X-gal staining (Fig. 4-12B and C; 4-13A-D), which was consistent with a report suggesting that the *hGFAP-Cre* line expresses Cre not only in differentiated glial cells but also in neural progenitor cells (Zhuo et al., 2001). In the cerebellum of *R26R/hGFAP-Cre* mice, most cells were positive for X-gal staining except the Purkinje cells;

X-gal staining was also scattered throughout the septum, thalamus, hypothalamus, midbrain, pons, and medulla (Fig. 4-12C). In addition, cells residing in the SVZ and in the RMS stained positive for X-gal (Fig. 4-13F), despite the lack of histological signs of neurodegeneration in these areas from *Egfr*$^{tm1Dwt/tm1Dwt}$, *hGFAP-Cre* brains. One clear difference between Cre expression in *R26R/Nestin-Cre* and *R26R/hGFAP-Cre* brains was in the choroid plexus, which showed positive X-gal staining in the *R26R/Nestin-Cre* brains but negative in *R26R/hGFAP-Cre* brains (Fig. 4-13E and F).

Western blot analysis shows extensive loss of EGFR in *Egfr*$^{tm1Dwt/tm1Dwt}$, *Sox2-Cre* (*Nestin-Cre*, and *hGFAP-Cre*) brains

Western blot analysis was used to verify that the *Egfr*^{tm1Dwt} allele was converted to the *Egfr*$^{\Delta}$ alelle via Cre expression in the brains. The brains were separated into two parts, one containing the prosencephalon consisting of the cortex, olfactory bulb, septum, thalamus and hypothalamus and the other containing the mesencephalon and rhombencephalon consisting of the midbrain, cerebellum, pons and medulla. Both parts from brains of *Egfr*$^{tm1Dwt/tm1Dwt}$, *Sox2-Cre* (as well as *Nestin-Cre* and *hGFAP-Cre*) mice displayed complete loss of EGFR, indicating that the *Egfr*^{tm1Dwt} allele is disrupted efficiently by all the Cre transgenic lines (Fig. 4-14A-C).

Discussion

Egfr null mice develop neurodegeneration in the cortex and olfactory bulb and die before weaning, even after placental defects have been rescued. This result raises the question of what cell types are affected. To identify the underlying defects, *Egfr* conditional

knockout mice were crossed to three different *Cre* lines. *Egfr*$^{tm1Dwt/tm1Dwt}$, *Sox2-Cre* mice should have *Egfr* disrupted in the entire neonate, while *Egfr*$^{tm1Dwt/tm1Dwt}$, *Nestin-Cre* should result in *Egfr* disruption throughout the entire brain. *Egfr*$^{tm1Dwt/tm1Dwt}$, *hGFAP-Cre* mice should have a more restricted disruption of *Egfr,* being primarily restricted to glial lineages including astrocytes, oligodendrocytes and microglias as well as some neurons. The results demonstrated that *Egfr*$^{tm1Dwt/tm1Dwt}$ mice with *Sox2-Cre* or *Nestin-Cre*, but not *hGFAP-Cre,* have neurodegeneration in the cortex, olfactory bulb, and growth retardation consistent with those from *Egfr* null mice (Sibilia et al., 1998; Threadgill et al., 1995). Based on these results, the likely explanation is that EGFR has a direct impact on neuronal survival. However, it has been shown that *hGFAP-Cre* line not only expresses Cre in glial cells but also in precursor cells of the cerebral cortex (Zhuo et al., 2001), the most extensive site of neurodegeneration.

When *R26R* was used to identify differences between *Nestin-Cre* and *hGFAP-Cre*, a very similar Cre expression pattern was observed in the cortex and olfactory bulb (Fig. 4-12B and C; 4-13A-D) indicating that Cre was not only expressed in the astrocytes but also in the neurons by *hGFAP*. Confirming this result, western blot analysis showed extensive loss of EGFR in the cerebral cortex of *Egfr*$^{tm1Dwt/tm1Dwt}$, *Nestin-Cre* as well as *Egfr*$^{tm1Dwt/tm1Dwt}$, *hGFAP-Cre* mice. These results suggest that neurodegeneraton in the cortex and olfactory bulb of *Egfr* null mice is not a primary effect of EGFR loss in the dying cells.

Previous report has suggested that neurodegeneration in the cortex and olfactory bulb of *Egfr* null mice is due to the death of *Egfr* deficient cortical astrocytes (Wagner et al., 2006). An *in vitro* co-culture system was used to show that the increased neuronal death was caused by *Egfr* null cortical astrocytes that no longer provide enough neurotropic support for

neuronal survival, whereas *Egfr* null midbrain astrocytes are not affected and can support midbrain neuronal survival. Based on this conclusion, the neurodegenerative phenotype should have been evident in *Egfr*$^{tm1Dwt/tm1Dwt}$, *hGFAP-cre* mice since *Egfr* is disrupted in cortical astrocytes. However, *Egfr*$^{tm1Dwt/tm1Dwt}$, *hGFAP-Cre* mice did not show the neurodegenerative phenotype. Since *Cre* expression may be incompletely penetrant, raising the possibility that there may be enough astrocytes expressing *Egfr* to secrete sufficient neurotrophic factors to support neuronal survival. If this is the case, cell number should be reduced in the cortex and olfactory bulb. However, when compared to wildtype mice, no detectable reduction in cortical or olfactory bulb cell number was detected in *Egfr*$^{tm1Dwt/tm1Dwt}$, *hGFAP-Cre* mice. Furthermore, X-gal staining and western blot analysis did not support differential *Cre* expression in the cortex and olfactory bulb from *Egfr*$^{tm1Dwt/tm1Dwt}$ carrying *hGFAP-Cre* versus *Nestin-Cre*. Therefore, it is not likely that inefficient *Cre* expression leads to protection from the neurodegenerative phenotype in *Egfr*$^{tm1Dwt/tm1Dwt}$, *hGFAP-Cre* mice.

Abnormalities were also observed in the areas surrounding the lateral ventricle in the brains from *Egfr*$^{tm1Dwt/tm1Dwt}$, *Sox2-Cre* (and *Nestin-Cre*) mice including a reduced thickness of the corpus callosum, smaller fimbria of the hippocampus and cell loss in the SVZ and RE, thus enlarging the lateral ventricle compared with wildtype mice (Fig. 4-8A-D). The cells that reside in the SVZ are mostly astrocytes, which are also neural stem cells that develop into neuroblasts and migrate along RMS to the olfactory bulb, where they differentiate into granular and periglomerular interneurons (Doetsch et al., 1999; Garcia et al., 2004; Merkle et al., 2004). Because of damages in the SVZ and RE, it is not surprising that cell loss was observed in the granular layer of olfactory bulb in *Egfr*$^{tm1Dwt/tm1Dwt}$, *Sox2-Cre* (and *Nestin-*

Cre) mice (Fig. 4-9B and D). Although loss of EGFR caused neuronal or astroctic death in these areas, this must be secondary since similar cell death was not observed in *Egfr*$^{tm1Dwt/tm1Dwt}$, *hGFAP-Cre* mice (Fig. 4-8E and F); the data showed that those cells were positive for X-gal staining in *R26R/hGFAP* brains (Fig. 4-13F). If loss of EGFR causes neuronal death directly, *Egfr*$^{tm1Dwt/tm1Dwt}$, *hGFAP-Cre* mice should display damage in the olfactory bulb subsequent to the neural stem cells differentiating into interneurons. Similarly, if loss of EGFR directly causes astrocytic death, which in turn led to neuronal death, then damage in the SVZ should have been seen in the *Egfr*$^{tm1Dwt/tm1Dwt}$, *hGFAP-Cre* mice.

Based on results presented herein, it is unlikely that cell loss in the cortex, olfactory bulb and SVZ is a direct effect from loss of EGFR. Rather, the neurodegeneration occurring in *Egfr*$^{tm1Dwt/tm1Dwt}$, *Sox-Cre* (and *Nesin-Cre*) mice is a secondary effect. Additionally, since *Egfr*$^{tm1Dwt/tm1Dwt}$, *hGFAP-Cre* mice did not display neurodegeneration in any of the three areas primarily affected in the other *Cre* crosses, the neurodegeneration that does occur in the cortex, olfactory bulb and SVZ may result from a common primary event. One possibility that connects the three regions is the choroid plexus-cerebrospinal fluid (CP-CSF) system.

CSF is primarily produced by the choroid plexus (Speake et al., 2001), flowing through the ventricular system and into the subarachnoid space; it is eventually absorbed by the arachnoid villi and returned to venous circulation (Di Terlizzi and Platt, 2006). The CSF serves as a cushion to protect the brain. Other functions of CSF include protection of the brain during blood pressure fluctuation, regulation of the chemical environment of the CNS, nutrient transport and detoxification (Di Terlizzi and Platt, 2006; Emerich et al., 2005; Redzic and Segal, 2004). It is possible that the neurodegeneration occurring in *Egfr* null and *Egfr*$^{tm1Dwt/tm1Dwt}$, *Sox2-Cre* (and *Nestin-Cre*) mice is due to a decrease in secretion of

important neuronal surivival factors or neurotrophic factors into the CSF. A major clue pointing toward the choroid plexus is the fact that the choroid plexus in *R26R/Nestin-Cre* mice were positive for X-gal staining, while being negative in *R26R/hGFAP-Cre* mice (Fig. 4-13E and F). Additionally, the morphological changes in the choroid plexus epithelium in *Egfr*$^{tm1Dwt/tm1Dwt}$, *Sox2-Cre* (and *Nestin-Cre*) mice were not observed in *Egfr*$^{tm1Dwt/tm1Dwt}$, *hGFAP-Cre* mice (Fig. 4-11A-F). An abnormally functioning choroid plexus may lead to a reduced secretion of CSF and/or a decrease in the secretion of nutrients (e.g. glucose, amino acids), growth factors (e.g. insulin-like growth factor II, transforming growth factor β), and neurotrophic factors (e.g. nerve growth factor [NGF], neurotrophin-4 [NT-4]) (Redzic and Segal, 2004; Timmusk et al., 1995). Neurotrophic or growth factors secreted by the choroid plexus have been shown to have therapeutic potential. Neurite outgrowth from hippocampal neurons is promoted when co-cultured with choroid plexus ependymal cells (Kimura et al., 2004). Similarly, when the choroid plexus is grafted into the adult rat spinal cord, it can promote the growth of regenerating axons in the injured dorsal funiculus (Ide et al., 2001). Additionally, encapsulated choroid plexus from neonatal pigs transplanted into rat striatum can protect acetyltransferase (ChAT) positive neurons in a rat model of Huntington's disease (Borlongan et al., 2004).

An abnormal choroid plexus may also cause alteration of the chemical environment within the brain. A possible mechanism is through alteration of ionic concentrations, especially Na^+, Cl^-, K^+, and Ca^{2+}, leading to depolarization of neurons and an increased uptake of Ca^{2+}, which can induce neuronal apoptosis (Mattson, 2006; Mattson et al., 2001). Alternatively, impairment of the choroid plexus may increase metal-induced neurotoxicity and oxidative stress since one of the functions of the choroid plexus is detoxification. The

choroid plexus contains high concentrations of glutathione, cysteine, metallothionein and protective enzymes such as superoxide dismutase, glutathione-s-transferase, glutathione peroxidase and reductase to sequester heavy metals, metalloid ions such as mercury (Hg), Cadium (Cd), Arsenic (As) and free-radical oxidative stresses that are harmful to cells in the CNS (Emerich et al., 2005; Zheng, 2001). Growing evidence links the choroid plexus to neurodegenerative diseases (e.g. Alzheimer's and Huntington's diseases) (Emerich et al., 2005). More importantly, it has been reported that EGFR is expressed by the choroid plexus ependymal cells in the rat, and some ependymal cells are neural progenitor cells (Itokazu et al., 2006).

If neurodegeneration in *Egfr* null and *Egfr*$^{tm1Dwt/tm1Dwt}$, *Sox2-Cre* (and *Nestin-Cre*) mice is a secondary event, then EGFR signaling is not directly required for neuronal or astrocytic survival. However, the loss of EGFR may make neurons or astrocytes more sensitive to the alterations in the chemical environment, reduced concentration of growth factors or an increase in neurotoxins or oxidative stresses since one function of EGFR is to prevent apoptosis. Further studies into the changes in the CSF of *Egfr* null mice, such as measuring ion concentrations may provide insights to whether an abnormally functioning choroid plexus leads to neurodegeneration.

The data collected in this study suggests the possibility of secondary effect for the neurodegeneration that occur in *Egfr* null and *Egfr*$^{tm1Dwt/tm1Dwt}$, *Sox2-Cre* (and *Nestin-Cre*) mice. Elucidation of the mechanism responsible for the neurodegeneration induced by *Egfr*-deficiency will provide new insights into the role of EGFR in the brain.

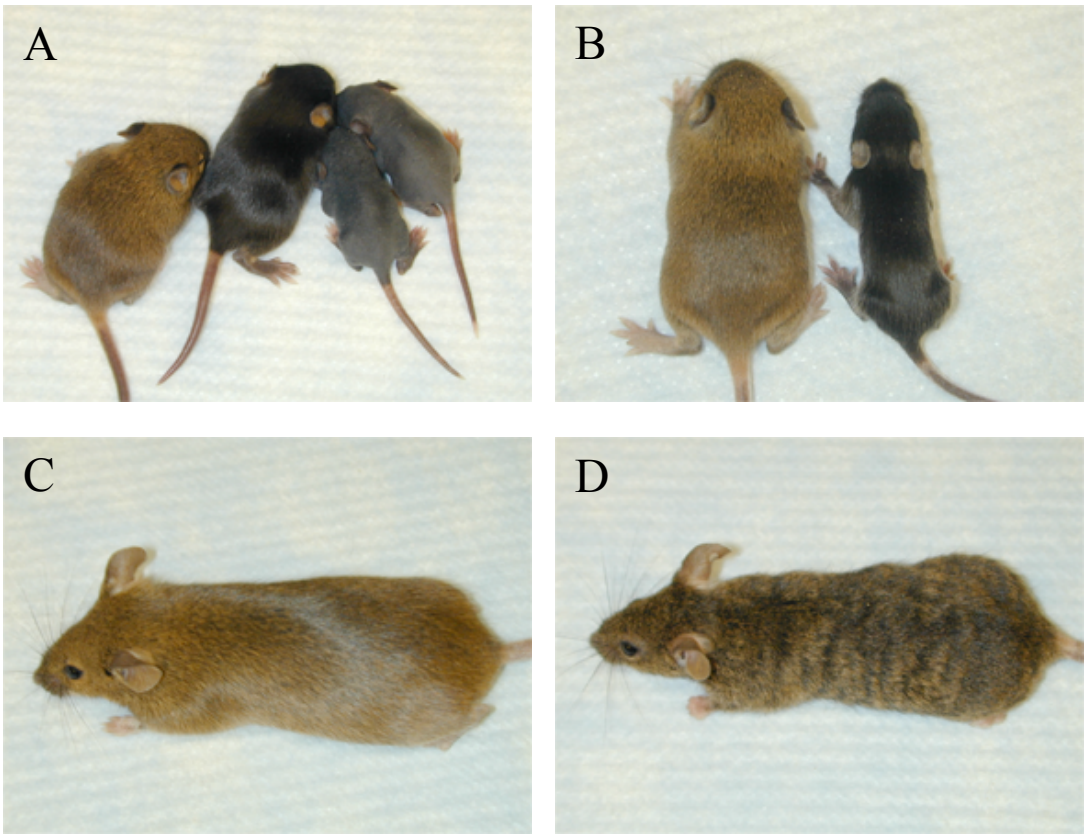

Fig. 4-1 Coat phenotypes of *Egfr* mutnat mice. (A) *Egfr*$^{tm1Dwt/tm1Dwt}$, *Sox2-Cre* mice (right two) displayed skin abnormalities and were smaller than their littermates. (B) *Egfr*$^{tm1Dwt/tm1Dwt}$, *Nestin-Cre* mouse (right) was smaller than its littermate. (C) Normal *Egfr*$^{tm1Dwt/+}$, *hGFAP-Cre* mouse. (D) *Egfr*$^{tm1Dwt/tm1Dwt}$, *hGFAP-Cre* mouse displaying a wavy coat.

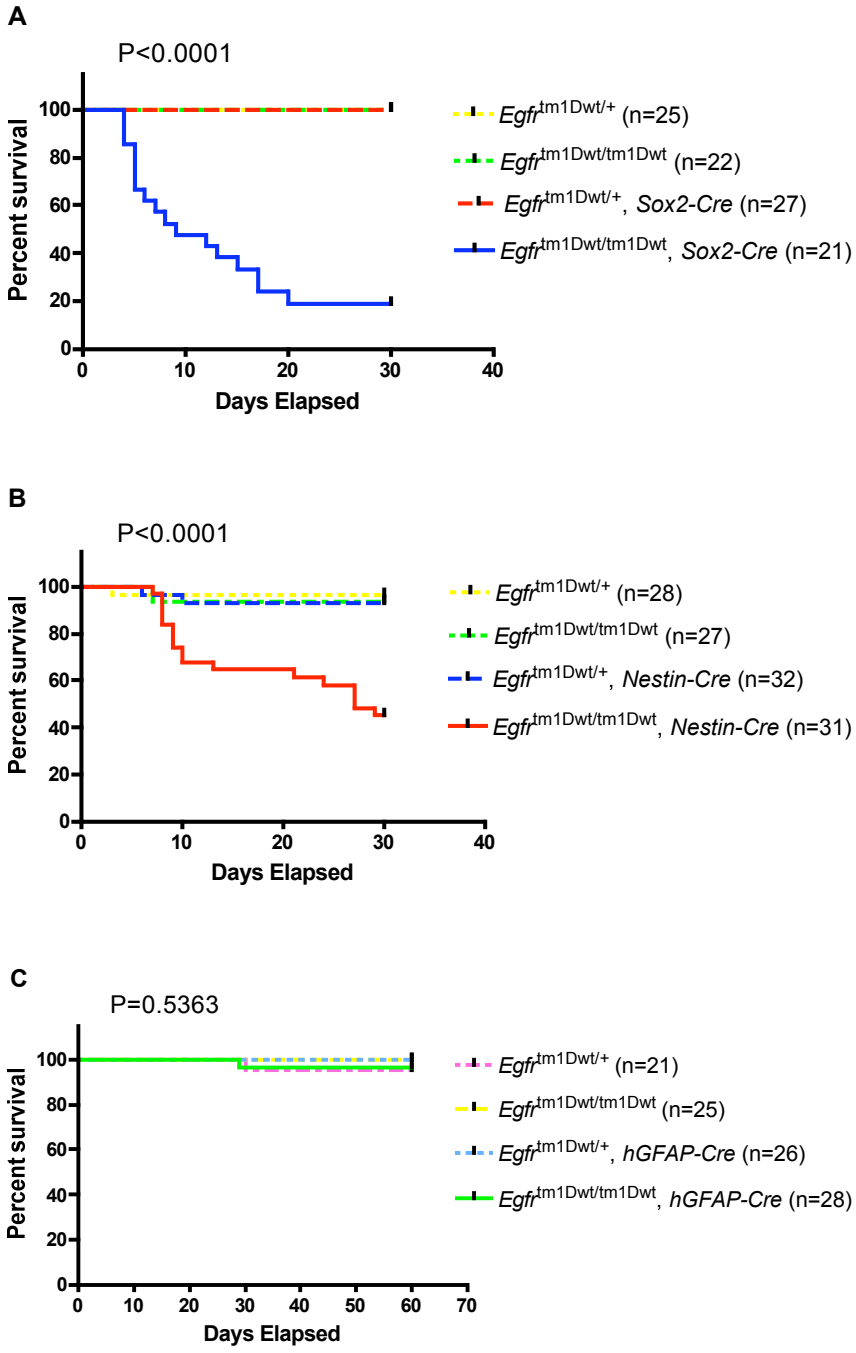

Fig. 4-2 Survival curves of *Egfr* mutant mice. (A) Survival of *Egfr*$^{tm1Dwt/tm1Dwt}$, *Sox2-Cre* mice was significantly lower than he control groups. (B) Survival of *Egfr*$^{tm1Dwt/tm1Dwt}$, *Nestin-Cre* mice was significantly lower than control groups. (C) No difference in survival between *Egf*$^{tm1Dwt/tm1Dwt}$, *hGFAP-Cre* mice and control groups.

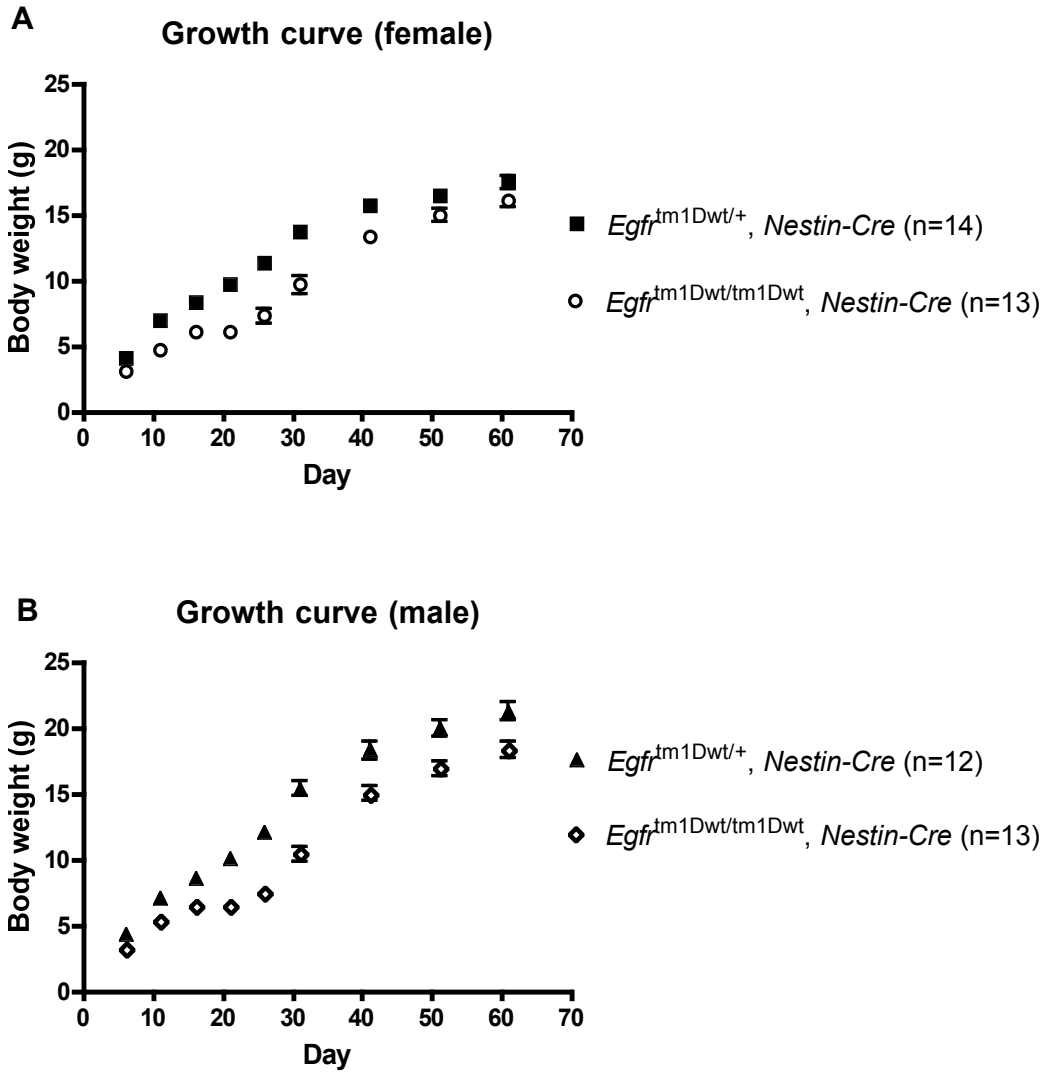

Fig. 4-3 Postnatal growth. (A and B) Female and male *Egfr*$^{tm1Dwt/tm1Dwt}$, *Nestin-Cre* mice display growth retardation compared to control groups.

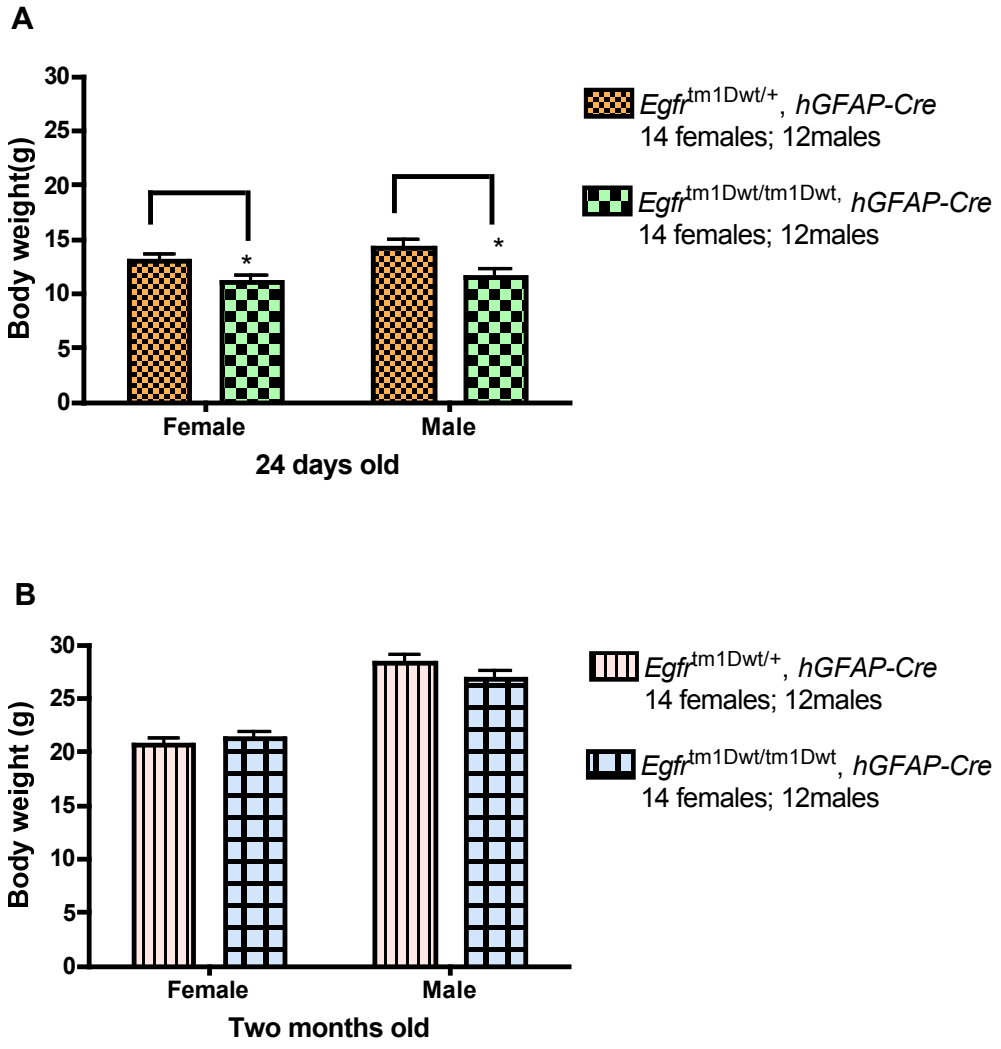

Fig. 4-4 Post-weaning body weights. (A) *Egfr*$^{tm1Dwt/tm1Dwt}$, *hGFAP-Cre* mice display growth retardation at weaning (11.05 ± 0.64 vs 13.02 ± 0.56 g, $p<0.05$ in female; 11.50 ± 0.74 vs 14.18 ± 0.71 g, $p<0.05$ in male). (B) Adult wildtype and *Egfr*$^{tm1Dwt/tm1Dwt}$, *hGFAP-Cre* mice have similar body weights at two months of age (21.25 ± 0.58 vs 20.63 ± 0.64 g, $p=0.48$ in female; 26.86 ± 0.64 vs 28.37 ± 0.73 g, $p=0.14$ in male).

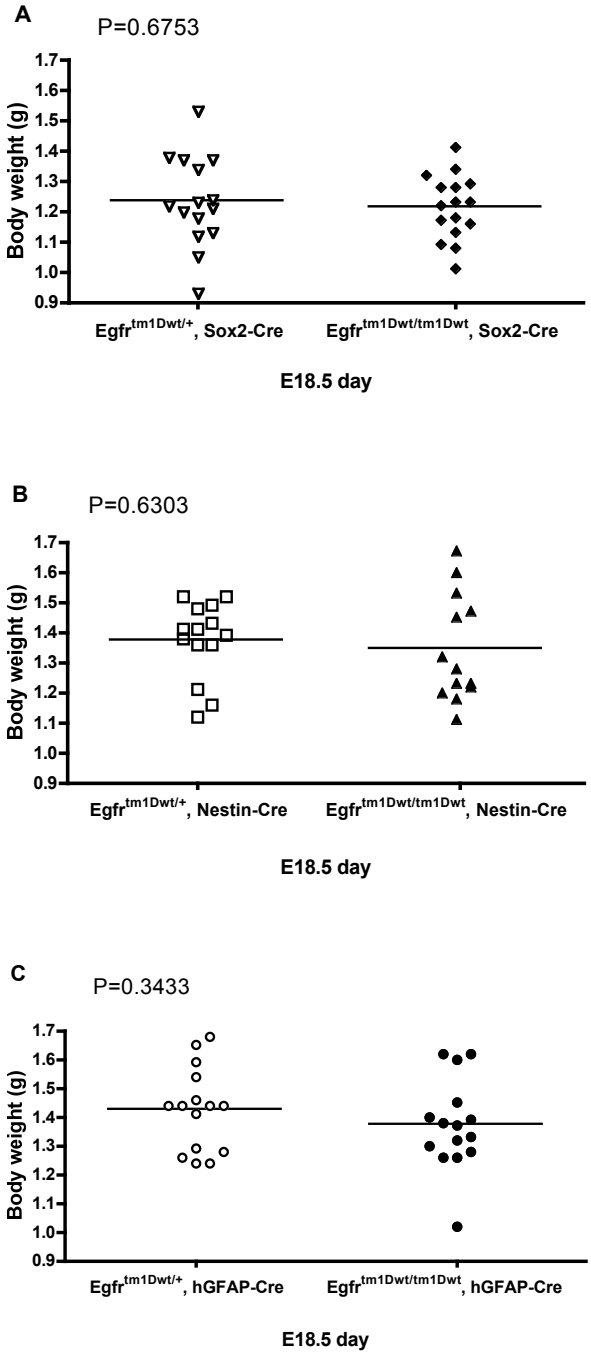

Fig. 4-5 Full-term body weights. (A-C) *Egfr*$^{tm1Dwt/tm1Dwt}$, *Sox-Cre* (*Nestin-Cre* and *hGFAP-Cre*) embryos at E18.5 display no differences in body weight compared with their control groups.

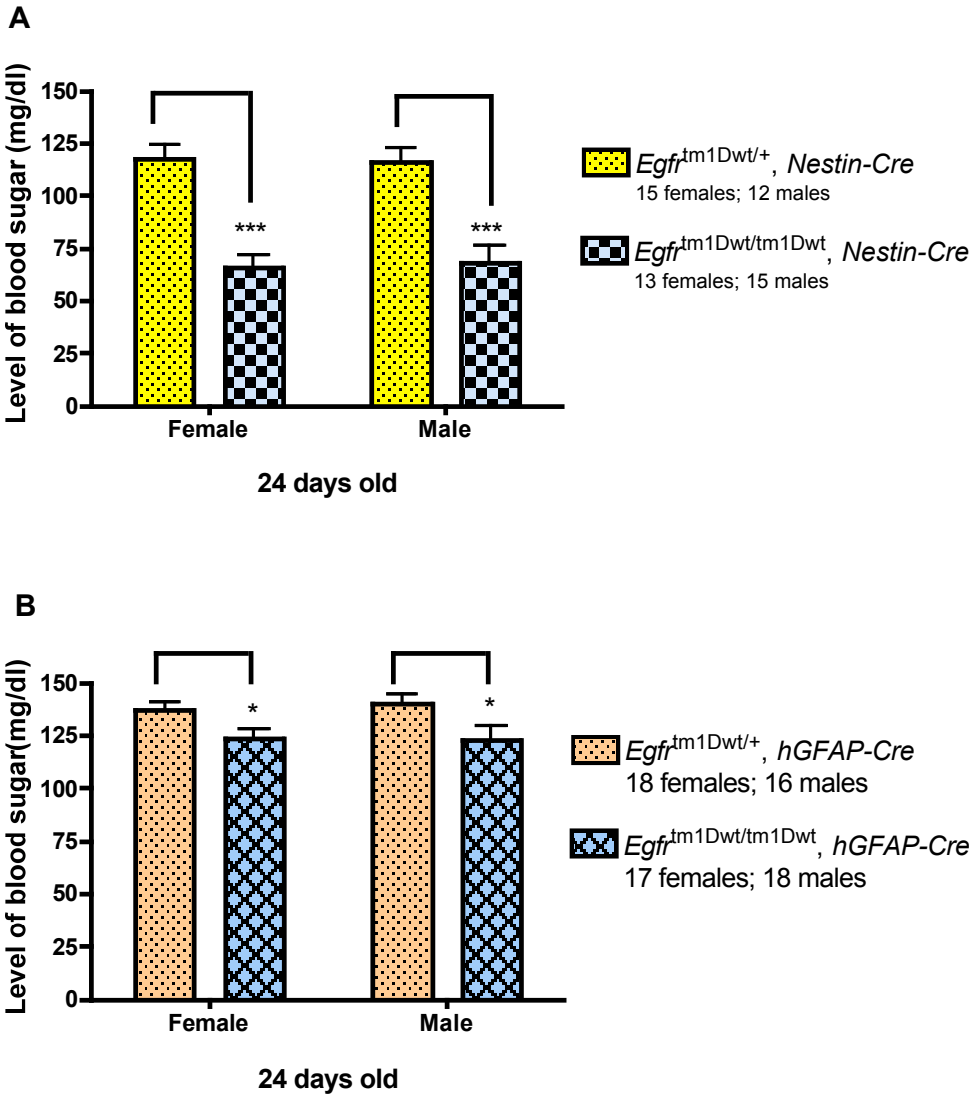

Fig. 4-6 Blood sugar levels. (A) *Egfr*$^{tm1Dwt/tm1Dwt}$, *Nestin-Cre* mice have lower blood sugar levels than their controls (65.5 ± 6.5 vs 117.5 ± 6.7 mg/dl, $p<0.001$ in female; 67.9 ± 8.4 vs 115.7 ± 6.8 mg/dl, $p<0.001$ in male). (B) *Egfr*$^{tm1Dwt/tm1Dwt}$, *hGFAP-Cre* mice have lower blood sugar levels than their controls (123.4 ± 4.3 vs 137 ± 3.8 mg/dl, $p<0.05$ in female; 122.8 ± 6.4 vs 140.1 ± 4.1 mg/dl, $p<0.05$ in male).

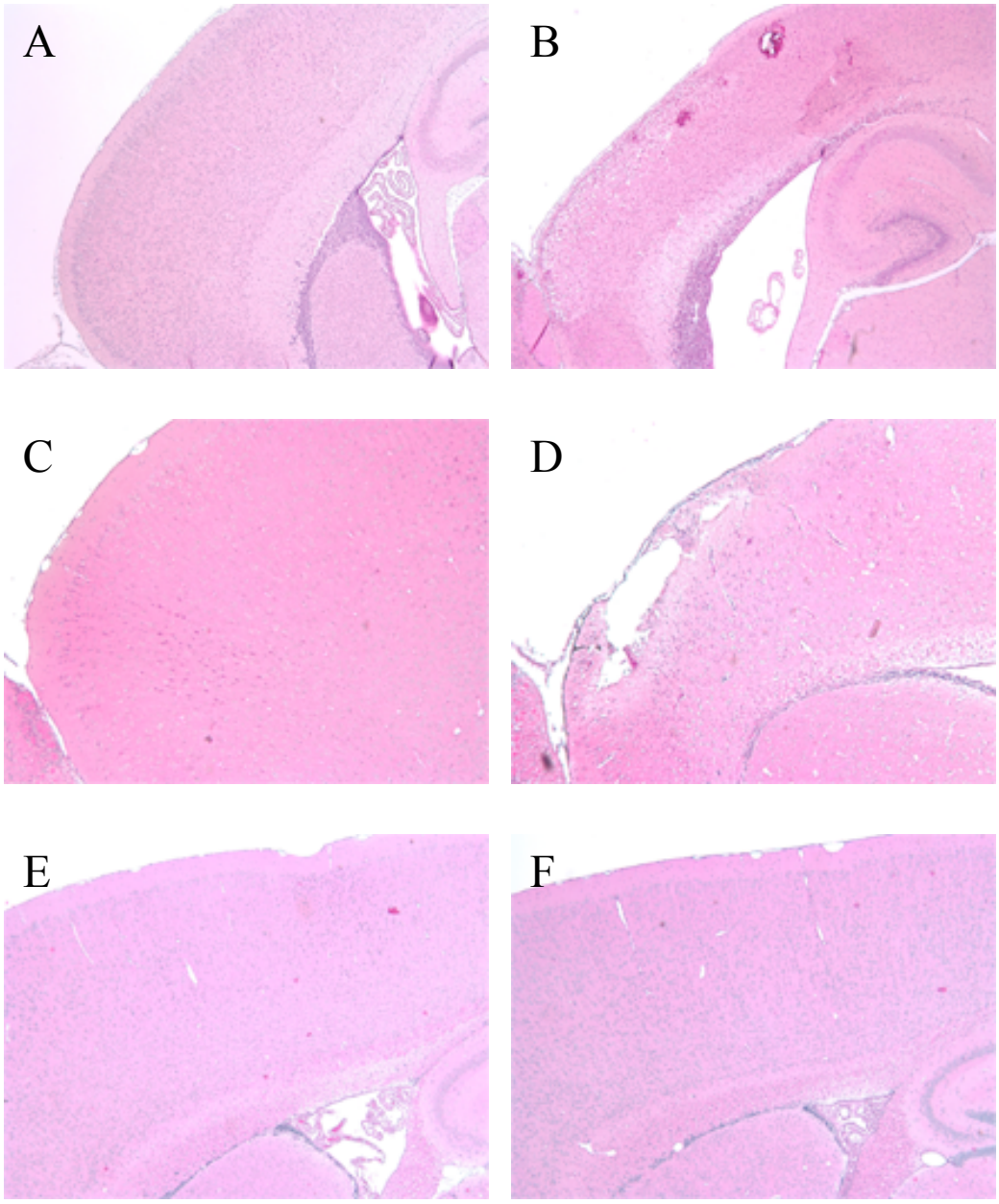

Fig. 4-7 Cortical histology. (A) Normal *Egfr*$^{tm1Dwt/+}$, *Sox2-Cre* cortex (P8). (B) Smaller *Egfr*$^{tm1Dwt/tm1Dwt}$, *Sox2-Cre* cortex with apoptotic cells and bleeding (P8). (C) Normal *Egfr*$^{tm1Dwt/+}$, *Nestin-Cre* cortex (P23). (D) Degenerative *Egfr*$^{tm1Dwt/tm1Dwt}$, *Nestin-Cre* cortex forming a cavity (P23). (E) Normal *Egfr*$^{tm1Dwt/+}$, *hGFAP-Cre* cortex (1M). (F) Normal *Egfr*$^{tm1Dwt/tm1Dwt}$, *hGFAP-Cre* cortex (1M). A-F, H&E stains, 50X

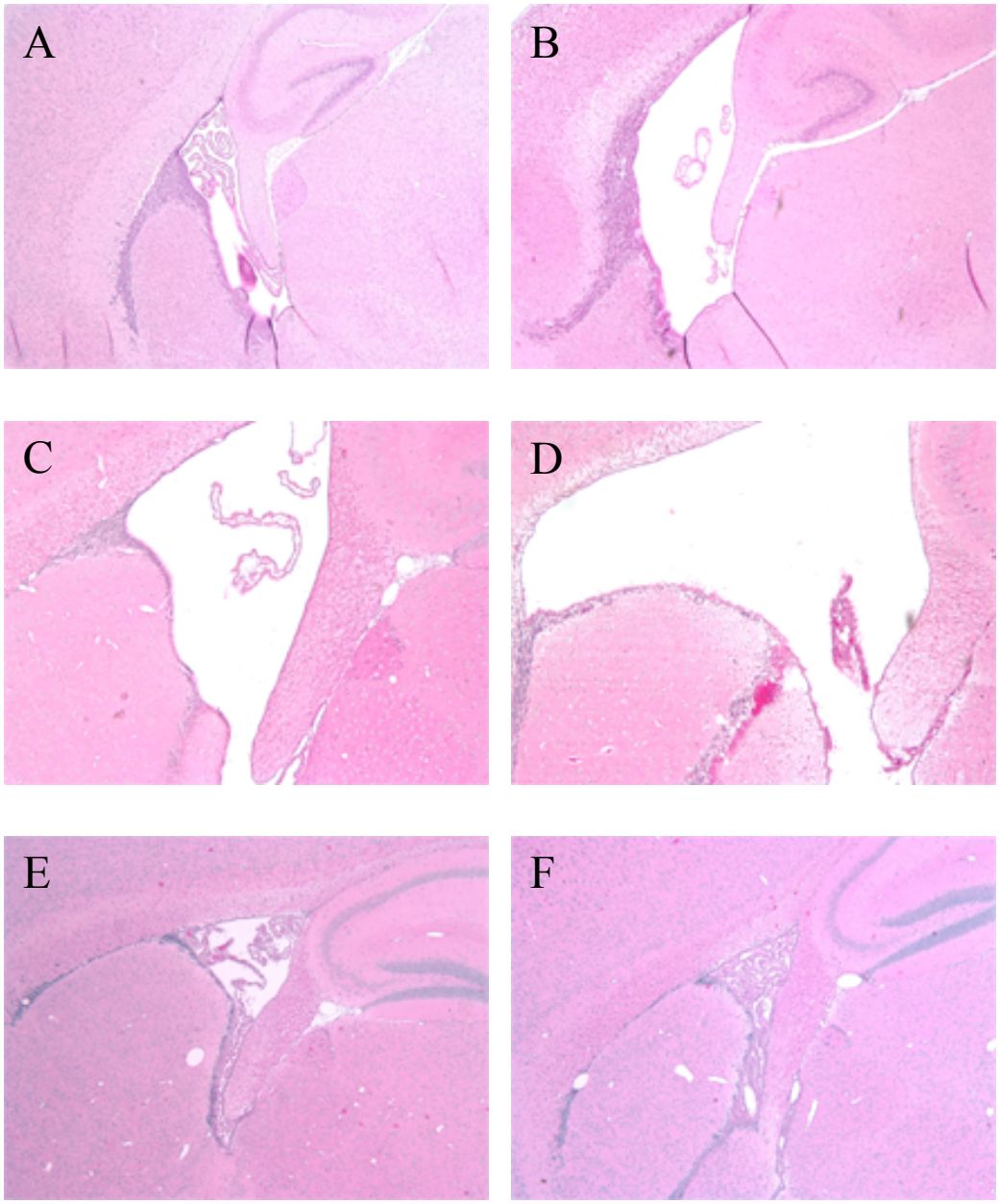

Fig. 4-8 Ventricular histology. (A) Normal phenotype in the areas surrounding the lateral ventricle of *Egfr*$^{tm1Dwt/+}$, *Sox2-Cre* brain (P8). (B) *Egfr*$^{tm1Dwt/tm1Dwt}$, *Sox2-Cre* brain displayed neurodegeneration with reduced thickness of corpus callosum, reduced fimbria of hippocampus, and cell loss in the SVZ and RE (P8). (C) Normal phenotype of *Egfr*$^{tm1Dwt/+}$, *Nestin-Cre* brain in the areas surrounding lateral ventricle (P23). (D) *Egfr*$^{tm1Dwt/tm1Dwt}$, *Nestin-Cre* brain displayed neurodegeneration with reduced thickness of corpus callosum, reduced fimbria of hippocampus, and cell loss in the SVZ and RE (P23). (E) Normal phenotype of *Egfr*$^{tm1Dwt/+}$, *hGFAP-Cre* brain in the areas surrounding lateral ventricle (1M). (F) *Egfr*$^{tm1Dwt/tm1Dwt}$, *hGFAP-Cre* brain displayed normal phenotype in the areas surrounding lateral ventricle (1M). A-F H&E stains, 50X.

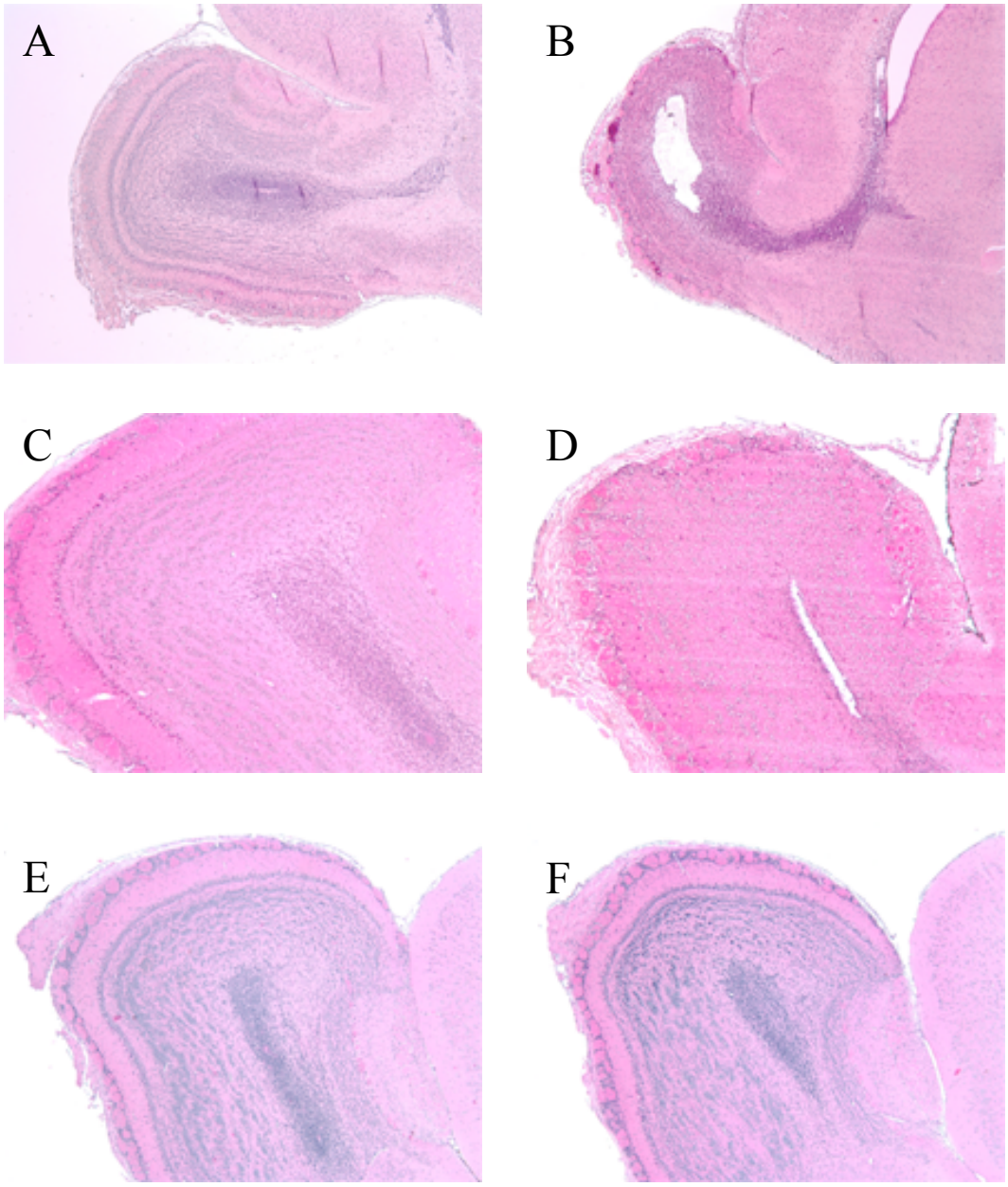

Fig. 4-9 Olfactory bulb phenotype. (A) Normal *Egfr*$^{tm1Dwt/+}$, *Sox2-Cre* olfactory bulb (P8). (B) *Egfr*$^{tm1Dwt/tm1Dwt}$, *Sox2-Cre* olfactory bulb displayed neurodegeneration with cell loss of mitral and granular cell layers as well as bleeding near the glomerular layer (P8). (C) Normal *Egfr*$^{tm1Dwt/+}$, *Nestin-Cre* olfactory bulb (P23). (D) *Egfr*$^{tm1Dwt/tm1Dwt}$, *Nestin-Cre* olfactory bulb displaying neurodegeneration with the disappearance of mitral cell layer as well as slight cell loss in the granular cell layer (P23). (E) Normal *Egfr*$^{tm1Dwt/+}$, *hGFAP-Cre* olfactory bulb (1M). (F) *Egfr*$^{tm1Dwt/tm1Dwt}$, *hGFAP-Cre* olfactory bulb showing no sign of neurodegeneration (1M). A-F H&E stains, 50X.

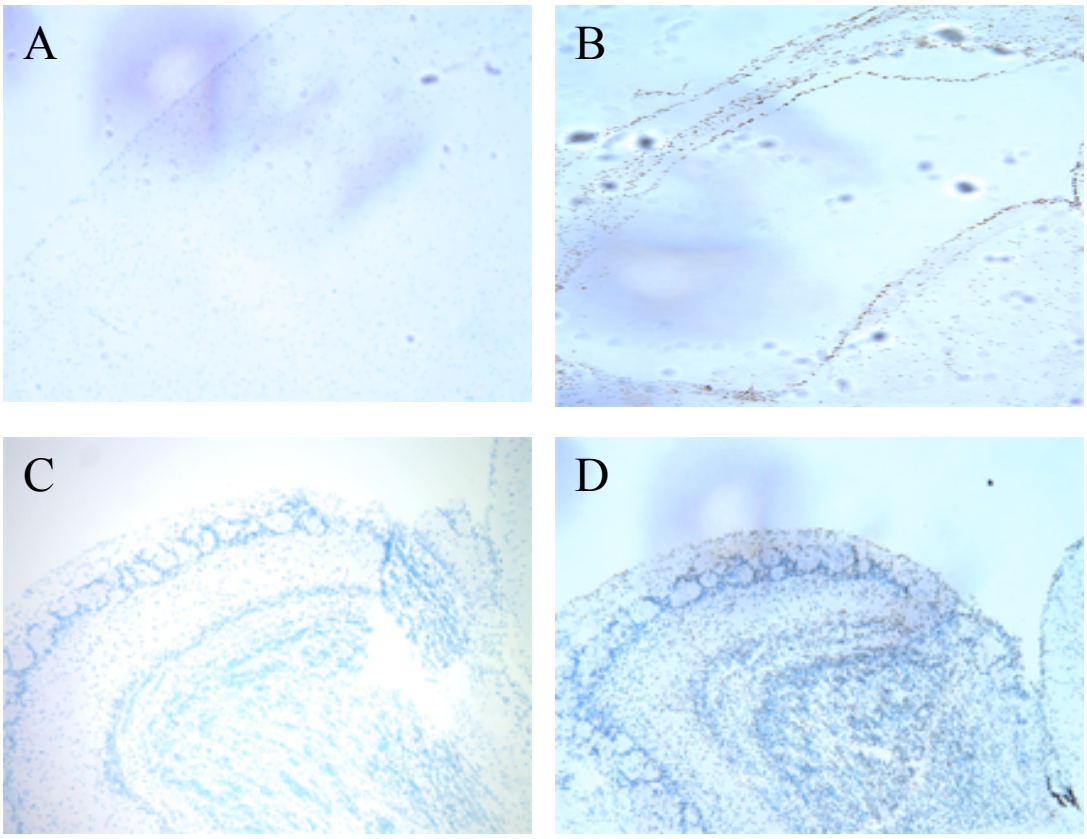

Fig. 4-10 TUNEL analysis. (A) *Egfr*$^{tm1Dwt/+}$, *Nestin-Cre* cortex displayed almost no apoptotic cells. (B) *Egfr*$^{tm1Dwt/tm1Dwt}$, *Nestin-Cre* cortex with apoptotic cells (brown spots) lining the border of the cavity caused by the neurodegenration. (C) *Egfr*$^{tm1Dwt/+}$, *Nestin-Cre* olfactory bulb displaying almost no apoptotic cells. (D) *Egfr*$^{tm1Dwt/tm1Dwt}$, *Nestin-Cre* olfactory bulb displaying many apoptotic cells throughout the olfactory bulb. A-D 50X.

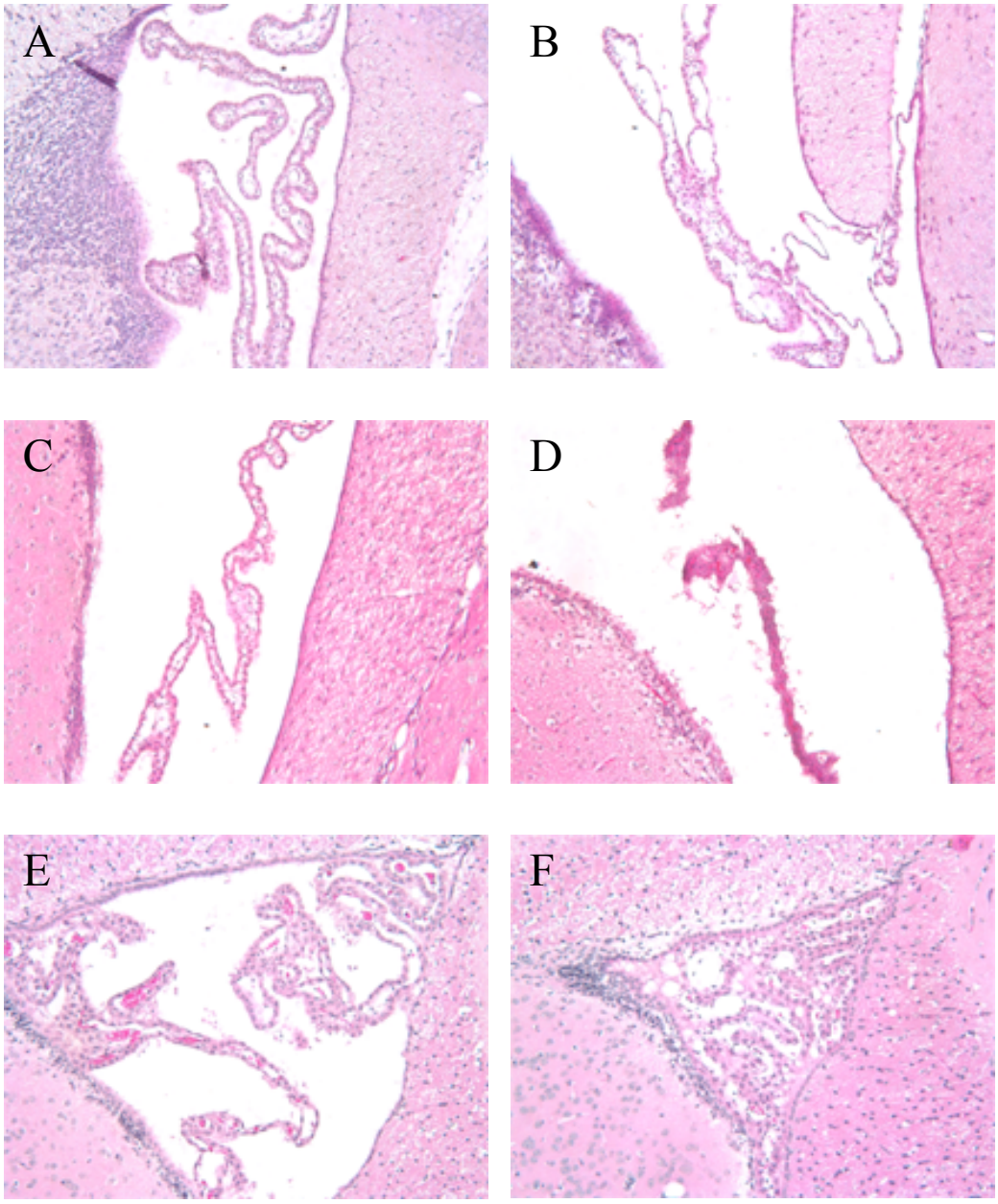

Fig. 4-11 Choroid plexus histology. (A) Normal *Egfr*$^{tm1Dwt/+}$, *Sox2-Cre* choroid plexus (P8). (B) *Egfr*$^{tm1Dwt/tm1Dwt}$, *Sox2-Cre* choroid plexus displaying less intact structure with loss of fibroblasts and collagen fibrils in the connective tissue of the villi (P8). (C) Normal *Egfr*$^{tm1Dwt/+}$, *Nestin-Cre* choroid plexus (P23). (D) *Egfr*$^{tm1Dwt/tm1Dwt}$, *Nestin-Cre* choroid plexus displaying abnormal shape with less cytoplasm in the choroid epithelial cells (P23). (E) Normal *Egfr*$^{tm1Dwt/+}$, *hGFAP-Cre* choroid plexus (1M). (F) *Egfr*$^{tm1Dwt/tm1Dwt}$, *hGFAP-Cre* choroid plexus did not display any abnormality (1M). A-F H&E stains, 200X.

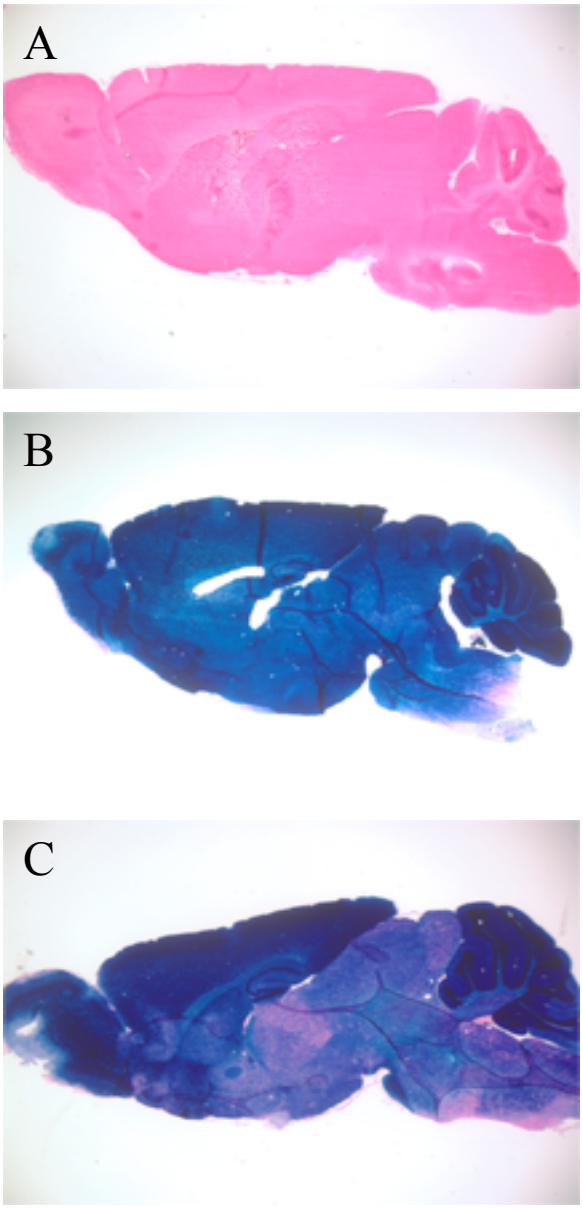

Fig. 4-12 Reporter X-gal staining. (A) *R26R* brain was negative for X-gal staining indicating no endogenous lacZ activity. (B) *R26R/Nestin-Cre* brain displaying extensive positive X-gal staining in the whole brain. (C) *R26R/hGFAP-Cre* brain displaying extensive X-gal staining in the cortex, olfactory bulb as well as cerebellum, and scattered X-gal staining throughout the septum, thalamus, hypothalamus, midbrain, pons and medulla. A-C 15X.

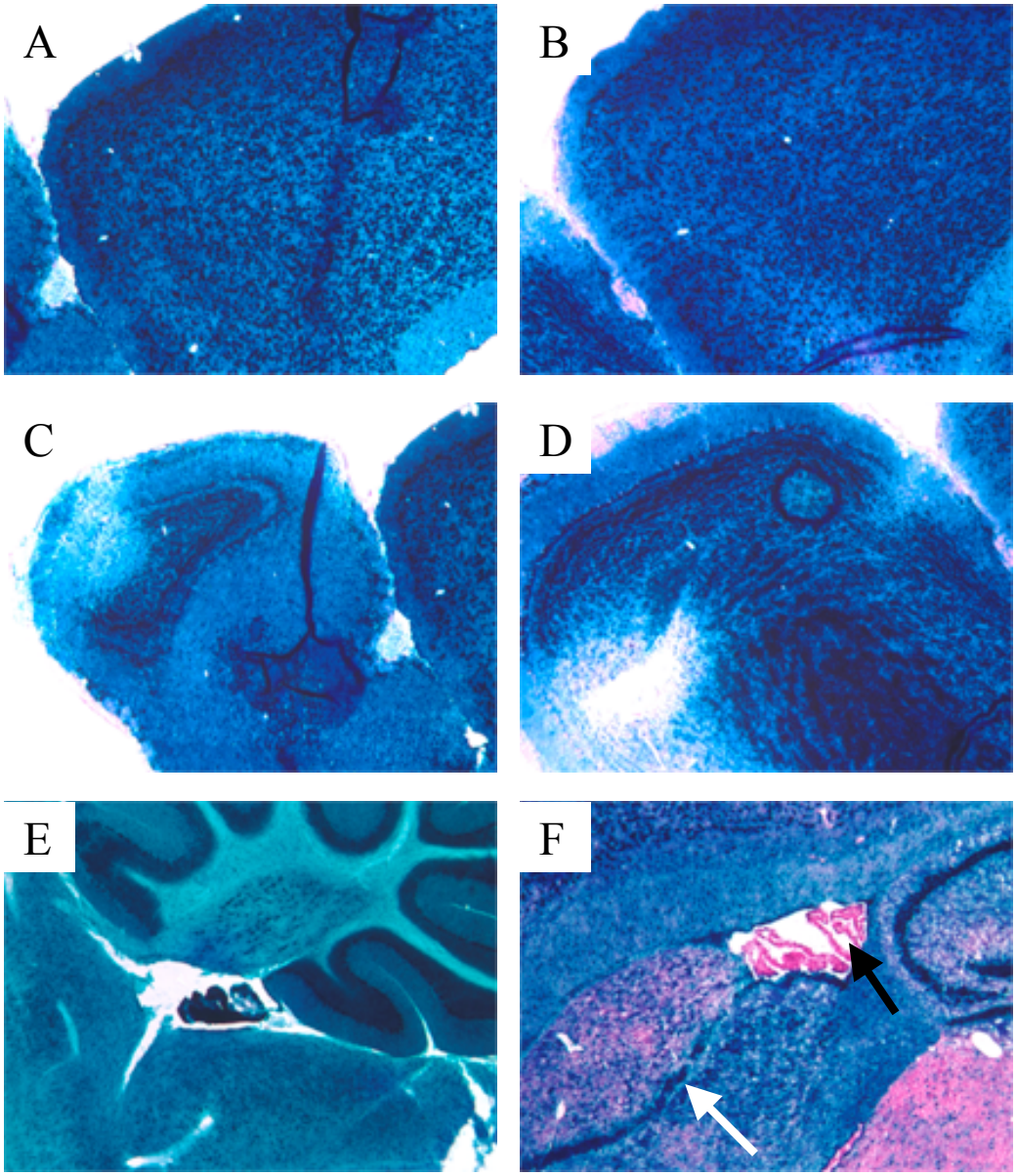

Fig. 4-13 Comparison of reporter X-gal staining. (A) *R26R/Nestin-Cre* cortex with X-gal staining. (B) *R26R/hGFAP-Cre* cortex with X-gal staining. (C) *R26R/Nestin-Cre* olfactory bulb with X-gal staining. (D) *R26R/hGFAP* olfactory bulb with X-gal staining. (E) *R26R/Nestin-Cre* choroid plexus with positive X-gal staining. (F) *R26R/hGFAP-Cre* brain displaying positive X-gal staining in the SVZ (white arrow) and RMS, but negative in the choroid plexus (black arrow). A-D 50X. E-F 100X.

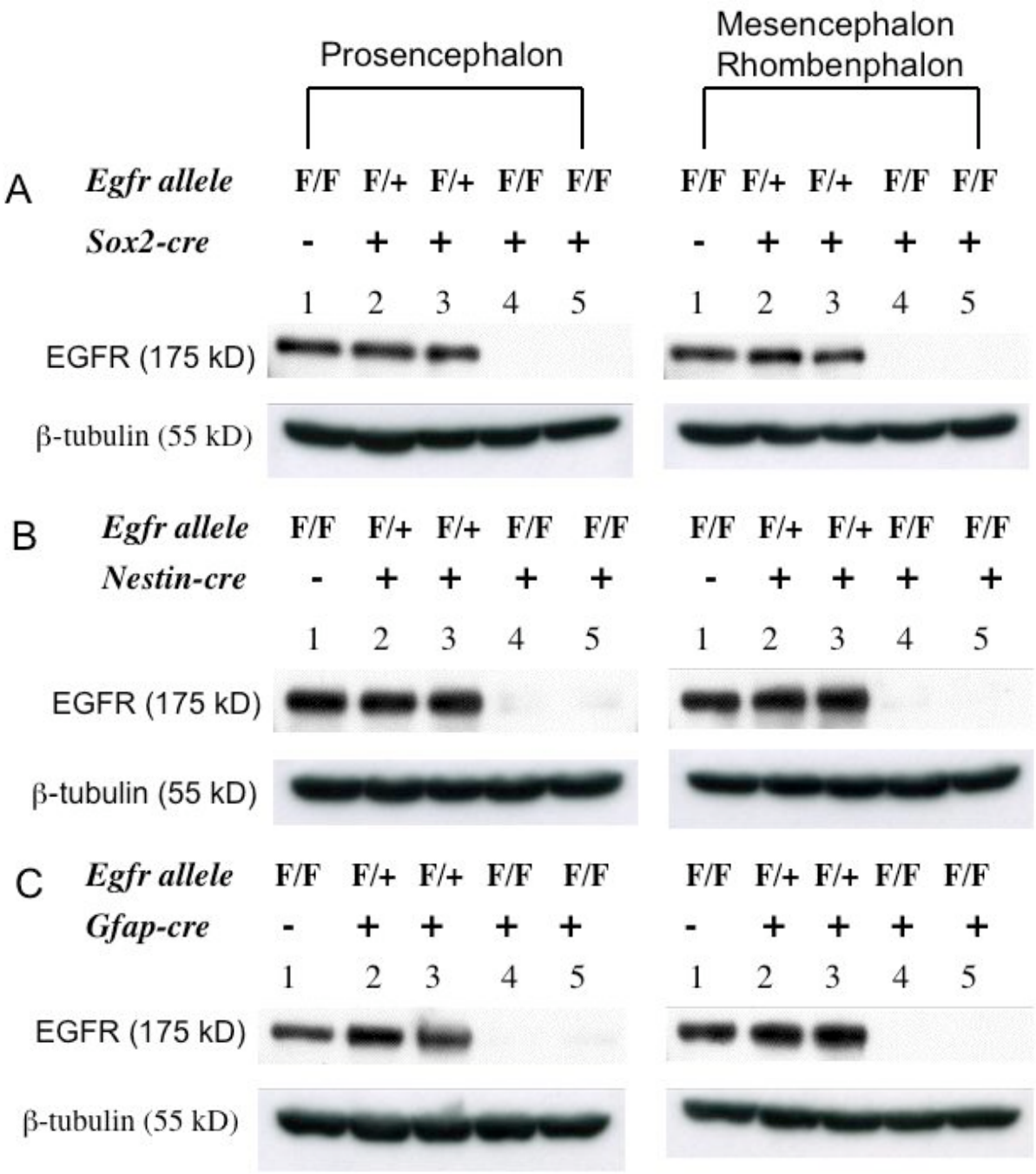

Fig. 4-14 Western blot analysis for EGFR expression. (A-C) Western blot analysis displaying the loss of EGFR in *Egfr*$^{tm1Dwt/tm1Dwt}$, *Sox2-Cre* (*Nestin-Cre* and *hGFAP-Cre*) brains. *Egfr*$^{tm1Dwt/tm1Dwt}$, *Sox2-Cre* (*Nestin-Cre* and *hGFAP-Cre*) brains were separated into two parts (prosencephalon and mesencephalon + rhombenphalon).

References

Aguirre, A., Dupree, J.L., Mangin, J.M., and Gallo, V. (2007). A functional role for EGFR signaling in myelination and remyelination. Nat Neurosci *10*, 990-1002.

Betz, U.A., Vosshenrich, C.A., Rajewsky, K., and Muller, W. (1996). Bypass of lethality with mosaic mice generated by Cre-loxP-mediated recombination. Curr Biol *6*, 1307-1316.

Borlongan, C.V., Skinner, S.J., Geaney, M., Vasconcellos, A.V., Elliott, R.B., and Emerich, D.F. (2004). Neuroprotection by encapsulated choroid plexus in a rodent model of Huntington's disease. Neuroreport *15*, 2521-2525.

Burrows, R.C., Wancio, D., Levitt, P., and Lillien, L. (1997). Response diversity and the timing of progenitor cell maturation are regulated by developmental changes in EGFR expression in the cortex. Neuron *19*, 251-267.

Caric, D., Raphael, H., Viti, J., Feathers, A., Wancio, D., and Lillien, L. (2001). EGFRs mediate chemotactic migration in the developing telencephalon. Development *128*, 4203-4216.

Ciccolini, F. (2001). Identification of two distinct types of multipotent neural precursors that appear sequentially during CNS development. Mol Cell Neurosci *17*, 895-907.

Close, J.L., Liu, J., Gumuscu, B., and Reh, T.A. (2006). Epidermal growth factor receptor expression regulates proliferation in the postnatal rat retina. Glia *54*, 94-104.

Di Terlizzi, R., and Platt, S. (2006). The function, composition and analysis of cerebrospinal fluid in companion animals: part I - function and composition. Vet J *172*, 422-431.

Doetsch, F., Caille, I., Lim, D.A., Garcia-Verdugo, J.M., and Alvarez-Buylla, A. (1999). Subventricular zone astrocytes are neural stem cells in the adult mammalian brain. Cell *97*, 703-716.

Emerich, D.F., Skinner, S.J., Borlongan, C.V., Vasconcellos, A.V., and Thanos, C.G. (2005). The choroid plexus in the rise, fall and repair of the brain. Bioessays *27*, 262-274.

Fox, I.J., and Kornblum, H.I. (2005). Developmental profile of ErbB receptors in murine central nervous system: implications for functional interactions. J Neurosci Res *79*, 584-597.

Garcia, A.D., Doan, N.B., Imura, T., Bush, T.G., and Sofroniew, M.V. (2004). GFAP-expressing progenitors are the principal source of constitutive neurogenesis in adult mouse forebrain. Nat Neurosci *7*, 1233-1241.

Goldshmit, Y., Greenhalgh, C.J., and Turnley, A.M. (2004). Suppressor of cytokine signalling-2 and epidermal growth factor regulate neurite outgrowth of cortical neurons. Eur J Neurosci *20*, 2260-2266.

Gritti, A., Frolichsthal-Schoeller, P., Galli, R., Parati, E.A., Cova, L., Pagano, S.F., Bjornson, C.R., and Vescovi, A.L. (1999). Epidermal and fibroblast growth factors behave as mitogenic regulators for a single multipotent stem cell-like population from the subventricular region of the adult mouse forebrain. J Neurosci *19*, 3287-3297.

Hayashi, S., Lewis, P., Pevny, L., and McMahon, A.P. (2002). Efficient gene modulation in mouse epiblast using a Sox2Cre transgenic mouse strain. Mech Dev *119 Suppl 1*, S97-S101.

Hayashi, S., Tenzen, T., and McMahon, A.P. (2003). Maternal inheritance of Cre activity in a Sox2Cre deleter strain. Genesis *37*, 51-53.

Ide, C., Kitada, M., Chakrabortty, S., Taketomi, M., Matsumoto, N., Kikukawa, S., Mizoguchi, A., Kawaguchi, S., Endoh, K., and Suzuki, Y. (2001). Grafting of choroid plexus ependymal cells promotes the growth of regenerating axons in the dorsal funiculus of rat spinal cord: a preliminary report. Exp Neurol *167*, 242-251.

Itokazu, Y., Kitada, M., Dezawa, M., Mizoguchi, A., Matsumoto, N., Shimizu, A., and Ide, C. (2006). Choroid plexus ependymal cells host neural progenitor cells in the rat. Glia *53*, 32-42.

Kimura, K., Matsumoto, N., Kitada, M., Mizoguchi, A., and Ide, C. (2004). Neurite outgrowth from hippocampal neurons is promoted by choroid plexus ependymal cells in vitro. J Neurocytol *33*, 465-476.

Koprivica, V., Cho, K.S., Park, J.B., Yiu, G., Atwal, J., Gore, B., Kim, J.A., Lin, E., Tessier-Lavigne, M., Chen, D.F*., et al.* (2005). EGFR activation mediates inhibition of axon regeneration by myelin and chondroitin sulfate proteoglycans. Science *310*, 106-110.

Lillien, L. (1995). Changes in retinal cell fate induced by overexpression of EGF receptor. Nature *377*, 158-162.

Liu, B., and Neufeld, A.H. (2004a). Activation of epidermal growth factor receptor causes astrocytes to form cribriform structures. Glia *46*, 153-168.

Liu, B., and Neufeld, A.H. (2004b). Activation of epidermal growth factor receptors directs astrocytes to organize in a network surrounding axons in the developing rat optic nerve. Dev Biol *273*, 297-307.

Lois, C., Garcia-Verdugo, J.M., and Alvarez-Buylla, A. (1996). Chain migration of neuronal precursors. Science *271*, 978-981.

Mattson, M.P. (2006). Neuronal life-and-death signaling, apoptosis, and neurodegenerative disorders. Antioxid Redox Signal *8*, 1997-2006.

Mattson, M.P., Duan, W., Pedersen, W.A., and Culmsee, C. (2001). Neurodegenerative disorders and ischemic brain diseases. Apoptosis *6*, 69-81.

Mazzoni, I.E., and Kenigsberg, R.L. (1994). Localization and characterization of epidermal growth-factor receptors in the developing rat medial septal area in culture. Brain Res *656*, 115-126.

Merkle, F.T., Tramontin, A.D., Garcia-Verdugo, J.M., and Alvarez-Buylla, A. (2004). Radial glia give rise to adult neural stem cells in the subventricular zone. Proc Natl Acad Sci U S A *101*, 17528-17532.

Redzic, Z.B., and Segal, M.B. (2004). The structure of the choroid plexus and the physiology of the choroid plexus epithelium. Adv Drug Deliv Rev *56*, 1695-1716.

Reynolds, B.A., Tetzlaff, W., and Weiss, S. (1992). A multipotent EGF-responsive striatal embryonic progenitor cell produces neurons and astrocytes. J Neurosci *12*, 4565-4574.

Schachtrup, C., Lu, P., Jones, L.L., Lee, J.K., Lu, J., Sachs, B.D., Zheng, B., and Akassoglou, K. (2007). Fibrinogen inhibits neurite outgrowth via beta 3 integrin-mediated phosphorylation of the EGF receptor. Proc Natl Acad Sci U S A *104*, 11814-11819.

Sibilia, M., Steinbach, J.P., Stingl, L., Aguzzi, A., and Wagner, E.F. (1998). A strain-independent postnatal neurodegeneration in mice lacking the EGF receptor. Embo J *17*, 719-731.

Sibilia, M., and Wagner, E.F. (1995). Strain-dependent epithelial defects in mice lacking the EGF receptor. Science *269*, 234-238.

Soriano, P. (1999). Generalized lacZ expression with the ROSA26 Cre reporter strain. Nat Genet *21*, 70-71.

Speake, T., Whitwell, C., Kajita, H., Majid, A., and Brown, P.D. (2001). Mechanisms of CSF secretion by the choroid plexus. Microsc Res Tech *52*, 49-59.

Threadgill, D.W., Dlugosz, A.A., Hansen, L.A., Tennenbaum, T., Lichti, U., Yee, D., LaMantia, C., Mourton, T., Herrup, K., Harris, R.C.*, et al.* (1995). Targeted disruption of mouse EGF receptor: effect of genetic background on mutant phenotype. Science *269*, 230-234.

Timmusk, T., Mudo, G., Metsis, M., and Belluardo, N. (1995). Expression of mRNAs for neurotrophins and their receptors in the rat choroid plexus and dura mater. Neuroreport *6*, 1997-2000.

Tronche, F., Kellendonk, C., Kretz, O., Gass, P., Anlag, K., Orban, P.C., Bock, R., Klein, R., and Schutz, G. (1999). Disruption of the glucocorticoid receptor gene in the nervous system results in reduced anxiety. Nat Genet *23*, 99-103.

Tropepe, V., Sibilia, M., Ciruna, B.G., Rossant, J., Wagner, E.F., and van der Kooy, D. (1999). Distinct neural stem cells proliferate in response to EGF and FGF in the developing mouse telencephalon. Dev Biol *208*, 166-188.

Wagner, B., Natarajan, A., Grunaug, S., Kroismayr, R., Wagner, E.F., and Sibilia, M. (2006). Neuronal survival depends on EGFR signaling in cortical but not midbrain astrocytes. Embo J *25*, 752-762.

Wang, S.L., Shiverick, K.T., Ogilvie, S., Dunn, W.A., and Raizada, M.K. (1989). Characterization of epidermal growth factor receptors in astrocytic glial and neuronal cells in primary culture. Endocrinology *124*, 240-247.

Xiang, Y.Y., Dong, H., Wan, Y., Li, J., Yee, A., Yang, B.B., and Lu, W.Y. (2006). Versican G3 domain regulates neurite growth and synaptic transmission of hippocampal neurons by activation of epidermal growth factor receptor. J Biol Chem *281*, 19358-19368.

Zheng, W. (2001). Toxicology of choroid plexus: special reference to metal-induced neurotoxicities. Microsc Res Tech *52*, 89-103.

Zhuo, L., Theis, M., Alvarez-Maya, I., Brenner, M., Willecke, K., and Messing, A. (2001). hGFAP-cre transgenic mice for manipulation of glial and neuronal function in vivo. Genesis *31*, 85-94.

CHAPTER 5

CONCLUSIONS AND FUTURE DIRECTIONS

Gene targeting technology is a powerful tool to study gene function in mouse models. Constitutional knockout of *Egfr* in mice results in placental defects with mice dying pre- or perinatally. This limits the study of EGFR in later stages of development or physiological functions in adults. Thus, the generation of an *Egfr* conditional allele was needed to overcome this limitation. The *Egfr* conditional allele, $Egfr^{tm1Dwt}$, possessed wildtype function since $Egfr^{tm1Dwt/-}$ mice were viable, fertile and did not display any detectable abnormal phenotype. The $Egfr^{\Delta}$ allele, resulting from *EIIa-Cre*-mediated inactivation of *Egfr* by deletion of exon 3, was confirmed to function as a null allele by demonstrating that $Egfr^{\Delta/\Delta}$ embryos on a 129,B6 mixed genetic background die at midgestation due to placental defect identical to that of *Egfr* null embryos. In order to analyze EGFR function within the brain, three *Cre* transgenic lines (*Sox2-Cre*, *Nestin-Cre*, *hGFAP-Cre*) were used. $Egfr^{tm1Dwt/tm1Dwt}$, *Sox2-Cre*, as well as *Nestin-Cre* and *hGFAP-Cre*, mice were generated. Only $Egfr^{tm1Dwt/tm1Dwt}$, *Sox2-Cre* and *Nestin-Cre* mice displayed neurodegeneration similar to *Egfr* null mice surviving to birth, while $Egfr^{tm1Dwt/tm1Dwt}$, *hGFAP-Cre* mice did not show any neurodegeneration. This result confirms that neurodegeneration is independent of placental defects, and is the major cause of postnatal lethality in mice lacking EGFR. In the current study, the data also suggests that neurodegeneration is a secondary effect. However, we can

not completely rule out the possibility that EGFR signaling is directly required for neuronal or astrocytic survival. Therefore, it will be necessary to use neuron-specific and astrocyte-specific *Cre* lines in future studies. The data suggests that the choroid plexus is a potential cause of the neurodegeneration, thus examination of CSF composition would be a promising avenue for additional studies.

The current study not only presents the necessity of EGFR within the brain, but also presents new mouse models that can be used as a platform for exploring other EGFR functions *in vivo*. Nearly 20% of $Egfr^{tm1Dwt/tm1Dwt}$, *Sox2-Cre* mice survive for more than one month due to mosaic deletion of *Egfr*. Some of the surviving mice have been examined but showed no overt neurodegeneration supporting neurodegeneration as a likely cause for postnatal lethality in *Egfr* null mice. Although the surviving mice did not display an obvious neurodegenerative phenotype, they may be a valuable model for examining possible phenotypes developing in other tissues since $Egfr^{tm1Dwt/tm1Dwt}$, *Sox2-Cre* mice possess no or very low EGFR activity in all tissues. Likewise, surviving $Egfr^{tm1Dwt/tm1Dwt}$, *Nestin-Cre* and *hGFAP-Cre* mice can be used in other studies. Although these mice did not display a neurodegenerative phenotype, they did nonetheless show growth retardation at early postnatal stages. Additional experiments have been performed feeding $Egfr^{tm1Dwt/tm1Dwt}$, *hGFAP-Cre* mice between 12-14 weeks of age a high fat diet for 3 months. The mean weight gain of $Egfr^{tm1Dwt/tm1Dwt}$, *hGFAP-Cre* mice was significantly lower than that of $Egfr^{tm1Dwt/tm1Dwt}$ control mice. Therefore, surviving $Egfr^{tm1Dwt/tm1Dwt}$, *Nestin-Cre* and *hGFAP-Cre* mice may be good models for investigating a role for EGFR in metabolism.

The *Egfr* conditional mouse model should also be a good platform for cancer research. Many types of cancers overexpress EGFR leading to proliferation, survival and

metastasis, and EGFR is a recognized therapeutic target for cancer treatment. Thus, by combining mouse cancer models with the *Egfr* conditional model, the role of EGFR in cancer biology can be evaluated to develop better strategies for cancer treatment. For example, EGFR is a therapeutic target for the treatment of colorectal cancer. However, clinically there are still at least 20% of colorectal cancers do not express EGFR, which means that those cancer cells may not rely on EGFR signaling. Other studies have used the Apc^{Min} mouse model for colorectal cancer in combination with tissue-specific deletion of *Egfr* in the epithelial cells of intestine using the *Villin-Cre* transgene. Apc^{Min}, $Egfr^{tm1Dwt/tm1Dwt}$, *Villin-Cre* mice display a significant reduction in polyp number reconfirming the importance of EGFR signaling for colorectal cancer development. These mice also provide an opportunity to examine polyps in which EGFR signaling is not necessary for development, and to identify compensatory signaling pathways that may be used by colorectal cancers lacking EGFR. More importantly, this should support new strategies for the treatment of colorectal cancer.

As EGFR is a major regulator of cellular signals, there is good reason to believe that EGFR has many unexplored functions. The *Egfr* condtional allele described herein will be a powerful tool to unravel other EGFR functions. As the reservoir of *Cre* lines increases, knowledge about EGFR function within specific cell types or tissues can be expanded.